UNIVERSITÀ DEGLI STUDI DI NAPOLI FEDERICO II

School of Polytechnic and Basic Sciences

PhD School in Earth, Environment and Resources Sciences

XXX cycle

PhD Thesis

Seismological and gravimetric surveys in Italian active tectonic areas

Advisor

Dott. Valeria Paoletti

PhD Student

Paola Luiso

Co-Advisors

Dott. Germana Gaudiosi INGV-OV

Dott. Rosa Nappi INGV-OV

2016/2017

Summary

In this thesis, I present a new multiparametric method aimed at investigating the neotectonic activity of three areas of the Apennines characterized by different Quaternary tectonic environments: the Thyrrhenian inner margin of the Southern Apennines, the backbone of the Central Apennines, and the foredeep-foreland at the transition zone between the Southern and Central Apennine belts.

The method consists in a multiparametric data analysis in GIS (Geographic Information System) environment which integrates faults, earthquakes and gravimetric lineaments. This is for characterizing the geometry (strike, dip direction, angle and depth) and activity of buried/silent active faults (Massico and San Giuliano di Puglia areas). We used the Monte Bove, Vettore and Paganica capable faults for calibration as they are located along the epicentral areas of the recent seismic sequences of 2009 and 2016, where an outstanding geological and geophysical database is available.

The structural setting of the study areas was investigated by performing *Multiscale Derivative Analysis* (MDA; Fedi, 2002), a valuable tool for identification and interpretation of complex geologic structures (such as faults) with density contrast. This method is especially suitable for detecting and characterizing faults not directly visible at the surface and that were not described before.

I analysed the correlation between the earthquakes location and the MDA maxima of the Bouguer anomaly field. To infer the characteristics of active fault planes in the areas with good correlation between the MDA signals and the epicentres, I performed a combined interpretation of 2D re-localized hypocentral sections and the images resulting from the *Depth from Extreme Points* method (DEXP; Fedi, 2007).

So, the chosen study areas are: *i)* the Paganica and the Mt. Vettore-Mt. Bove areas (central Apennines), hit by 2009 and the 2016 seismic sequences, respectively; *ii)* the Mt. Massico horst characterized by lower energy seismicity, but clear gravimetric signatures; *iii)* the San Giuliano di Puglia area (southern Apennines), hit by 2002–2003 seismic sequences. This choice was based either on the areas' high seismic hazard (for the Paganica and the Mt. Vettore-Mt. Bove areas), and/or on the presence of clear gravimetric signatures, combined with a good knowledge of quaternary geological structures in the complex geodynamic environment of the Apennine chain.

In all the cases, both the gravimetric and seismological analyses yielded clear information about the geometry of the fault plains. These good results show the effectiveness of this new multiparametric approach to identify and characterize active (capable or not) structures, known or un-known in literature. In addition, this approach allows revealing if the structure is active along all the fault plain or only partially, and detecting its direction and dip angle. So, it can be successfully employed in areas of the Apennine chain with a high potential hazard with buried and/or silent faults.

1 Introduction

The Apennine Chain is an east-verging belt developed in Neogene times above a west-dipping subduction. The eastward migration of the thrusts is associated with the opening of the back-arc extensional Tyrrhenian Sea basin. Since the Early Pliocene (for the southern Apennine) and the late Miocene (for the northern Apennine), the basin extended progressively to the east, causing the drowning of the internal sector of the orogenic wedge and the formation of coastal grabens (peri-Tyrrhenian basins) along the SW flank of the chain. During the Quaternary, the Apennine chain experienced NE–SW extension leading to the formation of intra-montane basins along NW–SE-to WNW–ESE-oriented extensional belts. In central and southern Italy, this tectonic environment is mainly reflected in well-exposed NW–SE normal fault alignments (Lavecchia et al., 2012), responsible for major historical (Rovida et al., 2011) and instrumental earthquakes.

The aim of this study is to identify and constrain the geometry of active, outcropping and buried fault systems of three areas of the Apennines characterized by different Quaternary tectonic environments: the Thyrrhenian inner margin of the Southern Apennines (Massico area), the backbone of the Central Apennines (Paganica and the Mt. Vettore-Mt. Bove), and the foredeep-foreland of the Apennines (San Giuliano di Puglia). This is done through an integrated analysis of faults, earthquakes and gravimetric lineaments. The integration of the information from different datasets has a key role in understanding the behaviour of the active faults when they are buried or silent.

In detail, the study areas (yellow boxes in Fig.1) are: *i)* the northern margin of the Campanian Plain, with the NE–SW fault systems bordering the Mt. Massico horst, characterized by low energy seismicity (M_{Wmax}=4.8); *ii)* the central Apennines hit by 2009 (M_{Wmax}=6.1) and the 2016 seismic sequences (M_{Wmax}=6.5), with surface ruptures of the Paganica and the Mt. Vettore-Mt. Bove faults, respectively; *iii)* the eastern Molise area hit by 2002–2003 seismic sequences (M_{Wmax}=5.8) of the San Giuliano di Puglia (southern Apennines).

Three thematic data sets have been generated for the study areas in GIS environment: “fault”, “earthquake” and “gravimetric” data sets, to collect and integrate all existing information. More specifically:

- the fault dataset consists of the collection of tectonic structures extracted from different catalogues and scientific papers, vectorialized in an ad-hoc dataset with an associated table of attributes containing information about each structure;
- the earthquake dataset contains the instrumental and historical earthquakes extracted from the available catalogues and a-relocation of the Massico seismic events (to improve the location accuracy for this area);
- the gravimetric dataset consists of lineaments identified by the MDA maxima of the Bouguer anomaly. *Multiscale Derivative Analysis* (MDA) relies on the high-resolution properties of the *Enhanced Horizontal Derivative* (EHD; Fedi and Florio, 2001). The maxima of the MDA map represent lineaments contacting lithologies with different density. The MDA method allows exploring potential field data at different scales and highlighting regional, intermediate and local structural trends. Thus, it represents a valuable tool for the interpretation of geologic structures. The MDA maps provide an almost complete representation of the structural framework of the study areas. Most of the known geological elements of the Apennine system are clearly shown at intermediate and short scales, along with several trends indicating structures that do not have any reference at the surface (buried faults). This is, for instance, the case of some regional linear trends in the foredeep area.

The analysis of the correlation between faults, earthquakes and MDA maxima allowed highlighting different possible scenarios in the study areas. Moreover, the geometry and depth extent of the studied faults was constrained through a *Depth from Extreme Points* (DEXP, Fedi, 2007; Fedi and Pilkington, 2011) analysis on gravity data, combined with the information derived from 2D hypocentral sections.

My thesis is organized as follows: Section 2 gives a description of the geological and seismotectonic framework of the study areas to better understand their geodynamic evolution and constrain the results of the present study with those from literature. Section 3 describes the collection of the three datasets: the “fault dataset”, the “earthquake dataset” (that includes earthquake re-location at Mt. Massico) and the “gravimetric dataset” (that includes a description of the MDA method). Section 4 describes the comparison of the three data sets in GIS environment and 2D combined sections of DEXP images and hypocenters.

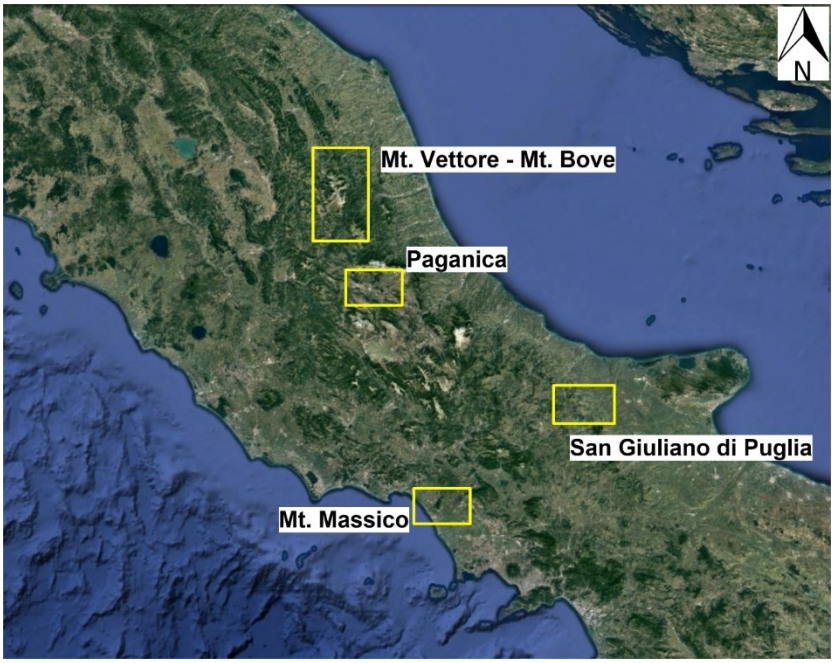

Fig.1 Location of the study areas in the frame of peninsular Italy.

2 Geological and seismotectonic framework of the areas

The Apennine Chain can be described as a complex thrust and fold belt system, built between the Lower Cretaceous and the Quaternary, as consequence of the convergence between the African and European Plates (Malinverno and Ryan, 1986; Doglioni, 1991).

This fold-and-thrust belt extends from peninsular Italy to Sicily for a length of ~1500 km, linking the western Alps to the Maghrebian chain of north Africa.

The thrust belt can be subdivided into the arcuate segments of the northern, central and southern Apennines (Ghisetti and Vezzani, 1997; Patacca and Scandone, 2007), bounded by the Olevano-Antrodoco Line to the NW (Salvini and Vittori, 1982; blue line in Fig. 2), and the Ortona-Roccamonfina Line to the SE (Ghisetti and Vezzani, 1983, 1991, red line in Fig. 2). The northern-central arc is composed of thrust systems structured as embricated fans in piggy-back sequences. The southern one, characterized by a greater shortening than the northern one, is built as duplex systems with overthrusting of the internal units onto the eastern edge of the Apulian platform (Mostardini and Merlini, 1986; Bally et al., 1986).

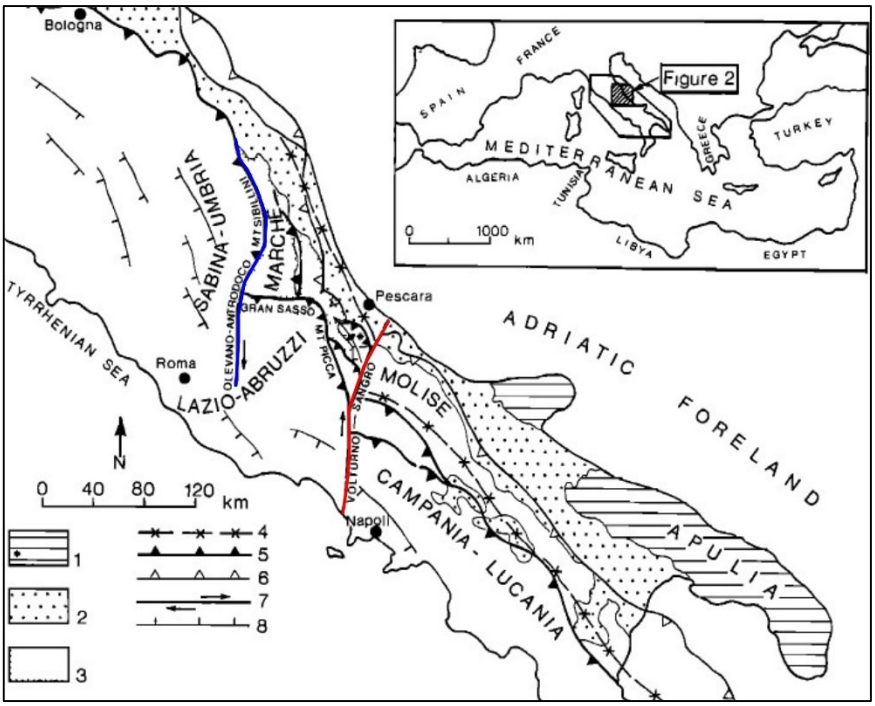

Fig.2 *Strctural sketch of the Apenninic chain. 1) Apulia foreland; 2) Adriatic foredeep; 3) Laga flysch basin; 5) major thrust faults; 6) buried thrust faults; 7) strike-slip faults; 8) normal faults; blue line: Olevano-Antrodoco Line; red line: Ortona-Roccamonfina Line (modified after Ghisetti and Vezzani, 1991).*

Since the Miocene the compressional phase, was characterized by the built of the Apennine chain with the development of NW–SE thrust and fold systems (Patacca et al., 1990, 2008, and references therein).

From the late Miocene, an eastward migration of the orogenic front and of the foredeep-foreland system was accompanied by an extensional collapse of the inner domains of the thrust belt. This process culminated in the crustal thinning and foundering of the Tyrrhenian basin (Fig. 3), interpreted by several authors (e.g., Malinverno and Ryan, 1986; Channell and Mareschal, 1989; Patacca et al., 1990, 1993; Patacca and Scandone, 2004; Doglioni, 1995) as a back-arc basin behind the retreating Apulia-Adriatic slab and the formation of coastal grabens (peri-Tyrrhenian basins) along the SW flank of the chain, accompanied by extensive volcanism.

From Pliocene to Pleistocene, the Apennine chain experienced NE–SW extension leading to the formation of intra-montane basins along NW–SE-to-WNW–ESE-oriented extensional normal fault systems superimposed onto the compressional thrust belt, and controlling the intense seismicity of the Apennine chain.

The seismicity is rather diffuse all along the Apennines and the strongest activity is concentrated in the backbone of the chain with $5 \leq M_w \leq 7$ historical normal faulting earthquakes occurring with

recurrence intervals ≥1 ka (Vittori et al., 1991; Pantosti et al., 1993, 1996; Giraudi and Frezzotti, 1995). In central Italy, the seismogenetic normal faults have well-exposed SW to SSW-dipping high-angle (Roberts and Michetti, 2004). Seismic events with M_W > 6.0 struck this sector in the last century (i.e., the M_W = 7.0 Fucino earthquake in 1915), as well as in recent times (M_W= 6.0, Colfiorito, 1997; M_W= 6.3, L'Aquila, 2009; M_W= 6.2 and M_W= 6.5, central Italy, 2016 seismic sequence). On the contrary, in southern Italy, west-dipping active faults crop out with less continuity, while an eastward-dipping normal fault system seems to be the most relevant structure and accounts for the seismicity recorded in the region (Pantosti and Valensise, 1990; Pantosti et al., 1993; Brozzetti, 2011; Brozzetti et al., 2012; DISS Working Group, 2015). The M_W= 6.9 1980 Irpinia earthquake represents the most energetic event associated with this extensional belt. Within this evolutionary trend, foreland to hinterland transects across the Apennines provide a progressive evolution from young, newly generated seismogenetic normal faults (to the east), to progressively older and more mature faults (to the west) that fail to generate large earthquakes.

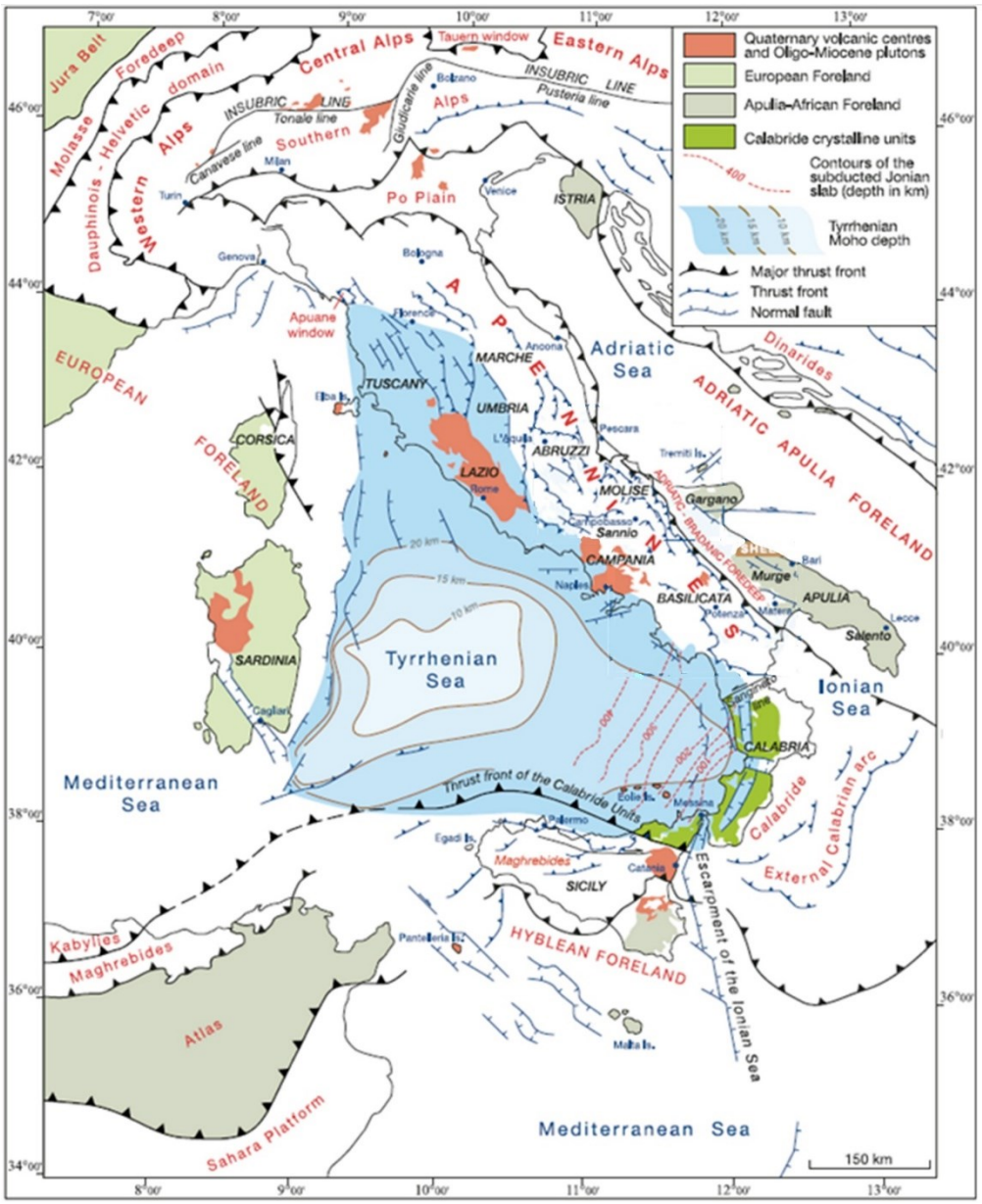

Fig.3 *Structural scheme of Italy and surrounding regions (modified after Vezzani et al., 2010).*

2.1 Paganica and Mt. Vettore — Mt. Bove (Abruzzo region)

The Umbria-Marche-Abruzzo intra-Apennine extensional belt consists of three alignments of Quaternary normal and normal-oblique faults, named respectively: external (from Mt. Vettore to Mt. Gorzano), intermediate (from Gubbio to Colfiorito, Norcia, L'Aquila and the Middle Aterno Valley), and internal (from the Rieti Basin to the Salto Valley and the Fucino Basin; Lavecchia et al., 2012; Fig.4), with NW–SE strike. The strike offsets the Mio-Pliocene fold-and-thrust structures and generates intra-mountain depressions (the Rieti, Norcia, Leonessa, Colfiorito, Fucino, Sulmona and L'Aquila basins) and minor depressions that are located in mountainous areas (the Salto and Turano

valleys, Campo Imperatore, Campo Felice and Castelluccio plains). The depressions are filled with continental deposits of Plio-Quaternary age (Cosentino et al., 2017; Miccadei et al., 1997; Bosi et al., 2003).

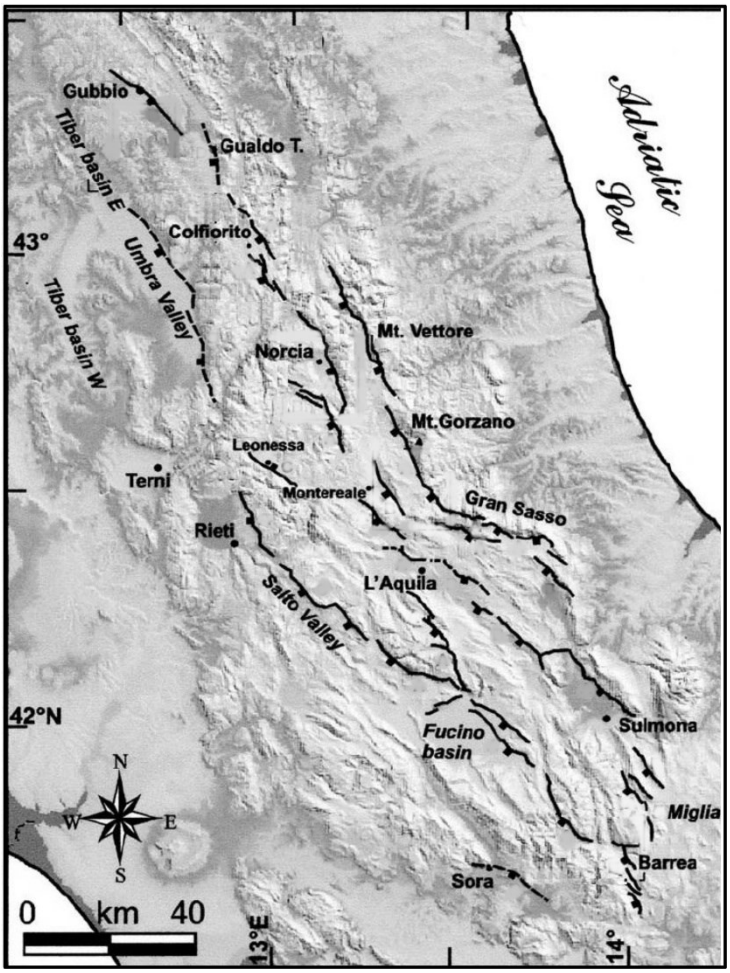

Fig.4 *Sketch of the main Quaternary active normal fault and intra-mountain depressions (modified after Boncio et al., 2004).*

Through the last 100 years, two major events with $M_w > 5.5$ struck the internal alignment: the one of Avezzano in 1915 with M_s 6.9 and the event of Barrea in 1984 with M_w 5.9. Four earthquakes hit the intermediate alignment: Gubbio 1984, M_w 5.6; Colfiorito 1997, M_w 6.0; Norcia 1979, M_w 5.9; L'Aquila 2009, M_w 6.1. No instrumental events with $M_w > 4.5$ were associated with the external alignment until the 2016 Amatrice seismic sequences with M_w= 6.5.

Paganica

The 2009 April 6 (M_w= 6.1) L'Aquila earthquake and its aftershocks sequence (Scognamiglio *et al*., 2010; Herrmann *et al*., 2011; Valoroso *et al*., 2013) hit a densely populated area in the Middle Aterno Valley (central Apennines) and caused heavy damage in the town of L'Aquila and surrounding

villages. As reported also by historical records (Tertulliani *et al*. 2009; Rovida *et al*. 2011), this region is one of the most active areas of Italy and was frequently struck by destructive earthquakes. The main historical earthquakes occurred in 1461 with M_w= 6.5 (I_{max}=X) close to the L'Aquila town and in 1703 with two main shocks with M_w= 6.8 (near Norcia) and M_w= 6.7 (near Pizzoli, L'Aquila; Rovida et al., 2016). It is estimated that their recurrence time is between 700 and 1000 years with an extension rate of 1mm/yr (Galadini and Galli, 2000; Emergeo Working Group, 2016). The 2009 L'Aquila earthquake sequence well fits the seismotectonic context of the area: seismologic, geodetic, DInSar and geological data clearly indicate that the Paganica - San Demetrio fault system (PSDFS) is the seismogenic fault of the M_w= 6.1, April 6 2009 main-shock. The focal mechanism indicates a fault plane with N140° direction and dipping about 45–50° to the SW (Chiaraluce, 2012; Valoroso et al., 2013), in agreement with the regional SW–NE extensional stress field active in the region.

The Paganica normal fault, the seismogenetic fault responsible of the 2009 L'Aquila mainshock, is in coincidence with the PSDFS (Fig.5), which bounds to the northeast the Aterno River valley. Here it shows a complex surface expression, with several synthetic and antithetic splays affecting the Quaternary basin continental deposits (Vezzani and Ghisetti, 1998; Boncio et al., 2004; ISPRA catalogue, 2006; Pucci et al., 2015).

Before the 2009 earthquake, the geometry and activity of the PSDFS was only roughly known. It was mapped as uncertain or buried fault (Fig. 6; Vezzani and Ghisetti, 1998; Boncio et al., 2004; Pace et al. 2006; Galli et al. 2010). During the 6 April main shock, this fault created a limited coseismic surface displacement observed for a total length > 3 km, consisting of a complex set of small scarps (up to 0.10 – 0.15 m high) and open cracks with a direction in agreement with the focal mechanism of the main seismic events (Falcucci et al., 2009; Emergeo Working Group, 2010; Vittori et al., 2011). Other discontinuous breaks occurred with a trend ranging from N120° to N170°, to north and south of the main alignment of ruptures. In this case, the length of the surface faulting may overcome 6 km (Emergeo Working Group, 2010). Other cracks are detected along the antithetic structures of Bazzano and Monticchio-Fossa (Fig. 5).

The total extension of the epicentral area has a length of 50 km along the NW-SE direction, with earthquakes confined below 2 km (Chiarabba et al., 2009; Chiaraluce et al., 2011). This suggests that only minor slips took place on the shallower portion of the fault, in agreement with surface observations. Elastic dislocation modelling suggests over 80 cm of slip at depth in the fault and the area with highest values of surface subsidence is located towards the south-eastern end of the

surface ruptures (Wilkinson et al., 2017). There is a general discrepancy between the length of the seismologically and geodetically modelled fault (up to 18 km), the limited size of the primary continuous coseismic surface ruptures (3-6 km), and the significant morphological expression of the PSDFS. This stimulated a debate about the maximum rupture length of the PSDFS and its capability to generate earthquakes stronger than the 2009 main shock, with much larger rupture length and displacement.

Based on the analogies in the distribution of the intensities in areas with the strongest effects, Tertulliani et al. (2009) and Atzori et al. (2009) suggest that both the 1461 and 2009 events are caused by the same structure: the Paganica fault. Palaeoseismological studies across different segments of the Paganica and San Demetrio faults returned different results: Galli et al. (2010) suggested that the Paganica fault caused both the M_w 6.7 Aquilano earthquakes in 1461 and on the 2nd of February 1703. Whereas Cinti et al. (2011) recognized five paleo-events which include the 1461 one but not the 1703 earthquake. Based on the long-term fault scarp geomorphology, however, they also suggested that the Paganica fault could generate larger earthquakes.

Soon after the mainshock, an intense aftershock sequence started to spread NW–SE, bilaterally, releasing five relevant events (M_w 5.0 to 5.5; Chiaraluce *et al.*, 2011).

The seismic sequence reactivated four well-distinguished fault sources differing in geometry, size and the degree of involvement (Fig. 6; Lavecchia et al., 2012):

1) the SW dipping Paganica fault system activated during the 6 April mainshock (M_w 6.1) from the surface to a depth of ~10.5 km;

2) the NE dipping hidden Ocre source activated during the strongest aftershocks (9 April, M_w 5.4) at depths between 11 km and 16 km;

3) the W-SW dipping Mt. Gorzano fault activated by four relevant aftershocks (6 to 13 April, M_w ~5.0 to 5.5) at depths between 6 km and 12 km;

4) the W-SW dipping Montereale fault system and its continuation into the S dipping Mt. San Franco fault activated at depths between 6 km and 10 km in a large number of minor events with M_w up to 3.6.

The epicentral area of the 2009 L'Aquila sequence is crossed by the external and intermediate fault alignments (Chiaraluce et al., 2001; Lavecchia et al., 2012). The epicentral area propagated in time further to the northwest towards the epicentral area of the Norcia 1979 earthquake, migrating from the Paganica fault (intermediate alignment) to the Gorzano fault (external alignment). Conversely, to the south, seismic activity remained nearly completely locked roughly at the northern boundary

of the Middle Aterno Valley fault system. The geological map and section of the area are shown in Figure 5.

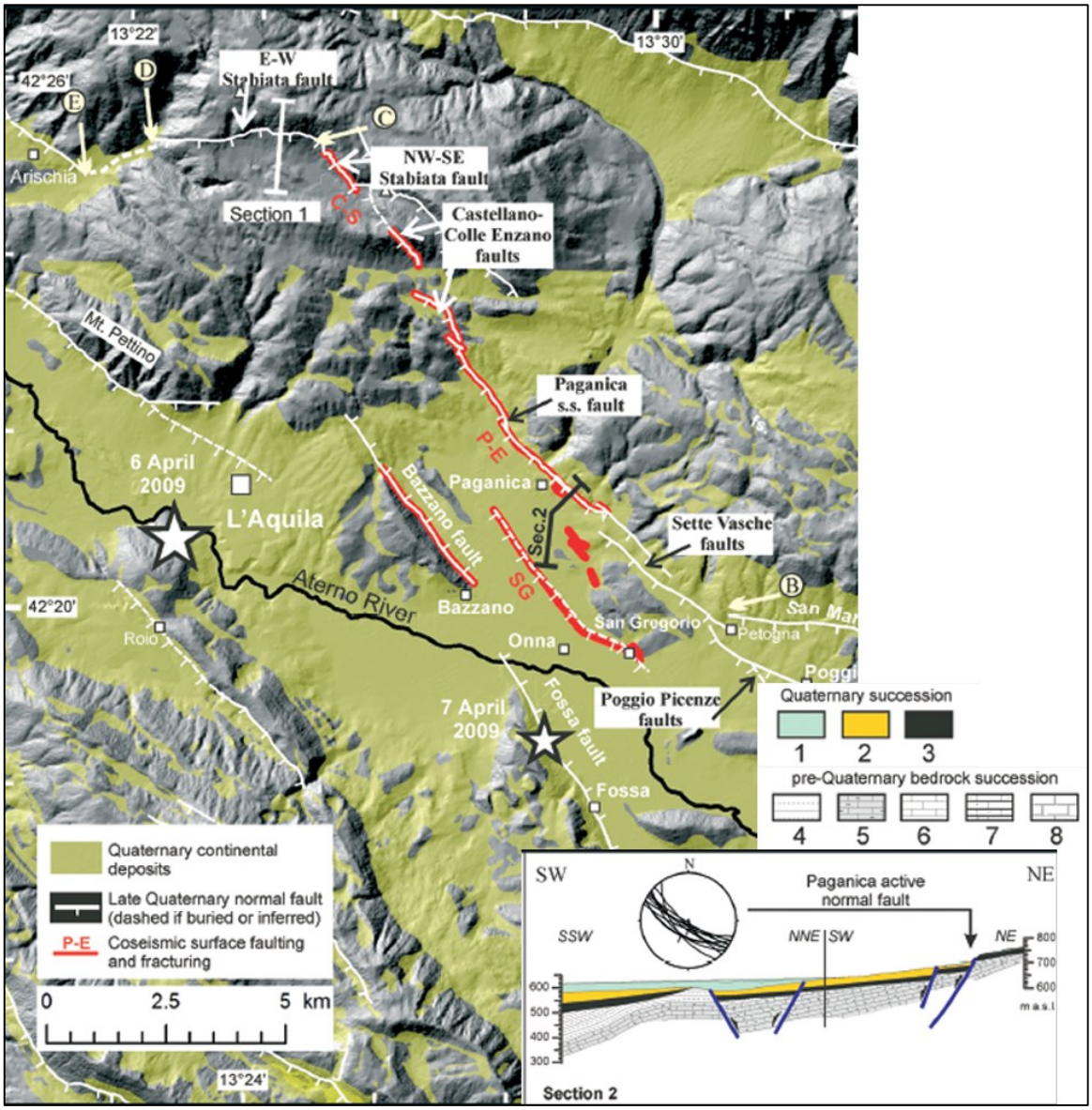

Fig. 5 *Geological map of the Paganica area. Below is shown the geological sections across the Paganica fault zones; 1) to 3): continental deposits of Late Pleistocene-Holocene (1), Middle Pleistocene (2) and Early Pleistocene (3) age; 4) Marne with Cerrogna and Marne a Orbulina fms (Langhian-Tortonian); 5) Bisciaro and Scaglia Cinerea fms (Oligocene-Aquitanian); 6) Scaglia detritica fm (Cenomanian-Late Eocene); 7) Marne a Fucoidi fm (Aptian-Cenomanian); 8) Maiolica fm (Late Titonian-Barremian) (modified after Lavecchia et al., 2014).*

Mt. Vettore – Mt. Bove

On August 24th, 2016, the M_w 6.0 Amatrice earthquake started a seismic sequence in central Apennines that lasted for months (and it is still ongoing), causing numerous casualties and infrastructure damage (Galli et al., 2016).

The sequence included three mainshocks: the M_w 6.0 Amatrice earthquake, the M_w 6.1 event that occurred on October 26th 2016 and the M_w 6.5 Norcia earthquake that occurred on October 30th, 2016. The M_w 6.5 earthquake is the largest event that struck Italy since the 1980 M_w 6.9 Irpinia earthquake.

These mainshocks have been accompanied by more than sixty thousand aftershocks-foreshocks including five earthquakes with $5.4< M_w <5.9$ (Chiaraluce et al., 2017). The three mainshocks (M_w 6.1, 6.0 and 6.5) occurred at depths of between ~7 and ~9 km along the Mt. Vettore Fault System (MVFS; Lavecchia et al., 2017; Mildon et al., 2017; Tinti et al., 2016), which cut through the heterogeneous marl and clay carbonate sedimentary succession of central Apennines.

Focal mechanisms of the three main events show a normal faulting plane 50° SW dipping and striking N150°. Such a main plane is interconnected at shallower depths with a set of synthetic and antithetic splays of different dimensions located both on the main fault's footwall and hanging wall. It is worth noting that the entire fault system is constrained at about 7–8 km of depth by a 2–3-km-thick layer gently dipping to the east activated during the 2016-17 seismic sequence (Chiaraluce et al., 2017). The seismic sequence was confined within the upper 10–12 km of the crust and the volume affected by the aftershocks extends for about 80 km, with NW–SE and NE–SW directions between the towns of Camerino to the north and Pizzoli to the south. The distribution of seismicity also suggests the activation of an antithetic NE-dipping extensional fault below the Norcia basin.

The main active tectonic structures in the area affected by the 2016-2017 seismic sequence are the Mt. Vettore – Mt. Bove (VBFS), the Laga Mountains (also known as Mt. Gorzano fault), the Norcia and the Montereale fault systems (see Fig. 4). The sequence occurred in the seismic gap between the 1997–98 Colfiorito seismic sequence (M_w 5.4 and M_w 5.9 earthquakes; Fig. 6) and the 2009 L'Aquila earthquake (M_w 6.3). It was generated by Mt. Vettore – Mt. Bove fault system (between Colfiorito and Campotosto areas) that represents the easternmost active extensional fault zones of the southern Umbro-Marchean Apennine ridge, characterized by normal to transtensive behavior (Pizzi et al., 2002).

The historical seismicity correlated with the most external fault system of the Umbria-Marche-Abruzzi Apennine ridge is characterized by absence of strong energy- seismicity along the Mt. Bove

- Mt. Vettore - Vettoretto sector, suggesting that the fault system was “silent” until the 2016 seismic sequence (Galadini and Galli, 2000); with the only exception of the Amatrice area in the hanging wall of the northern Mt. Gorzano fault, which was struck by the October 1639 earthquake (M_w 5.9) (Rovida et al., 2016). This event heavily damaged Amatrice and the surrounding villages. Galli et al. (2016) suggest that the 1639 earthquake might be a twin of the 2016 M_w 6 event, rupturing the same southern fault strand. In pre-historical times, these faults were all seismogenic. Before 2016 earthquakes, paleoseismological surveys show that recurrence intervals for M_w= 6 events are always greater than 1000 years and sometimes greater than 2000 years (Galadini and Galli, 2003; Galli et al., 2008). The combined analysis of paleoseismological data and long-term seismicity shows that activation of the faults could generate earthquakes of M_w = 6.5–7.0. The extension rate ranges between 0.7 and 1.6 mm/yr (Galadini and Galli, 2000; Emergeo Working Group, 2016).

Coseismic ruptures were observed along several fault planes belonging to the main fault system, both on synthetic and antithetic splays (Fig. 7; Pucci et al., 2017). The average strike is N155°, mainly the SW side down, in very good agreement with long-term surface expression of the VBFS. The large-scale deformation zone of the VBFS at the surface ranges from 70 to 3000 m in width (distance between fault splays), while the width of each displacement zone (single fault splay) ranges from 3 to 60 m (distance between overlapping or en-echelon ruptures). The average vertical offset is 0.5 m even though some coseismic ruptures display throw > 1 m, with maxima of ~2.0 m along the so-called Cordone del Vettore fault scarp (Civico et al., 2017). The structural pattern and kinematics of the observed coseismic effects appear to be independent from morphology and lithology, affecting both bedrock and different bodies of unconsolidated deposits.

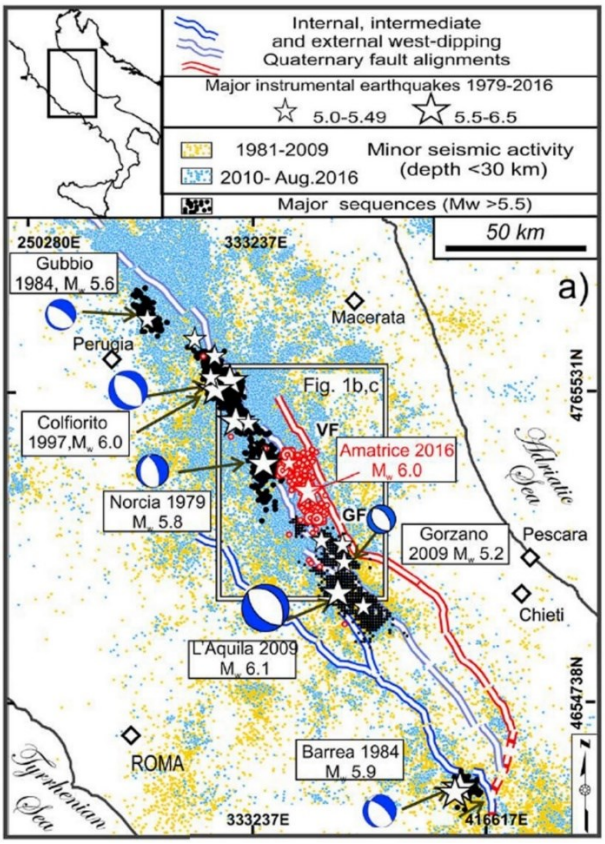

Fig.6 *Background seismicity of the Paganica and Mt. Vettore – Mt. Bove areas since 1981, with major instrumental sequences and active fault alignments (modified after Lavecchia et al., 2012).*

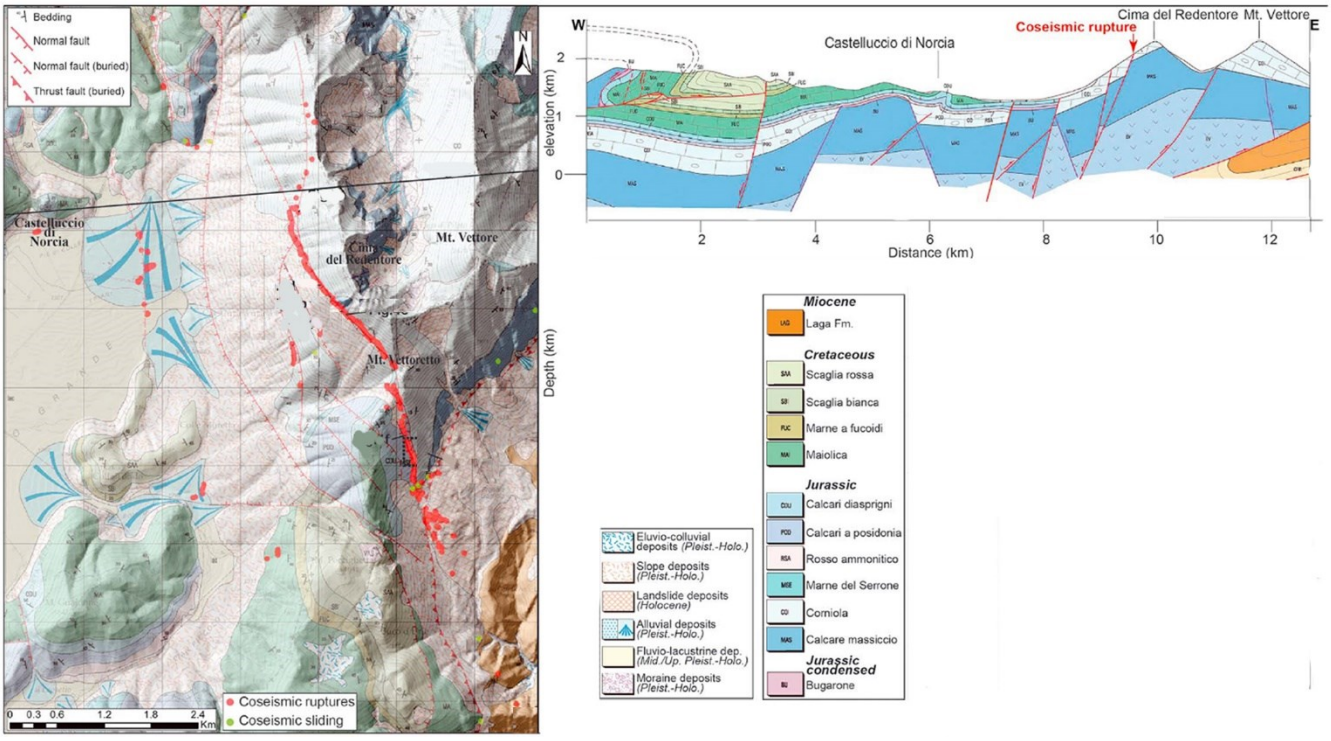

Fig. 7 *Distribution of the coseismic geological effects collected in the Mount Vettore area (Pucci et al., 2017). On the right, geological cross section (modified after Pierantoni et al., 2013).*

Mt. Massico (Campania region)

The Massico Mount is a NE–SW trending carbonate horst that separates the two NW–SE Garigliano and Volturno depressions, above the Campanian-Latial margin of the Tyrrhenian basin (Fig. 8).

Since the early Pliocene, the Tyrrhenian basin extended progressively to the East, involving the internal sector of the orogenic wedge and causing the formation of coastal grabens (peri-Tyrrhenian basins) along the western flank of the chain. The main fault pattern of this margin is characterized by high-angle NE–SW and NW–SE trending structures that formed different sedimentary basins (Volturno, Garigliano, Fondi, and Pontina plains). Moreover, E–W, N–S and NNW–SSE oriented faults systems have contributed to the recent collapse of the plains with a vertical subsidence rate of about 2 mm/y during Quaternary (Brancaccio et al., 1991; Cinque et al., 2000). Remarkable volcanic activity that occurred mainly along the western margin of the Campanian plain, originating the Roccamonfina, Campi Flegrei, Ischia, Procida and Somma-Vesuvius districts, was an important consequence of the Quaternary extension.

The northern sector of the Mount Massico is wedged under the Roccamonfina deposits. From NE toward SW, Mt. Massico consists of Trias dolomitic units that change to Jurassic-Cretaceous limestone and then to heterogeneous clay Miocene units (Fig. 8; Billi et al., 1997).

Geological and geophysical studies on land show that the Massico area is well-defined by NE–SW, N–S and NW–SE normal faults, which dislocate the massif with down-thrown blocks along normal faults in different directions: NW direction to the Garigliano plain, SE direction towards the Volturno plain, and SW in the direction of the coastal plain (Billi et al., 1997; Bruno et al., 2000). Few hundred metres of fault displacement (slip rates: 2–2.5 from 1.45 Ma to present, and 0.2–0.5 from 36 ka to present; Cinque et al., 2000) put the quaternary deposits of the plain in contact with the carbonatic and silico-clastic deposits of Mt. Massico.

Geochemical studies reveal a large depth of the faults bordering the Mt. Massico. In both sides of Mt. Massico, it was found the presence of ^{3}He, a primary gas mantle, arising along deep fault systems (Amoresano et al., 2015; Corniello et al., 2015). Moreover, the geochemical characteristics of springs along the southern side of Mt. Massico are similar to that measured in the Phlegrean Fields district (Cuoco et al., 2017; Tedesco, 1997), suggesting the sharing of a common Campanian mantle source. On the other side, gas samples collected on the northern fault of Mt. Massico show a ^{3}He R/Ra ratios similar to the northern Latial volcanism (Cuoco et al., 2017; Barberi et al., 2007; Chiodini et al., 2007), suggesting a common Latial mantle origin.

Evidence of buried fault systems on land (Billi et al., 1997) and offshore (Bruno et al., 2000; Torrente et al., 2010; Milia and Torrente, 2011) in the Gaeta and Naples Gulfs, have been identified by seismic profiles. The interpretation of offshore seismic reflection data (Bruno et al., 2000) shows that the in-land southern NE–SW striking fault delimiting the Massico horst propagates off-shore and is translated south-eastward. This horizontal dislocation of Mt. Massico suggests left lateral movements for the ESE–WNW to E–W faults. These faults, which are located on the maximum gradient of the E–W elongated magnetic alignment of 41PL (Bruno et al., 2000), are responsible for the S-SE translation of the offshore sector of the Mt. Massico horst. The NE–SW faults that affect the southern side of the Mt. Massico horst represent the southern tip of the ORL (Ortona–Roccamonfina Line) and show seismic features consistent with normal movements (Bruno et al., 2000; de Alteriis et al., 2006).

The seismicity of the Campanian plain, including Mt. Massico, is characterized by few earthquakes with energy (M_w maximum = 4.8) lower than that of the Apennine chain. The southern Apennines seismicity is concentrated mostly along the NW–SE striking normal faults of the backbone in the shallower 15–20 km of the crust, with destructive events (I_o = X–XI MCS; Rovida et al., 2016). The Massico area presents minor seismicity, characterized by swarms and moderate energy earthquakes (M_w<5.5), occurring along the NE–SW structures, such as for the ORL bordering the north-western margin of the Campanian plain and on NW–SE carbonate massifs bordering the plain. Small segments of the ORL are seismically active and move in response to both the NE–SW regional extension of Southern Apennines, and to the NW–SE longitudinal extension (Oldow et al., 1993; Milano et al., 2008).

The low slip rate and low level of seismicity of the faults bordering the Massico horst suggests that these faults were capable (Michetti et al., 2005; Wilkinson et al., 2017) with significant potential for generate earthquake of M_w greater than 6.5 earthquakes. Today, these faults are characterized by small magnitude earthquakes and hydrothermal activity, but are no more capable.

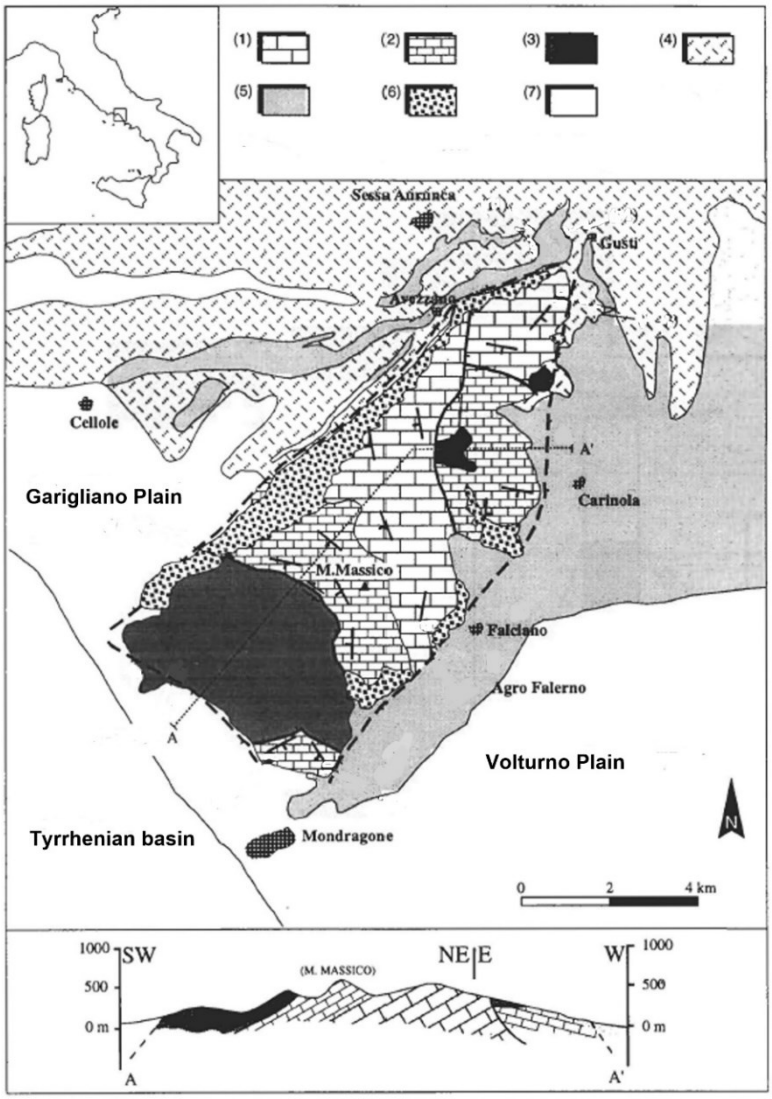

Fig.8 *Geo-structural sketch of Mount Massico; 1) limestone and dolomites of the carbonate platform facies (upper Trias-Jurassic); 2) limestone and dolomites of the carbonate platform facies (Cretaceous-lower Miocene); 3) terrigeneous deposits (Miocene); 4) pyroclastic deposits of Roccamonfina volcano (upper Pleistocene); 5) pyroclastic deposits of the Phlegraean Fields (upper Pleistocene); 6) loose or mildly cemente debris deposit and alluvial fans (Holocene); 7) continental transitional deposits and fine-grained sand of present beach and mobile dune (Holocene); AA' trace of the geologic cross-section shown in the lower part of the figure (modified after Billi et al., 1997).*

2.2 San Giuliano di Puglia (Molise region)

On October 31, 2002, at 10:32 UT, a strong earthquake of M_w= 5.7 (M_l= 5.4) struck the Molise region in southern Italy, followed by a similar magnitude on November 1. The earthquake caused the collapse of a school building, with 28 casualties and major damages in hundreds of private buildings. The area struck by the 2002 Molise seismic sequence falls between the Apennines axial zone and the Apulia-Gargano foreland, both corresponding to well-identified seismogenic zones (Fig. 9; Chiarabba et al., 2005). This sequence occurred in a region where, based on historical and instrumental seismicity, no comparable earthquakes occurred in the last 1000 years. Nevertheless, the area is surrounded by high-level seismicity zones.

The CPTI15 catalogue (Rovida et al.,2016) reports only a few large earthquakes in the surrounding areas: the 1125 earthquake in the immediate vicinity of the present sequence. Little is known about this event, that might have reached I_{max} VIII-IX: the Apenninic sequence of December 1456, which caused heavy damages and reached MCS intensity I_{max} XI; the Gargano sequence of the summer of 1627, which also caused damages, assessed as I_{max} X; the July 1805, Matese earthquake, which produced effects up to I_{max} X.

The main neighboring seismogenetic structures are: Gargano (60–100 km at East), San Severo (30–40 km at East), Foggiano (50–80 km at South-East), Beneventano - Irpinia (40–80 km at South) and the Bojano basin (40–50 km at west). All these faults have generated earthquakes of high magnitude (M_S = 6.5 – 7) and have damaged the eastern part of Molise (Galli and Molin, 2002).

Focal depths and mechanisms of the Molise sequence aftershocks show different characteristics from the seismicity located within the southern Apennine chain. The seismicity in the southern Apennine is focused in the shallowest 10-15 km of depth along normal faults, NW-SE striking. The 2002 Molise sequence, nucleating at a depth between 10 and 24 km, appears to be confined to the lower parts of the crust. All focal solutions show nearly pure strike-slip mechanisms with tensional axes oriented NE-SW, roughly parallel to those of the normal faulting events in southern Apennines (Pondrelli et al., 2002).

The aftershocks alignment suggests that the rupture occurred on a EW plane of focal solution, with a dextral fault motion (Fig. 10; Pondrelli et al., 2002). Purely strike-slip focal mechanisms are uncommon for relatively large events in the Italian peninsula, especially along the Apennines. The Molise sequence shows some similarities with the last Apennine foredeep seismic sequence, occurred in May 5, 1990 near Potenza (M_w=5.8), southern Italy. The entire 1990 sequence was

characterized by 20 km-deep and strike-slip events (Di Luccio et al., 2005). Both sequences occurred in the foredeep rather than within the Apennines chain. The only known active structure in the area with similar kinematics is the Mattinata fault located in the Gargano Promontory, east of the region hit by the seismic sequence. Following Di Bucci and Mazzoli (2003), the 2002 Molise seismic sequence suggests that Mattinata fault system (the important zone of dextral wrench faulting across the Adriatic–Gargano foreland area) may extend westward, beneath the allochthonous units that form the foothills of the Apennine chain in Molise. Moreover, the authors propose that this (buried) transcurrent structure within the Adria plate plays a major control on the seismotectonic behavior of the epicentral area of the 2002 Molise seismic sequence.

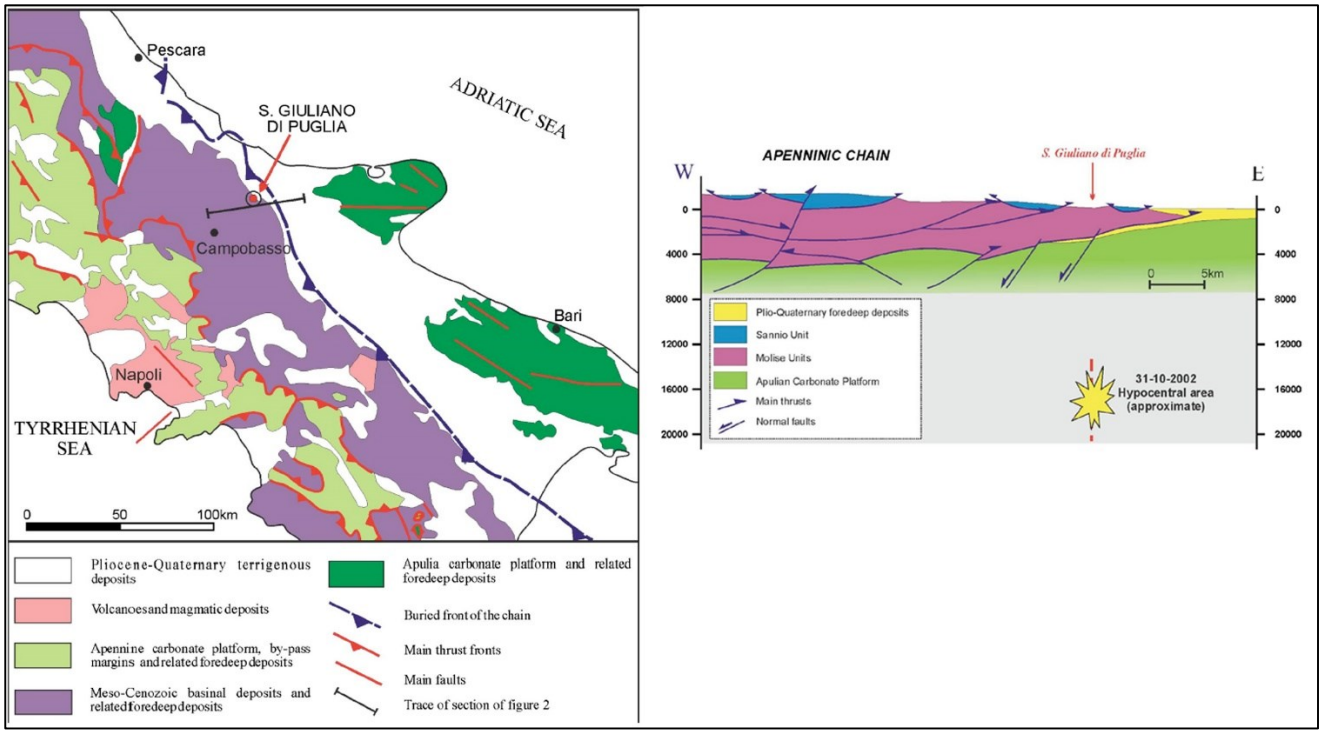

Fig. 9 *Geological sketch of the Southern Apennines with the trace of the geological section shown on the right (modified after Casciello et al., 2004).*

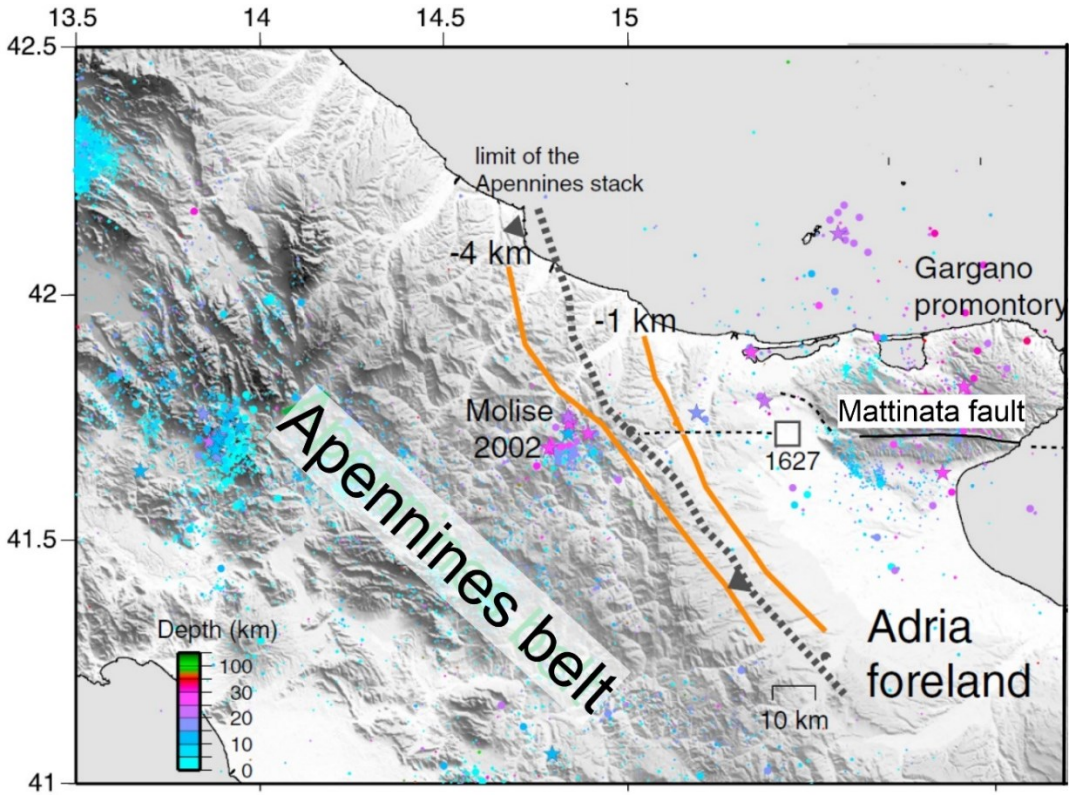

Fig. 10 *Map of the San Giuliano di Puglia area. Colored dots: hypocenters of past years seismicity; dashed line: limit of the Apennines stack at depth; orange lines: depth of the Apulian carbonate platform westward dipping below the Apennines belt. The approximate epicenter of the 1627 A.D., M 6.7 earthquake is shown (modified after Chiarabba et al., 2014).*

3 Integration of three database

The analysis of structural, seismological and gravimetric data consisted in the creation of databases in which the data, extracted from literature and the available catalogues, are merged together in GIS environment. Then, the different types of data have been compared to check the correlation between seismicity, faults and gravimetric lineaments. This allowed identifying the possible active faults and picking up the more interesting structures to be studied through a 2D analysis.

3.1 Structural database

The faults from the different catalogues (Ithaca catalogue, maps from CARG project and the Neotectonic Map of Italy) are vectorialized in an ad-hoc dataset. For each area, the fault dataset is obtained using different maps and scientific works and is correlated with a table of attributes containing important information about each structure, such as:

- ID number: a number to identify the fault in a specific catalogue;
- Age: the age of the activity of the fault, when the information is available;
- Name: some faults are named using the toponym of the nearest city;

- Geographic coordinates: latitude and longitude of the beginning and the end of the fault segment;
- Direction: the direction of a line created by the intersection of the fault plane and a horizontal surface relative to North;
- Dip: the angle between the fault and a horizontal plane;
- Length: linear extension of the fault segment.

For each area, the fault dataset is obtained using different maps and scientific works. The attribute tables, attached at the end of the thesis, is important to understand the faults' structure and the possibile correlation with the other database.

3.1.1 Paganica and Mt. Vettore – Mt. Bove areas

The structural database of the Paganica and Mt. Vettore – Mt. Bove areas (Fig. 11a, b, respectively) contains faults extracted from:

- Ithaca Catalogue, containing the capable faults in Italy whose characteristics are derived from scientific works (red lineaments in the Fig. 11a);
- EMERGEO Working Group catalogue (2016), containing structural lineaments derived from coesismic effects investigation (red lineaments in the Fig. 11b);
- Neotectonic Map of Italy with scale 1:500.000 published by Ambrosetti et al. (1987) containing the active faults in the last million years (blue lineaments in Fig. 11a, b). This map has been first vectorialized and then plotted above the shaded relief of the topography of the study areas;
- Geological Cartography of Italy with scale 1:50.000 from *Servizio geologico d'Italia* and CARG project, available at the web site: http://www.isprambiente.gov.it/ . The cartography is available only for the Paganica area (purple lineaments in the Fig. 11a);
- Faults from paleoseismological analyses (Galadini and Galli, 2003; yellow lineaments in the Fig. 11a, b).

An attribute table (shown at the end of the thesis) accompanies the datasets containing, for each fault, important information about the type of the fault, its age and dip and some notes specifying, i.e., if the fault is supposed.

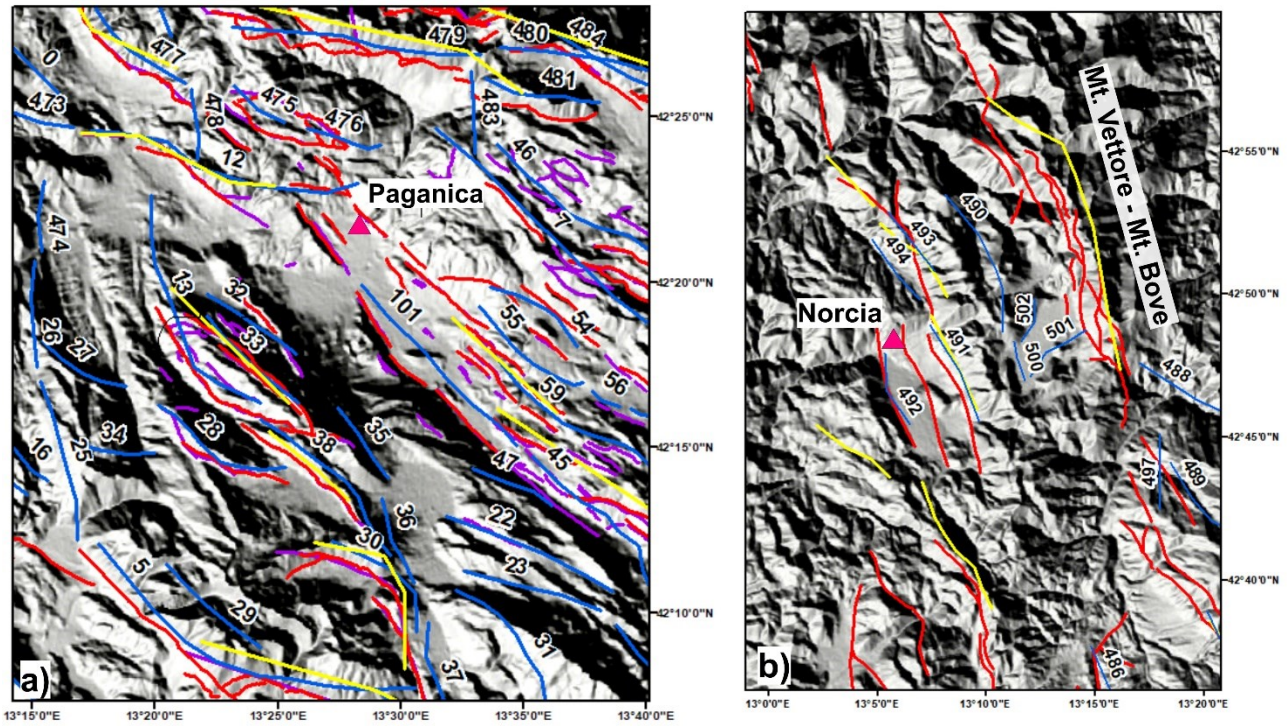

Fig. 11 *Structural database for: a) the Paganica area; b) the Mt. Vettore – Mt. Bove area. Red lines: faults extracted from ITHACA catalogue (in sub-plot a)) and EMERGEO W.G catalogue (in sub-plot b)); blue lines: faults extracted from the Neotectonic map of Italy (Ambrosetti et al., 1987); purple lines: faults extracted from CARG project; yellow lines: faults extracted from Galadini and Galli (2003). The location of the Paganica and Norcia towns is shown with a pink triangle. The attribute tables for Paganica and Mt. Vettore – Mt. Bove faults are shown in* ***Table 1*** *and* ***2,*** *respectively.*

3.1.2 Mt. Massico area

The structural database of the Mt. Massico area (Fig. 12) contains faults extracted from:

- Ithaca Catalogue (Red lineaments in Fig. 12);
- Neotectonic Map of Italy in scale 1:500.000 (Ambrosetti et al., 1987; blue lineaments in the Fig. 12);
- *Carta delle faglie tardo-quaternarie dell'Appennino meridionale* by Cinque et al. (2000) that contains the recently active quaternary faults (white lineaments in the Fig. 12).

I have also consulted some geological maps and scientific papers:

- *Carta Geologica dell'Appennino Meridionale* with scale 1:250.000 (Bonardi et al., 1988);
- Structural Map of Italy with scale 1:500.000 (Bigi et al., 1983);
- Scientific paper of De Rita and Giordano (1996).

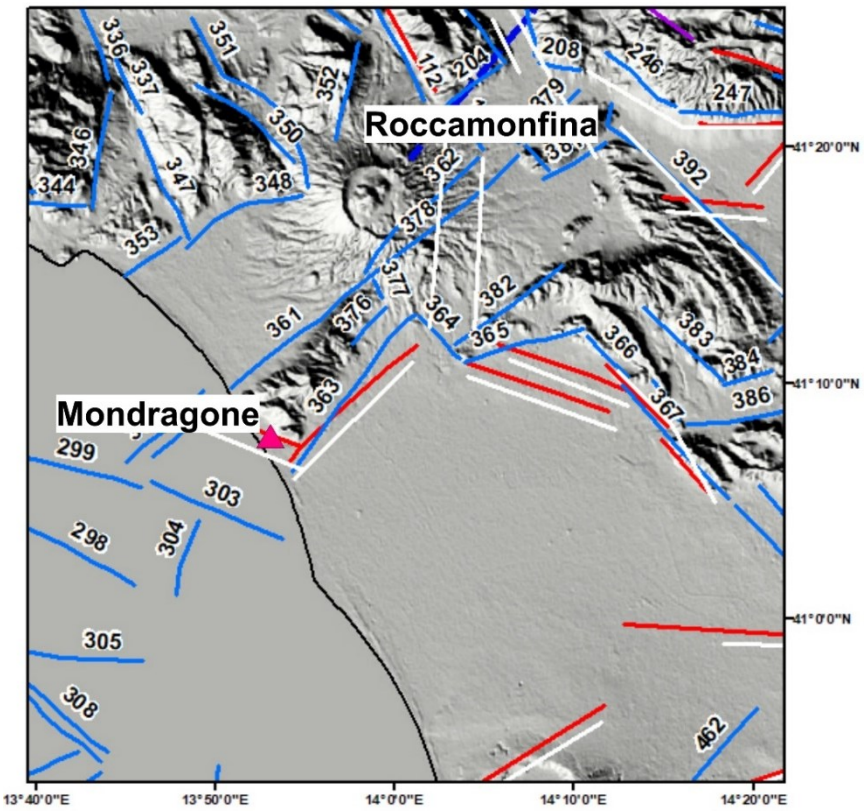

Fig. 12 *Structural database of the Mt. Massico area. Red lines: faults extracted from ITHACA catalogue; blue lines: faults extracted from the Neotectonic map of Italy (Ambrosetti et al., 1987); white lines: faults extracted from Cinque et al. (2000). The location of the Mondragone town is shown with a pink triangle. The attribute table is shown in* ***Table 3****.*

3.1.3 San Giuliano di Puglia area

The structural database of San Giuliano di Puglia (Fig. 13) contains faults extracted from:

- Ithaca Catalogue (Red lineaments in Fig. 13);
- Neotectonic Map of Italy with scale 1:500.000 (Ambrosetti et al., 1987; blue lineaments in Fig. 13);
- Geological-Structural Map of the Central-Southern Apennines in scale 1:250.000 (Vezzani et al., 2010) that is the final product of a long-term project focused on regional and structural geology of Italian Apennines. It contains the outcropping faults (green lineaments in Fig. 13) and the buried ones (orange lineaments in Fig. 13).
- *Carta delle faglie tardo-quaternarie dell'Appennino meridionale* by Cinque et al. (2000) that contains the recently active quaternary faults (white lineaments in the Fig. 13).

I have also considered the faults reported in scientific papers of Di Bucci and Mazzoli (2003), Mucciarelli et al. (2009) and Puglia et al. (2013).

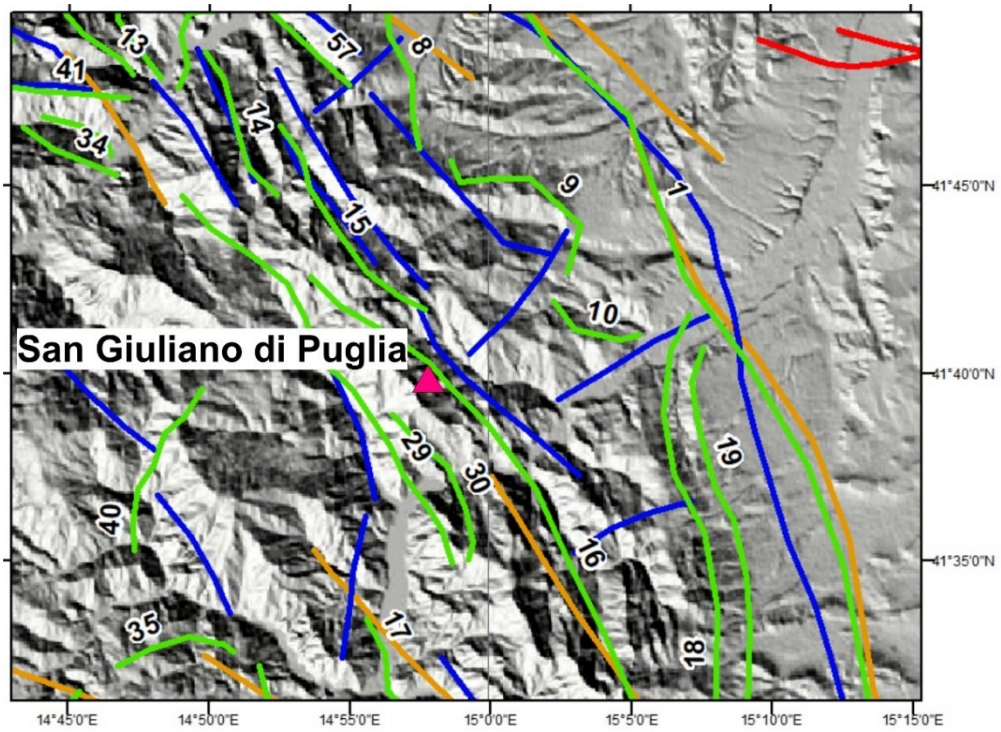

Fig. 13 *Structural database of the San Giuliano di Puglia area. Red lines: faults extracted from ITHACA catalogue; blue lines: faults extracted from the Neotectonic map of Italy (Ambrosetti et al., 1987); white lines: faults extracted from scientific work of Cinque et al. (2000); green and orange lines: structural and buried faults from Vezzani et al. (2000). The location of the San Giuliano town is shown with a pink triangle. The attribute table is shown in* ***Table 4.***

3.2 Seismological database

The seismological database contains the instrumental and historical earthquakes extracted from the available catalogues available on-line. For all the study areas, the historical earthquakes are extracted from the *Catalogo Parametrico dei Terremoti Italiani* (CPTI15 version; Rovida et al., 2016) that contains the seismological parameters (hypocentral location, intensity and the equivalent magnitude) of the historical earthquakes from year 1000 A.C. to 2015 A.C. In this thesis, I have considered the historical events until 1990. After this year, I have considered the instrumental earthquakes. The database of instrumental earthquakes is different for each study areas, even though the first step consisted in the extraction of the instrumental earthquakes from the ISIDe catalogue (Italian Seismic Instrumental and parametric Data-basE) that provides earthquake parameters since 1990 A.C. obtained by integrating locations performed in near-real time with data from the Italian Seismic Bulletin. ISIDe data contains the earthquakes detected by the Italian National Seismic Network and reviewed by INGV seismologists. For the Paganica, Mt. Vettore – Mt.

Bove and San Giuliano di Puglia areas, I have used the re-localized earthquakes provided by Chiaraluce et al. (2011) Michele et al. (2016) and Chiarabba et al. (2014), respectively.

3.2.1 Paganica and Mt. Vettore – Mt. Bove areas

The seismological database of the Paganica area contains the relocated earthquakes provided by Chiaraluce et al. (2011). The earthquakes have been recorded by the permanent Stations of the National Seismic Network (RSNC) managed by the Istituto Nazionale di Geofisica e Vulcanologia (INGV) until April 6, and then by stations of the INGV temporary network, available a few hours after the L'Aquila main shock. For two months after April 2009, Chiaraluce et al. (2011) used also a temporary network installed by the *Laboratoire de Géophysique Interne et Tectonophysique* (LGIT) of Grenoble. The smooth gradient velocity model (Fig. 14a) consists of a V_p velocity that increases linearly from V_0 (5.0 km/s) at the surface by 0.15 km/s per kilometre until the half space is reached at a depth of 10 km. The velocity within the half space is 6.51 km/s. The V_p/V_s ratio, for the foreshocks, is 1.90 and was determined by using a cumulative Wadati diagram (Chiaraluce et al., 2011). Chiaraluce et al. (2011) considered 2643 aftershocks with $M_l \geq 1.9$ and their waveforms were cut 50s and 120s before and after the origin time of the event, respectively. This led to have relocalization values with RMS (root mean square of the travel time residuals) < 0.2 s, ERH and ERZ (error of the horizontal and vertical components) < 1 km, Gap (azimuthal coverage of the stations around the event) < 200° and more than 8 P- and 4 S-readings. The events are plotted above the topography of the area (Fig. 14b), along with the historical earthquakes from CPTI15.

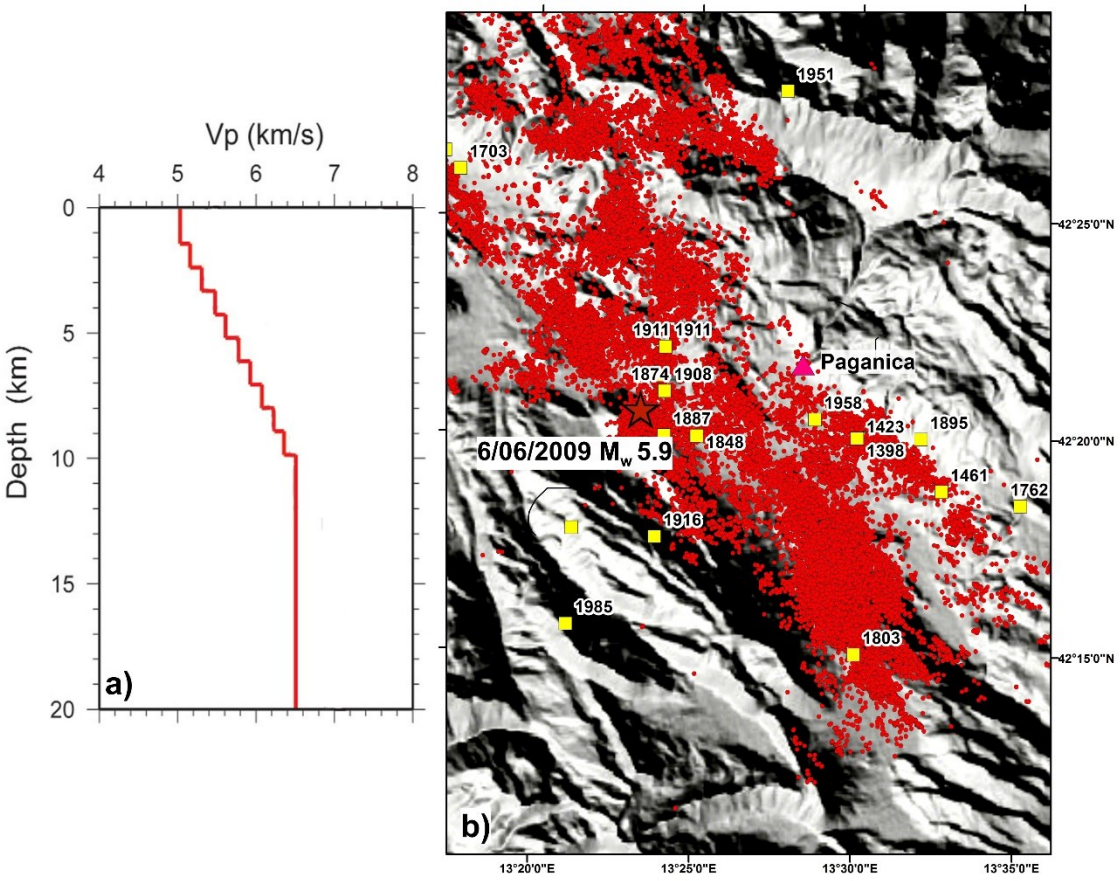

Fig. 14 *The seismological database of the Paganica area;* ***a)*** *Smooth gradient 1D velocity model used by Chiaraluce et al. (2011) for relocalization of the Paganica aftershocks (modified after Chiaraluce et al., 2011);* ***b)*** *red dots: relocated events; yellow squares: historical seismicity from CPTI15 (Rovida et al., 2016). The location of the Paganica town is shown with a pink triangle; red star: main shock of the 2009 seismic sequence.*

The seismological database of Mt. Vettore – Mt. Bove contains relocated earthquakes provided by Michele et al. (2016). The 8.340 earthquakes of the database were recorded by the National Seismic Network (RSN, INGV), the National Accelerometric Network (RAN, Civil Protection Department) and by 12 additional stations installed soon after the main shock (SISMIKO Team, 2016). Michele et al. (2016) used a 1D velocity model interpolated from the 1D velocity model of De Luca et al. (2009), in order to avoid seismicity scattering where velocity discontinuities were present (Fig. 15a). They reduced the errors using 143.825 P and 116.824 S arrival times. The V_p/V_s ratio was fixed to 1.85 using the Wadati method (1931). These arrangements led to have relocalization values with RMS ≤ 0.5 s, ERH ≤ 1.5 km, ERZ ≤ 2.0 km, Gap ≤ 180°. The events are plotted above the area's topography (Fig. 15b).

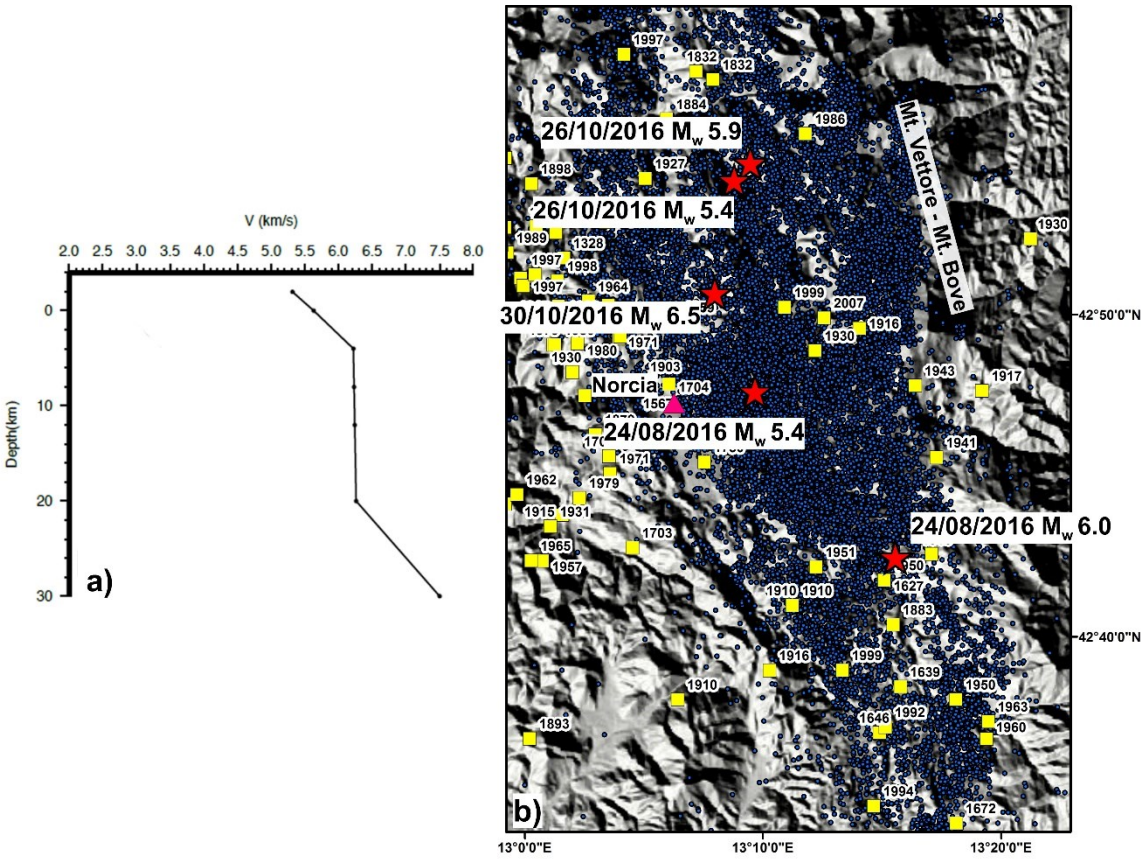

Fig. 15 *The seismological database of the Mt. Vettore – Mt. Bove area;* ***a)*** *Gradient 1D velocity model used by Michele et al. (2016) for relocalization of the Amatrice sequence (modified after Michele et al., 2016);* ***b)*** *dark blue dots: relocated events; yellow squares: historical seismicity from CPTI15 (Rovida et al., 2016). The location of the Norcia town is shown with a pink triangle; red stars: the strongest events of the 2016 seismic sequence.*

3.2.2 Mt. **Massico** area

The seismological database of Mt. Massico area contains earthquakes extracted from ISIDe catalogue and 70 events relocated with the aim of improving the quality of the focal parameters (latitude, longitude and depth).

I extracted the waveforms from the "Plinio" catalogue, from the OV - INGV website (http://sismolab.ov.ingv.it/sismo/index.php?PAGE=SISMO/last&area=Vesuvio&rmenu=on). The choice of the events to re-localize is based on some consideration:

a) Improving the location quality with a more accurate waveform analysis;
b) Increasing the number of the seismic phases for each earthquake to lower the value of RMS (the root-mean-square of the travel time residuals), ERH (error in the horizontal location) and ERZ (error in the depth location).

The work was performed in these phases:

a) Extraction of the waveform of the 70 seismic events from the "Plinio" catalogue since 2000;
b) Analysis of the seismic waveform by WinPick software (Scarpato et al., 2004);
c) Hypocentral location by Hypo71 software (Lee and Lahr, 1975) with the use of different V_p/V_s ratio and velocity models;
d) Creation of a new "earthquake dataset" containing the relocated hypocentral parameters.

I have first used the 2D velocity model of INGV – Osservatorio Vesuviano for the Campanian area with V_p/V_s = 1.73 and depth estimates = 10 km.

With this model, the re-localization highlighted low values of RMS (from 0.1 to 1.83) and ERH (from 1 to 9 km) but high values of ERZ up to 979 km. Thus, I made another re-localization using the same velocity model with fixed depth values = 10 km and V_p/V_s = 1.8. This model provided good values of RMS but very high values of ERH and ERZ.

Finally, I have applied another velocity model (Gaudiosi et al., 2010) obtained from the analysis of active seismic data (profile DSS and WARR) and passive seismic profiles (telesesmic receiver functions) that provides a V_p/V_s = 1.8 and a velocity gradient increasing with depth (Tab. 5).

The obtained results showed a high quality of the re-localization, especially for the events between the years 2006 and 2008 in which the ERH and ERZ values are less than 2.5 km and RMS values less than 0.5 s.

In Figure 16, the relocated events are plotted above the shaded relief of the topography of the area. In next section, I will use both the relocated events and those non-relocated extracted from the ISIDe catalogue for a more detailed analysis along hypocentral sections.

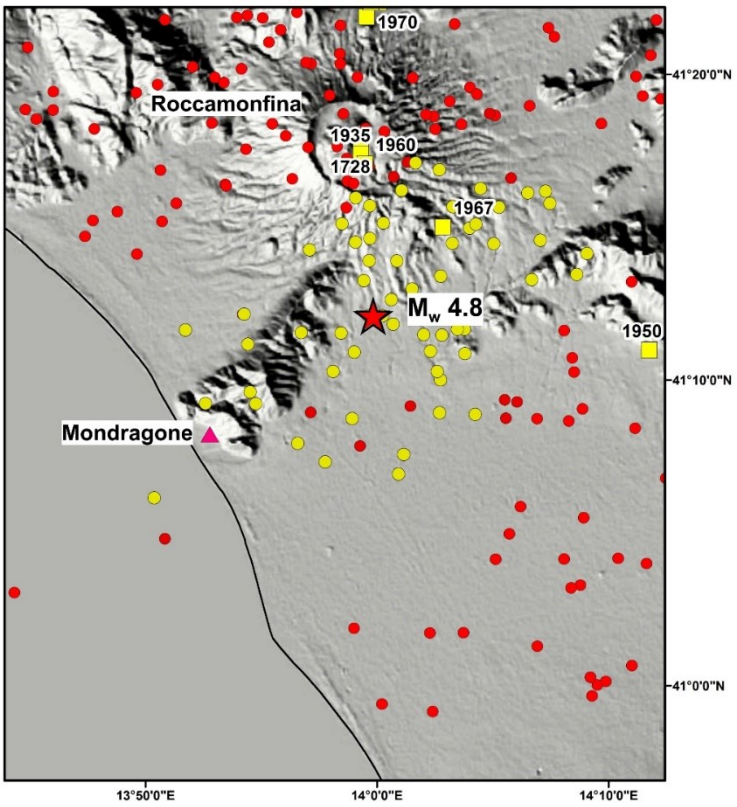

Fig. 16 *The seismological database of the Mt. Massico area. Yellow dots: relocated events with the velocity model extracted from Gaudiosi et al., (2010); yellow squares: historical seismicity from CPTI15 (Rovida et al., 2016); red dots: not-relocated events from ISIDE catalogue. The location of the Mondragone town is shown with a pink triangle; red star: the strongest event in the Mt. Massico area extracted from the CPTI15 catalogue.*

3.2.3 San Giuliano di Puglia area

The seismological database of the San Giuliano di Puglia area contains 1332 earthquakes relocated by Chiarabba et al. (2014). 3D velocity models have been computed by inverting 1594 P and 14441 S arrival times recorded at 37 seismic stations and rejecting data with residual times greater than 0.3 s. Data pre-processing consisted in: band-pass filtering the seismograms between frequencies of 25 and 40 Hz, normalizing the traces with three-component trace equalization, and deleting the energies associated with the arrivals of the P and S direct waves. After these arrangements, the final RMS was 0.14s (Latorre et al., 2010) and the hypocentral errors in the 3D model was less than 0.5 km in x, y, and z on average (Chiarabba et al., 2014). Specifically, in the layers from 8 to 12 km depth, the P wave model shows a main low V_p anomaly located in the central part of the area, surrounded by positive anomalies with $6.0 < V_p < 6.4$ km/s (Fig. 17a). This is caused by the westward deepening of the Apulian carbonate platform (Mariotti and Doglioni, 2000). The geometry of the Adria platform, depressed in the central part of the model and with 4.9 km/s velocity contour, well matches with the top of the carbonate units defined by S-P converted wave analysis (for more

details, see Latorre et al., 2010). At greater depths, very high V_p anomalies (higher than 6.4 km/s and 7.0 km/s) are found in distinct positive spots that cluster close to the fault at depth. The V_p/V_s model shows positive anomalies in the central area along the east trending fault between 8 and 10–12 km and a change from negative to positive anomalies crossing the fault from north to south below 12 km of depth (Chiarabba et al., 2014). The seismological database is shown in Fig. 17b.

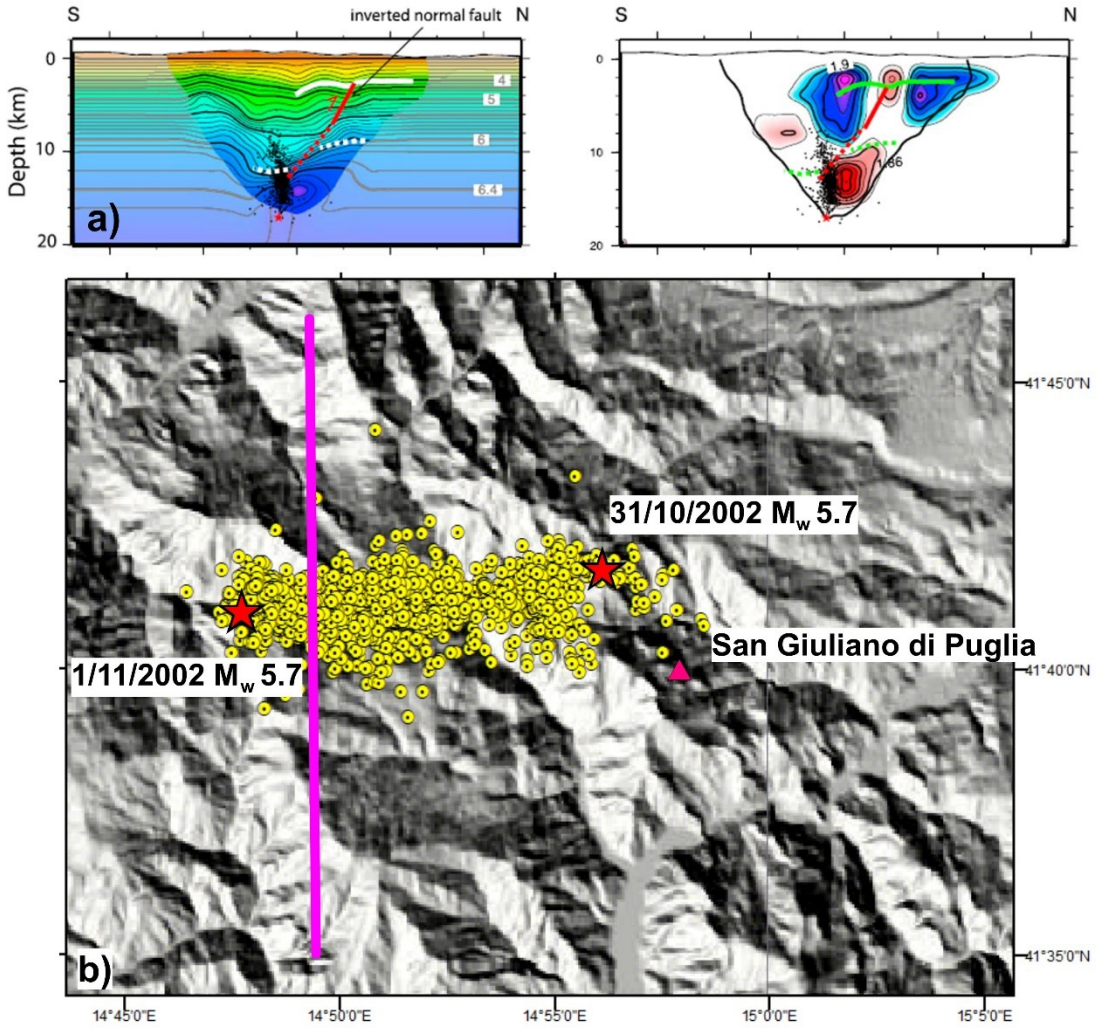

Fig. 17 *The seismological database of the San Giuliano di Puglia area;* ***a)*** *V_p and V_p/V_s model along a N-S profile (pink line in plot* ***b)*** *extracted and modified from Chiarabba et al. (2014). The white lines are the top (solid) or bottom (dashed) of the Apulian carbonate multilayer, from Latorre et al. (2010). Red lines represent some major faults visible in correspondence of velocity anomalies. Black solid dots: aftershocks; red stars: main shocks.* ***b)*** *yellow dots: relocated events provided by Chiarabba et al. (2014). The location of the San Giuliano town is shown with a pink triangle; red stars: main shocks. The pink line is the trace of the section shown in plot a.*

3.3 Gravimetric database

The use of gravimetric data is justified by the complexity of the geology in the Apennine chain where many sources related to different depths and extents are normally estimated to contribute the measured anomaly fields (Fedi et al., 2005). A classical problem of potential field interpretation arises from the fact that these single effects are merged together, and their identification and isolation is often difficult. In this study, the gravimetric data, with sampling rate of 1 km, are extracted from the *Bouguer Gravity Anomaly Map of Italy* published by CNR (Carrozzo et al., 1986). The input dataset has these characteristics:

- Density for the Bouguer correction: 2.4 g/cm^3;
- Normal gravity: U.G.G.I., (1984);
- Reference system: IGSN71.

The gravity anomaly field of central and southern Apennines (Fig. 18) shows the presence of negative and positive short-wavelength anomalies, together with regional ones, caused by density contrast of different lithologies (Fedi et al., 2005). The regional anomalies are represented by an elongated low running along the main axis of the Apennine chain and by an extended high, whose maxima is in the central area of the Tyrrhenian basin. In several cases, the anomalies coincide with carbonate units or basin structures (Fedi et al., 2005).

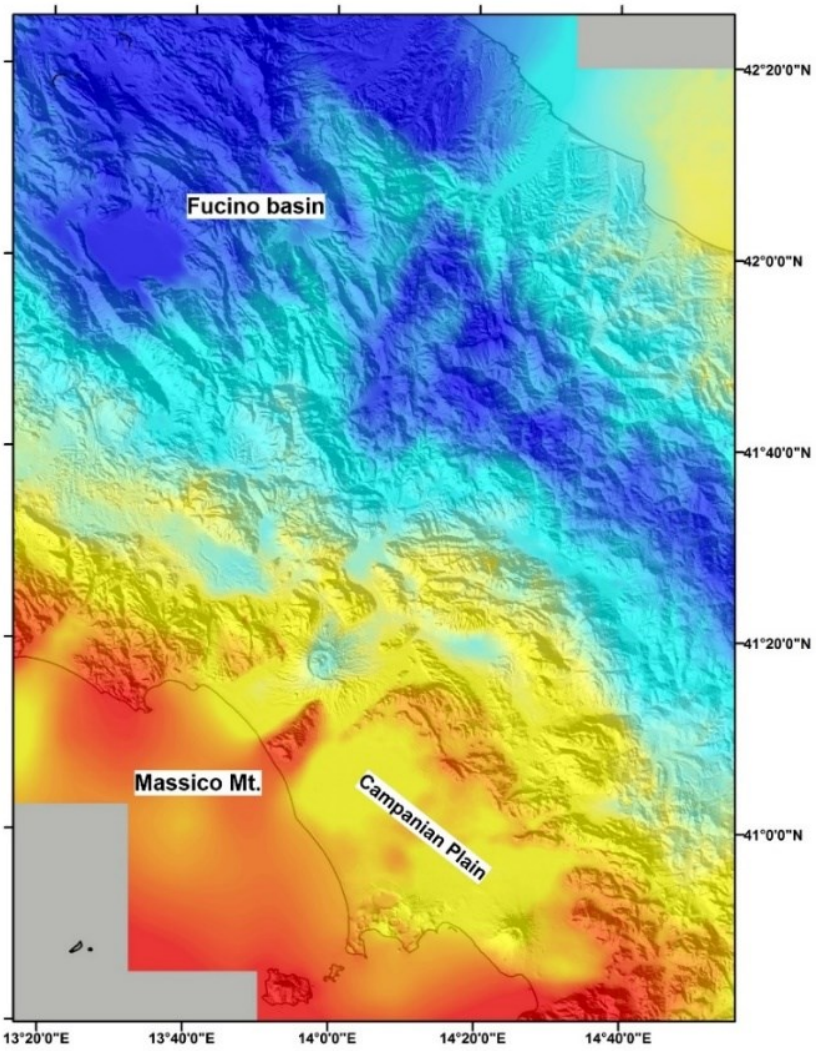

Fig. 18 *Sketch of the gravity anomaly field of the central and southern Apennines (modified after Fedi et al., 2005).*

In order to highlight the field contributions related to sources with different depth/extent, I have used the *Multiscale Derivative Analysis* (MDA; Fedi, 2002) of the Bouguer anomaly gravity field.

The *Multiscale Derivative Analysis* methods takes advantage from the variable resolution properties of EHD (*Enhanced Horizontal Derivative*; Fedi and Florio, 2001) that is formed by taking the horizontal derivative of a sum of vertical derivatives of increasing order (see eq. 1). The sum allows showing the structural features of the study areas and having a signal that is more complete and richer than any single term of the sum. The location of EHD maxima is used to outline the source boundaries. A key feature of MDA method is that it does not apply sharp component separation but enhances the contributions at different resolution that are present in the field.

According to Fedi and Florio (2001), the EHD is defined as:

$$\mathrm{EHD}(x,y)=\sqrt{\left(\frac{\partial \phi}{\partial x}\right)^2+\left(\frac{\partial \phi}{\partial y}\right)^2} \quad (1)$$

where:

$$\phi(x,y)=w_0 f(x,y)+w_1 f^{(1)}(x,y)+w_2 f^{(2)}(x,y)+\ldots+w_m f^{(m)}(x,y) \quad (2)$$

and

$f^{(1)}$, …, $f^{(m)}$ are the m-order derivatives and w_0…..w_m are the sets of weights.

The first term EHD_0, the last one EHD_m and the weights w_0. . .w_m of the equation (2) influence the flexibility of the EHD. The summation (2) starts with the scalar potential or any other term. Low order terms are affected by deeper sources or large-scale effects, whereas high order terms better represent small scale and shallow components. The last term EHD_m plays an important role about the resolution's details: the higher the order m, the better the sources' boundaries are defined. Finally, the set of weights w_m controls the influence of each summation term (Fedi and Florio, 2001). An accurate choice of the weights and the right combination of the different terms of the equation (2) allows enhancing the effects at scales from large to small, improving the effect related to the deeper or shallowest sources (Fedi, 2002). Fedi and Florio (2001) demonstrated the usefulness of this method considering the magnetic field generated by 3 prisms that simulates a complex geological structure, with sources at different depths (Fig. 19): two shallower prisms and a deeper one. As shown in the figure, the shallower sources' effect merges together and it is very difficult to recognize them from the analysis of the field (Fig. 19, plot a). Using the MDA, it is possible to separate the different sources' effects by choosing the number of the summation terms. When the summation is made by the first terms of the equation (2), the deepest source boundaries are better defined (Fig. 19, plot b). On the contrary, by using the last terms of the summation, the shallowest sources' boundaries are better delineated (Fig. 19, plot c, d).

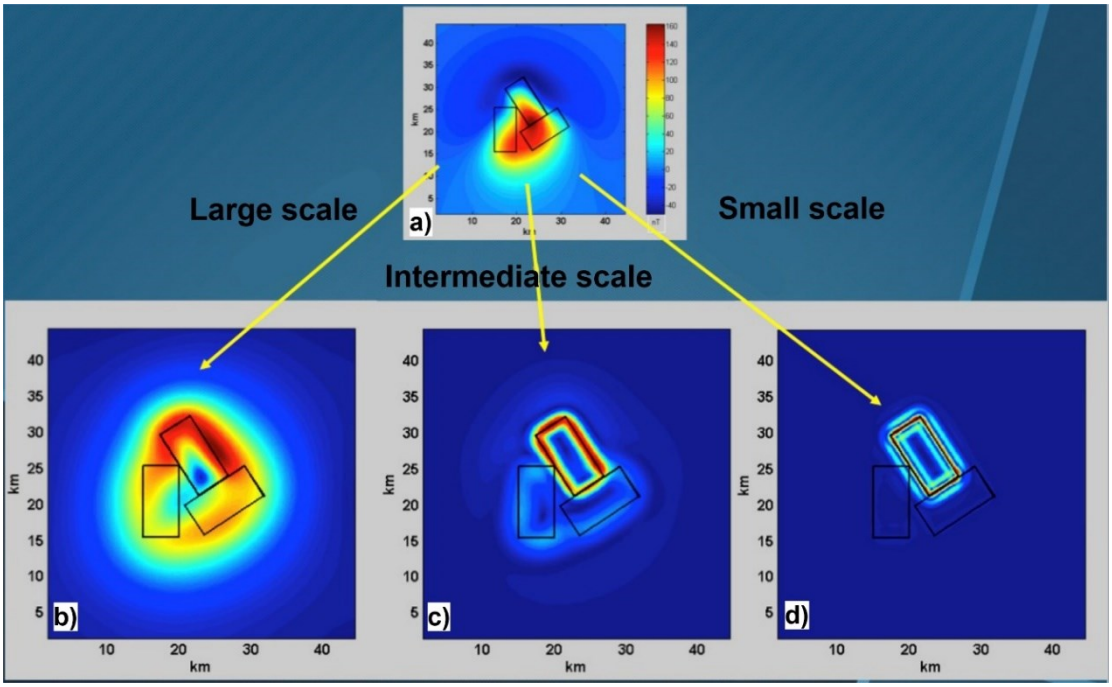

Fig. 19 *Synthetic magnetic field generated by three shallow and deep prismatic sources. In the sub-plots I show, the source boundary analysis using different scale of the MDA. (after Fedi and Florio, 2001).*

These results hold also for the gravimetric field. For this thesis, I used the MDA at medium scale (w_m = 5) for the Paganica, Mt. Vettore – Mt.Bove, San Giuliano di Puglia areas, that allows to highlight both shallow and deep structures, and short scale (w_m = 7) for the Mt. Massico area. The MDA maps of the study areas are shown in Fig. 20, plots a, b, c, d. In all the sub-plots of Fig. 20 some Apenninic and anti-Apenninic trends of anomalies are clear. The red values of the MDA map, highlighted by black lines, represent density contrasts, caused by the presence of fault that puts in contact lithologies with different density. The presence of topographic highs could also influence MDA maxima. For this reason, is important to understand the source of each gravimetric lineaments with the support of the seismicity. Thus, I created an attribute table, showed at the end of the thesis, in which, for each lineament, I reported:

- ID number: to identify the lineament;
- Correlation with topography: if the MDA lineament fits with a topographic feature the value of the correlation is “high”, if the lineament does not fit with a topographic high the value of the correlation is “low”;
- Correlation with faults: if the trend of the MDA lineament matches with the trend of the mapped faults, the value of the correlation is “high”, when there is no match between faults’ evidence on surface and MDA maxima the value of correlation is “low”;

- Correlation with earthquakes: if the MDA lineament overlaps a seismic clustering, the value of the correlation is “high”. On the contrary, if the MDA lineament matches with sporadic (or absent) seismicity the value of the correlation is “low”.
- Notes: some comments about the correlations are made. For examples, I specify:

- if the MDA lineament cuts a topographic high or a seismic clustering perpendicularly;
- if the MDA lineament is only partially correlated with topography or earthquakes.

In all the sub-plot in Fig. 20 the main gravimetric lineaments are correlated with an ID number to better identify them in the attribute tables.

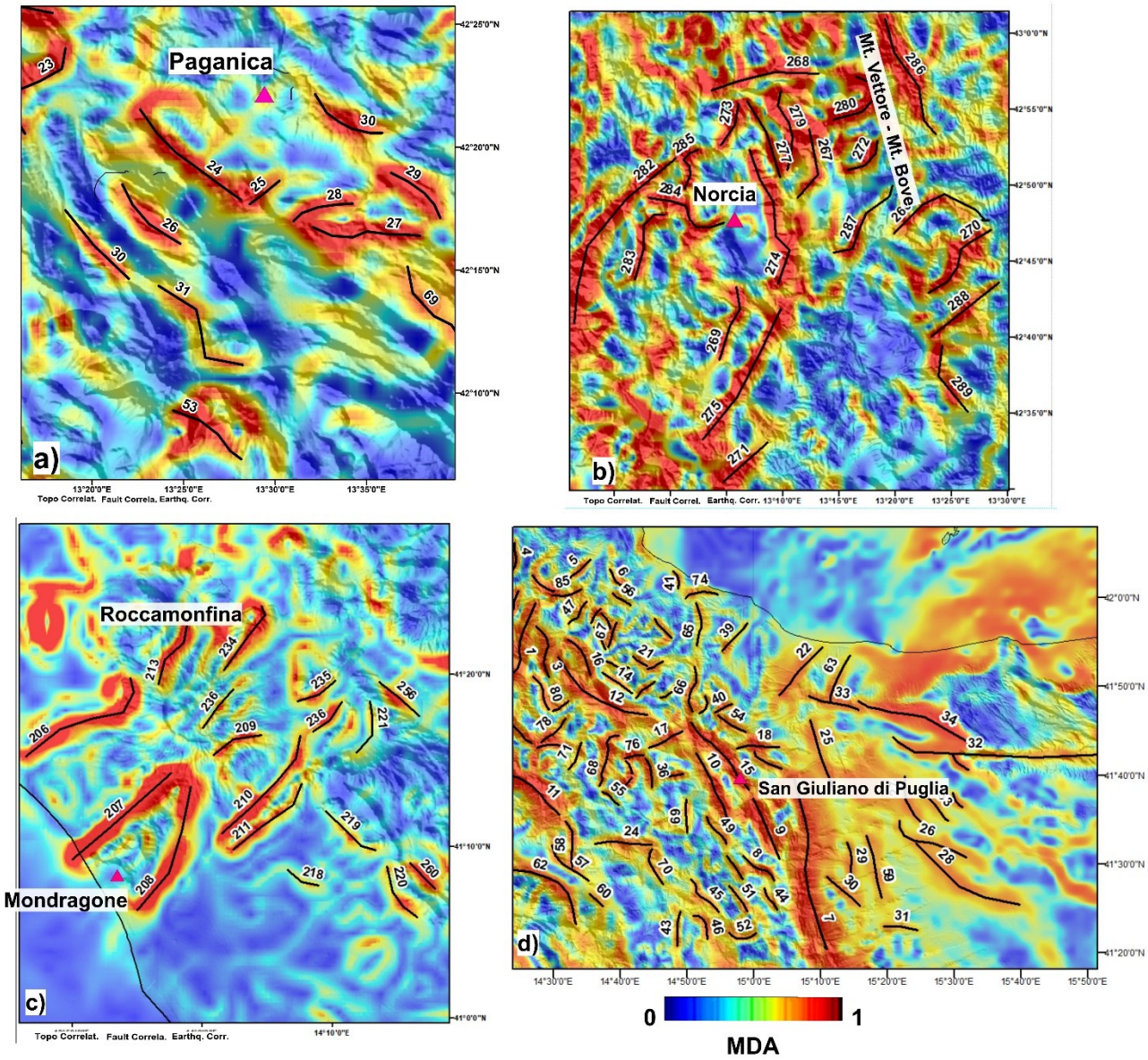

Fig. 20 *The gravimetric database of the study areas with attribute tables;* ***a)*** *MDA at medium scale in the Paganica area;* ***b)*** *MDA at medium scale in the Mt. Vettore-Mt.Bove area;* ***c)*** *MDA at short scale in the Mt. Massico area;* ***d)*** *MDA at medium scale in San Giuliano di Puglia area. Black lines: MDA maxima signals with ID numbers; The location of the main towns is shown with a pink triangle. The attribute tables for all the area are shown in* ***Tables 6a, b, c, d.***

4 Results: analysis and discussion

To analyse the correlation between faults, earthquakes and MDA lineaments, I have merged together all the database and plotted them on the shaded relief of the areas. The overlapping between structural, seismological and gravimetric database has the aim to identifying active faults, silent faults and inactive ones. All the investigated areas are affected by some MDA lineaments with Apenninic and anti-Apenninic directions. These follow the trend of the most of the topographic features but they are also present where the topographic highs are completely missing. For a better assessment of the correlation between faults, earthquakes and gravimetric lineaments, I have divided the analysis for areas. First, to clarify the final map with all the analysed data, I have simplified the structural dataset taken the most accredited faults (mapped in two catalogues at least) and marking them with black lines. All resulting faults, marked with an ID number, are correlated with an attribute table in which I specify the type (normal, inverse fault or thrust), the dip and the bibliographic sources from which the faults are extracted. In all the following figures the MDA maxima are marked by white lines. The attribute tables are shown in the end of the thesis.

4.1.1 Paganica and Mt. Vettore – Mt. Bove areas

As regards the correlation between faults, earthquakes and MDA maxima in the Paganica area, I see that at SW of the Paganica fault (ID 3), near the Roio Canetra fault (ID 6), there is a strong correlation between the earthquakes relocated by Chiaraluce et al. (2011) and a MDA maximum with an Apenninic trend highlighted with white line (Fig. 21a in the green ellipse). This maximum could be caused by the Paganica fault plain, which is SW dipping with an angle of 45° (Chiaraluce, 2012 and references therein). A different kind of correlation is found for the Lucoli fault (ID 4), SW of the Paganica fault. Here we see a strong correlation between the Lucoli fault, well reported in literature, and a MDA maximum (highlighted by a white line), but there are no earthquakes (green ellipse in Fig 21b). On the contrary, the Poggio Picenze fault (ID 11), SE of the Paganica fault, is a clear example of good correlation between fault reported in literature and relocated events, but with the total absence of MDA maxima (green ellipse in Fig 21c). This suggests the lack of density contrasts between the different lithologies along the fault.

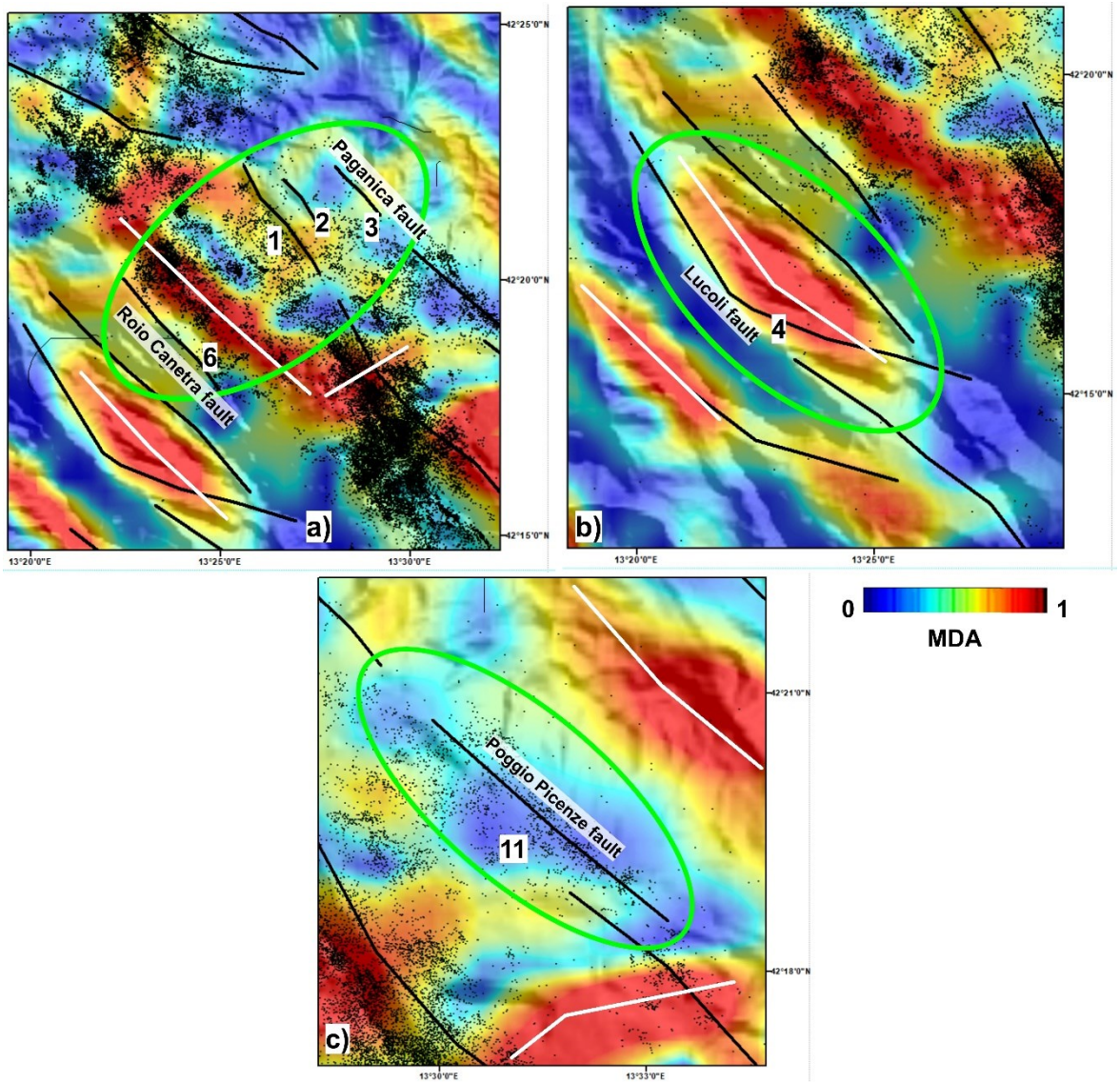

Fig. 21 *Merge of the structural, seismological and gravimetric datasets in the Paganica area;* ***a)*** *good correlation of the datasets on the Paganica fault;* ***b)*** *good correlation between gravimetric and structural datasets on the Lucoli fault;* ***c)*** *good correlation between structural and seismological datasets on the Poggio Picenze fault. Black lines: faults mapped in the most of the consulted catalogues and scientific papers; white lines: MDA maxima signals; black dots: earthquakes relocated by Chiaraluce et al. (2011); the attribute table for the Paganica area is shown in* ***Table 7.***

In order to confirm what I have hypothesized for the Paganica fault regarding the south-westward shift between the position of the fault and its MDA maximum, I performed a synthetic modelling (Fig. 22). The test regards the analysis, along a profile, of the gravity field generated by a 2D normal fault plain located from x_0= 7000 m to x_1=19500 m, having its top at 1000 m depth (as detected from the DEXP analysis, section 4.2.1) and its bottom at 10000 m depth and with a density contrast of 0,5 g/cm^3. Data spacing is 50 m. We note that the maximum value of the computed horizontal derivative (pink line) is located at x_n=13500 m, in correspondence with fault plain's middle (dashed green line). The synthetic data (gravity field and horizontal gradient) agree with the real data, confirming that

such a geometry of the fault could generate a shift between the position of the fault on the surface and its MDA maximum.

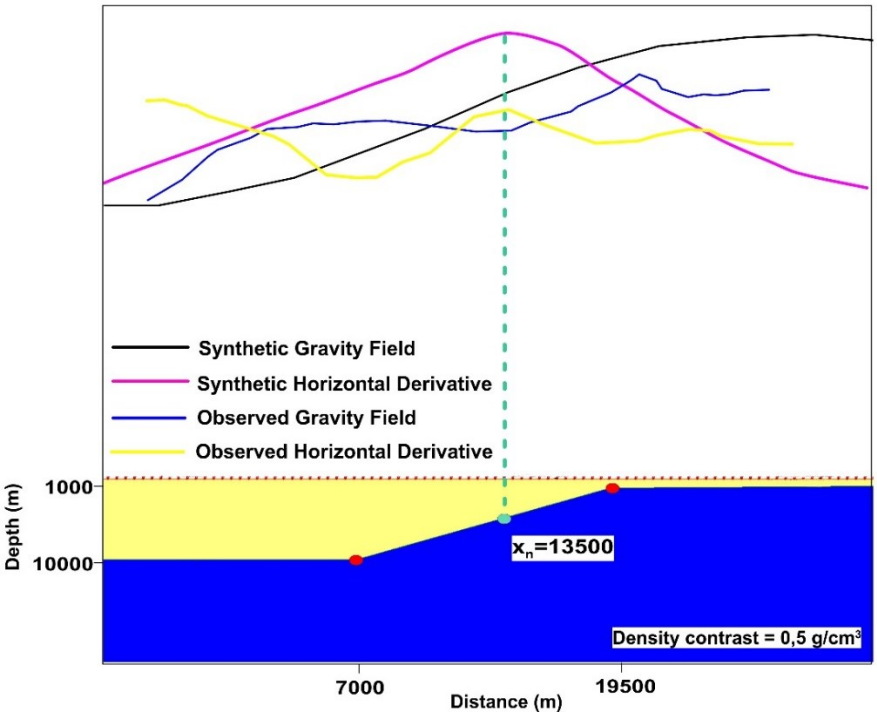

Fig. 22 *Synthetic modelling relative to a normal fault model.*

Then, I have analysed the correlation between the three datasets in Mt. Vettore – Mt. Bove area. In Fig. 23a (in the green ellipse) a MDA maximum, distant about 8 km far from the Mt. Vettore – Mt. Bove fault system (faults with ID 6, 7, 8) and having the same NNW-SSE direction, is overlapped to a high concentration of earthquakes relocated by Michele et al. (2016). The MDA maximum is located near the Norcia antithetic active fault system (ID 2, 3, 4). According to the seismological analysis of Chiaraluce et al. (2011) and Scognamiglio et al. (2016), the M_w 5.4 event, occurred 1 hr later the M_w 6.0 event (at 02:33 UTC), nucleated exactly at the intersection with the main fault plane and probably on this secondary structure. This could confirm the strong activity of the antithetic fault and the robust gravimetric signal that could generate. Thus, the MDA maxima of the area could be originated by the Mt.Vettore –Mt. Bove fault system (with a shift between the position of the fault on the surface and its MDA maximum, as in the case of the Paganica fault, see Fig. 23), and/or by the Norcia antithetic fault.

Instead, in Fig. 23b (in the green ellipse) we show a good correlation between the Amatrice fault (also known as Mt. Gorzano faults' system; ID 15) and a well concentrated earthquake swarms (north and SW of the Amatrice fault) that suggests a North-westward continuation of the fault plain

and a SW dip. Similarly to what seen before, the lack of MDA maxima in this case is evidence of the lack of density contrasts between the different lithologies along the fault (Fig. 23b).

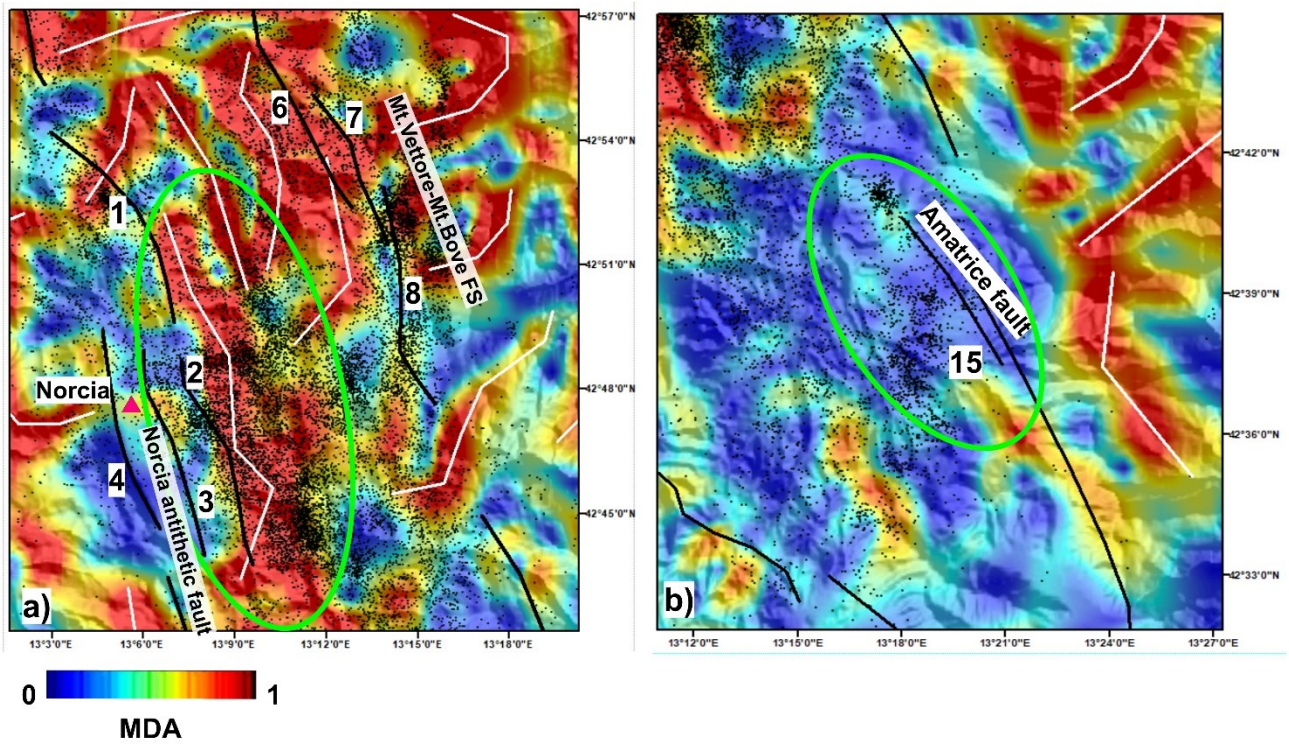

Fig. 23 *Merge of the structural, seismological and gravimetric datasets in the Mt. Vettore – Mt. Bove area;* ***a)*** *good correlation of the datasets on the Mt. Vettore – Mt. Bove fault system;* ***b)*** *good correlation between structural and seismological datasets at Amatrice fault. Black lines: faults mapped in most of the consulted catalogues and scientific papers; white lines: MDA maxima signals; black dots: earthquakes relocated by Michele et al. (2016); the location of the Norcia town is shown with a pink triangle; the attribute table for the Mt. Vettore – Mt. Bove area is shown in* ***Table 8.***

4.1.2 Mt. Massico area

Even though its seismicity is relatively low, in the Mt. Massico area the correlation between faults, earthquakes and MDA lineaments is very strong along the northern and southern sub-vertical faults bordering the massif (ID 1 and 6, respectively), as shown in Fig. 24. The red earthquakes are extracted from the ISIDe catalogue and were not relocated, the yellow ones are re-rilocalized using the velocity model of Gaudiosi et al. (2010). For details, see the paragraph 3.2.2. To the NE of the Mt. Massicco northern fault, the Vairano Patenora fault (ID 2 and 3) shows absence of MDA maxima but exhibits medium seismicity that links the Vairano Patenora fault with the northern fault of the Mt. Massico. In the following section, I investigated this connection through an analysis by DEXP images and hypocentral sections.

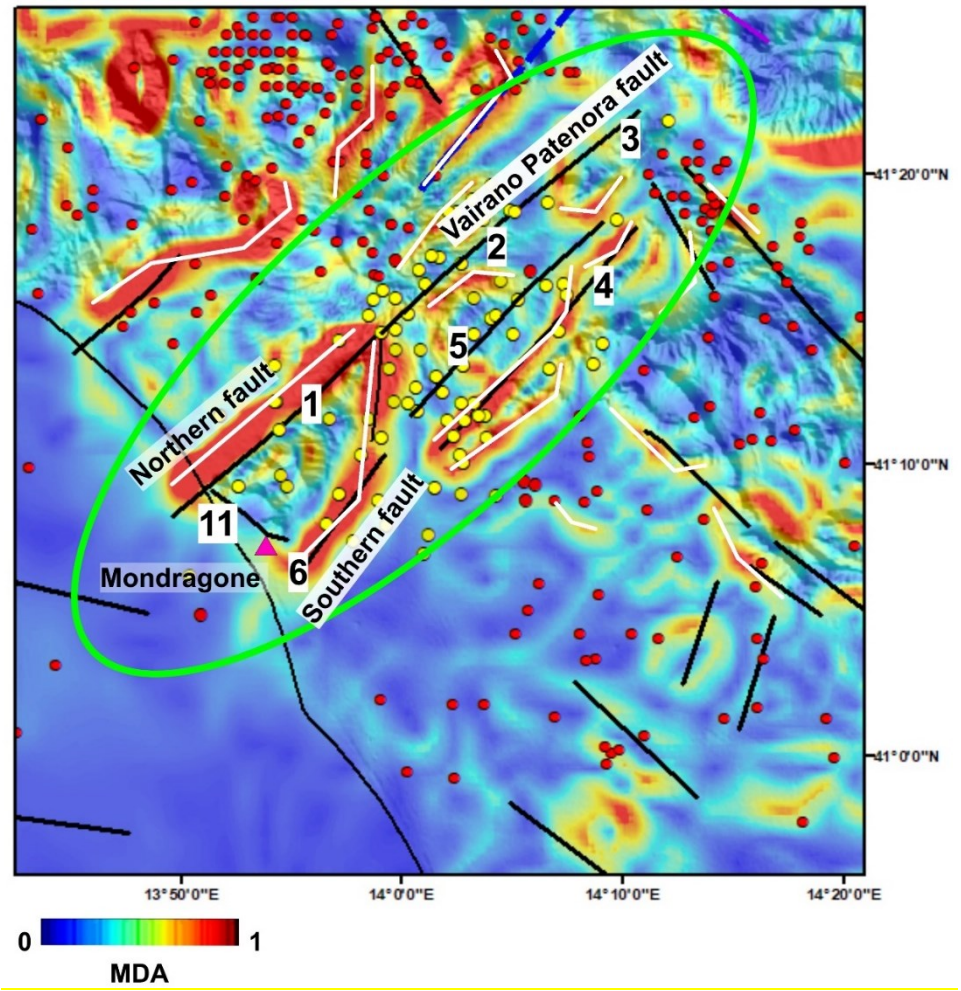

Fig. 24. *Merge of the structural, seismological and gravimetric datasets in the Mt. Massico area. Black lines: faults mapped in most of the consulted catalogues and scientific papers; white lines: MDA maxima signals; red dots: earthquakes from the ITHACA catalogue; yellow dots: earthquakes re-localized through the velocity model of Gaudiosi et al., (2010); the location of the Mondragone town is shown with a pink triangle; the attribute table for the Mt. Massico area is shown in* ***Table 9.***

4.1.3 San Giuliano di Puglia area

The correlation between faults, earthquakes re-localized by Chiarabba et al. (2014) and MDA lineaments in the San Giuliano di Puglia area is shown in Fig. 25 a, b. There is a strong correlation between MDA lineaments and low-angle thrust lineaments (ID 1, 2, 3; Vezzani et al., 2010; blue ellipse in Figure 25a with an Apenninic direction. The direction of the thrust is not in agreement with the E-W trend of seismic clusters (Fig. 25a). To the south of the seismic clusters, it is visible a small MDA lineament with E-W trend that is in matches with both the seismic cluster and the westward propagation of the Mattinata fault (ID 13; red ellipse in Fig. 25a; Valensise et al., 2004; Mucciarelli et al., 2009; Puglia et al., 2013). A first analysis of this correlation seems to suggest that the E–W

MDA lineament, that seems located in continuation with the Mattinata fault, is interrupted and covered by the strongest MDA lineaments with apenninic direction related to the low-angle thrusts. This interesting correlation will be more investigated in the next section.

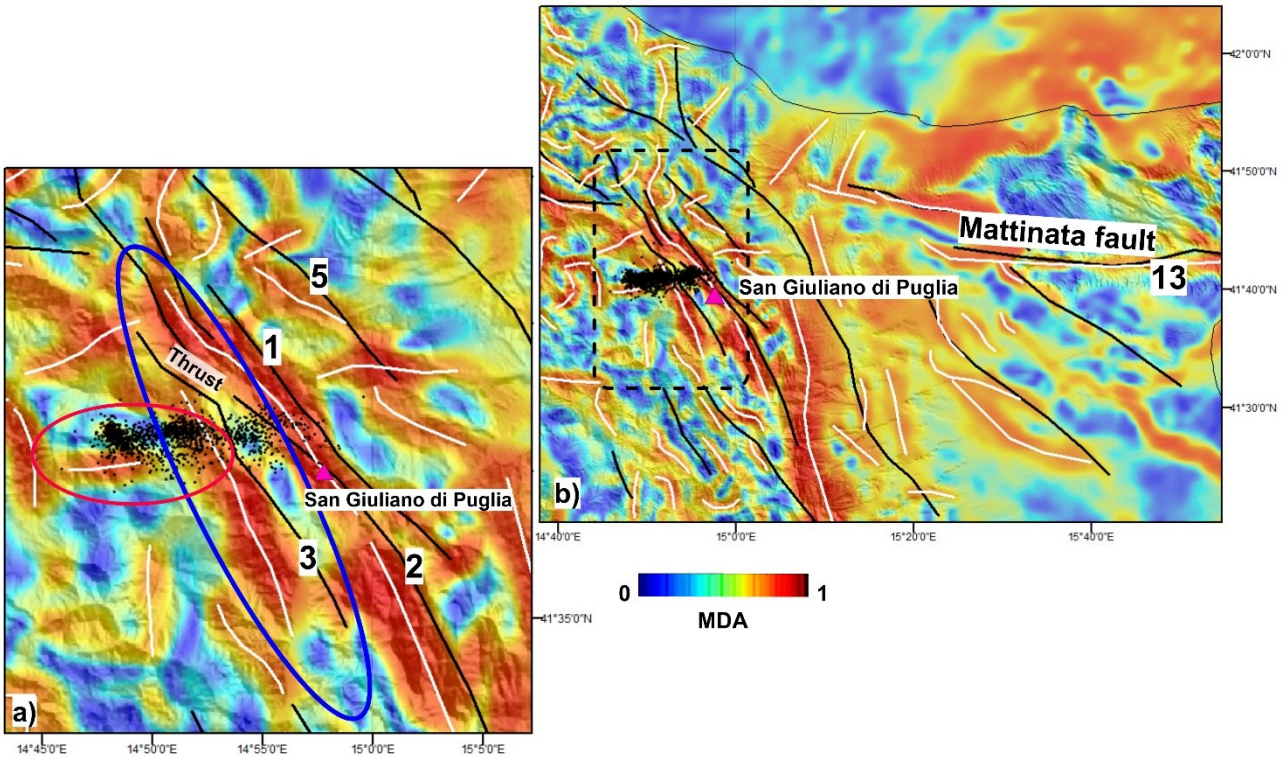

Fig. 25 *Merge of the structural, seismological and gravimetric datasets in the San Giuliano di Puglia area;* ***a)*** *Black lines: faults mapped in most of the consulted catalogues and scientific papers; white lines: MDA maxima; black dots: earthquakes relocated by Chiarabba et al. (2014);* ***b)*** *extended area; black dotted rectangle: area shown in sub-plot* ***a****. the location of the San Giuliano di Puglia town is shown with a pink triangle; the attribute table for the San Giuliano di Puglia area is shown in* ***Table 10.***

Now, considering the comprehensive analysis of these datasets in all the studied areas, we can highlight some possible scenarios of correlation between faults, earthquakes and MDA maxima:

1) The existence of active faults, revealed by a strong correlation between epicentral location, known fault positions and MDA maxima. This is the case of the faults edging the Massico horst, the faults of the Mt. Vettore – Mt. Bove faults system;

2) the presence of inactive or silent faults, such as the Lucoli fault, highlighted by good correlation of gravimetric lineaments with faults reported in geological maps, with lack of earthquakes;

3) The existence of faults correlated with weak MDA signal but marked by a good clustering of earthquakes. This is the case of the Amatrice fault (also known as Mt. Gorzano faults' system), where

the distribution of earthquakes suggests that the fault plain spreads through NW with a SW dipping fault plain. The absence of gravimetric lineaments could be explained by the fact that the fault plain puts in contact two lithologies with a similar density.
4) the existence of strong MDA signals correlated with a good clustering of earthquakes. This could suggest that the fault is active and buried. This is the case of the portion of the Paganica fault that is not mapped, and of the fault responsible of the San Giuliano di Puglia seismic sequences.
The correlation analysis on map can detect only if the fault is active or inactive (or silent), or if it is active but contacts lithologies with small density contrast. To analyse the geometry of the fault plains, I have used the DEXP method, a multiscale analysis on gravity data that provides an estimate of the sources' depth/extent. The results of the DEXP method were then merged with the hypocentral sections of the relocated events.

4.2 DEXP images and hypocentral sections

The DEXP images and the hypocentral sections were obtained along profiles mainly perpendicular to the investigated faults. The DEXP maxima are at about the depth to the top of the fault plains, but the images do not yield information about the bottom of these sources. The integration of this information from potential fields with that from the 2D analysis of the hypocentral data allows us to better constrain the geometry of the fault systems and infer their depth extent.

In detail, the *Depth from Extreme Points* method (DEXP; Fedi, 2007) provides an estimate of the sources' depth and of their *Structural Index* (an index relative to the sources' shape) by analysing the extreme points' position in a 3D field scaled with appropriate scaling functions of the continuation height (Fedi and Pilkington, 2011). The scaling function is in relation with the *Structural Index* (*N*) described in the theory of Euler deconvolution. The method is fast and stable because of the regular behaviour of the potential field with the height increasing. For this reason, the DEXP method can be useful for data with low signal/noise ratio. Moreover, the method can be applied also on vertical or horizontal derivative of the gravity/magnetic field, contributing to reducing the interferences between nearby anomalies (Fedi, 2007). The "key" for a correct use of the DEXP method is the "scaling function" τ defined as the derivate of the logarithm of the potential f on the log (z) ratio:

$$\tau\,(z)\frac{\partial \log[f(z)]}{\partial \log(z)} \qquad (3)$$

That, for a spherical source, is:

$$\tau_1(z) = -\frac{2z}{z-z_0} \qquad (4)$$

The scaling function is singular in the source region, where $z = z_0$. In the harmonic region, for an altitude $z = -z_0$, $\tau = -1$ (Fig. 26):

$$\tau_1(z = -z_0) = \frac{\partial \log[f_1(z)]}{\partial \log(z)}\Big|_{z=-z0} = -1 \qquad (5)$$

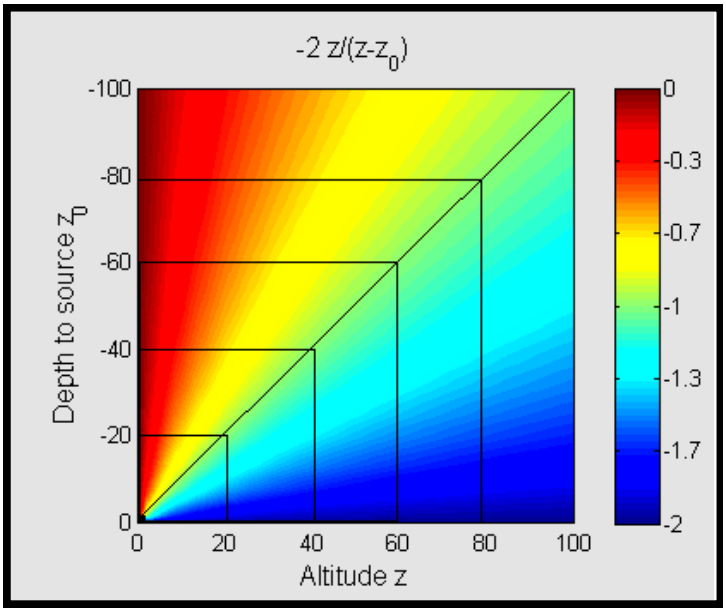

Fig. 26 *The scaling function τ_1 for n = -1. The "key" of the DEXP method is that τ_1 is = -1 when $z = -z_0$ (from Fedi, 2007).*

So:

$$\frac{\partial z f_1}{\partial z}\Big|_{z=-z0} = 0 \qquad (6)$$

This means that the function is obtained scaling the gravity field with a power law of the altitude z and exponent equal to 1:

$$W_{g1} = f_1 z \qquad (7)$$

and the equation (7) will give the extreme points at $x = x_0$, $y = y_0$, $z = -z_0$ as shown in Fig. 27 This function is called DEXP transformation on gravity field (Fedi, 2007).

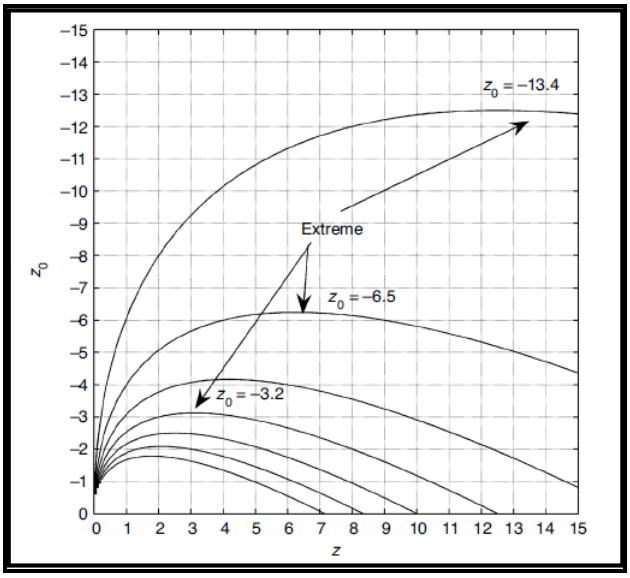

Fig. 27 *The function f_1 at $x = x_0$, $y = y_0$. From the surface $f_1(z,z_0)z$, for sources at depth z_0 is created a curve which ends correspond to the points $z = z_0$ (Fedi, 2007).*

It is possible to write a general equation, valid for the n^{th} vertical derivative of the gravity potential field:

$$W_n(z) = z^{Nn/2} f_n(z) \qquad (8)$$

where $N_n = (N+1)$ is the *Structural Index* of n-order of the source (Fedi, 2007).

A relation between "scaling exponent" and the *Structural Index* N exists (Fedi, 2007; Stavrev and Reid, 2007):

$$N_n = 2\alpha_n \qquad (9)$$

where α_n is the "scaling function".

The DEXP method involves three steps:

a) Estimate the *Structural Index* (*N*) of the DEXP function to different scales according to "scaling function" (equation 3);
b) Transformation of the potential field in the DEXP function *W* (equation 8), using the estimated value *N* as in step (a);
c) Determination of the source depth from the maximum value of *W*.

For all the study areas, before implementing the DEXP method, I have continued the gravimetric data upward to 10 km a.s.l and 20 km a.s.l. only for the Mt. Massico area, and considered the horizontal gradient of the gravimetric field previously scaled with the 4th vertical derivative for the Paganica, Mt- Vettore – Mt. Bove, San Giuliano di Puglia areas and with the 2nd ones for the Mt. Massico area to better visualize the horizontal density contrast. For all the areas, I used a structural index *N*=-1, which is appropriate for a contact-like structure (Fedi and Florio, 2002). The areas are analysed separately.

4.2.1 Paganica and Mt. Vettore – Mt. Bove areas

In the Paganica area, my combined analysis along a profile perpendicular to the main lineaments shows that the shallowest segment of the Paganica fault is clearly recognizable by the DEXP maxima, with a dip of about 45–50°, from 5 km depth to the surface (Fig. 28). From 4 km to 10 km the fault plain is marked by the distribution of hypocenters, following the same orientation of the DEXP signal (highlighted by a white line) dipping about 50°. This suggest that the top of the Paganica fault plain is at about 1 km m depth but the 2009 seismic sequence is generated by the activation of the sector from 5 km to 10 km depth, as confirmed by EMERGEO Working Group (2010) and Chiaraluce et al. (2011). On the SW sector of the DEXP profile there is a clear maxima signal generated by the nearby antithetic fault, NE dipping.

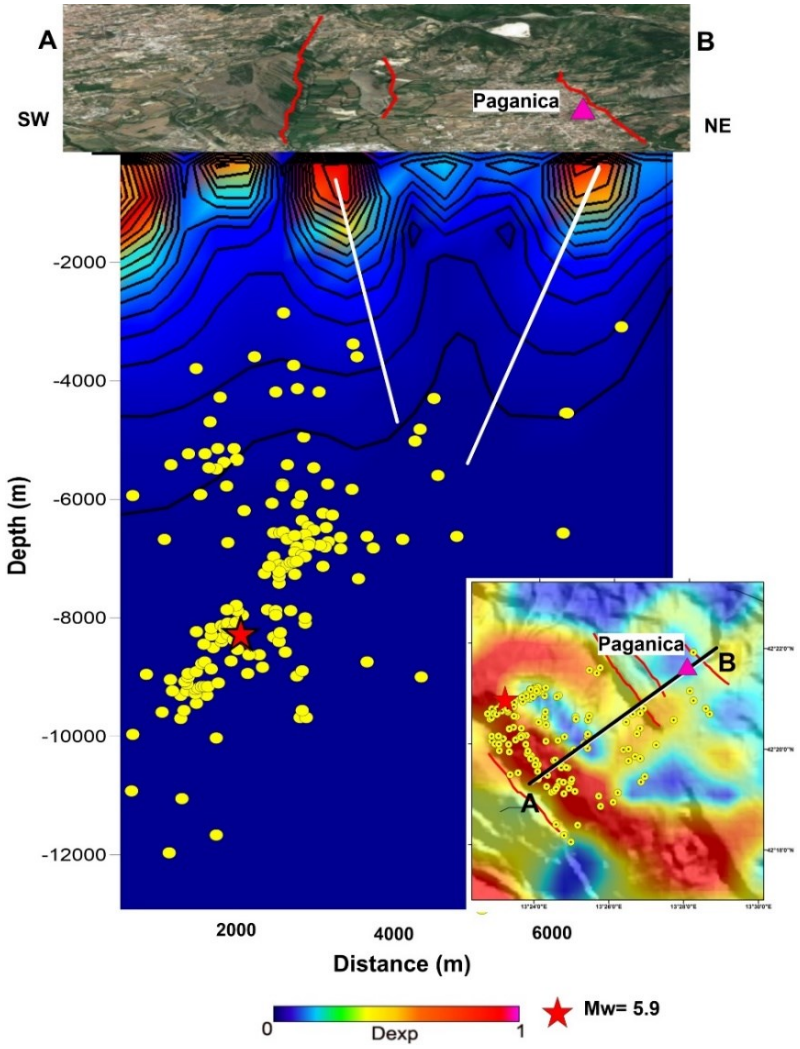

Fig. 28 *Combination of the DEXP image and hypocentral section at Paganica. The figure shows an agreement between the gravimetric and seismological evidences. White line: DEXP maxima; red star: main shock of the 6th of April 2009. To the right: sketch of the position of the AB profile (black line).*

About the Mt. Vettore – Mt. Bove area, I divided it in 12 sub-areas, with dimensions 4 km by 40 km (Fig. 29a; b), similarly to Chiaraluce et al. (2017). The sub-areas are represented by the white boxes identified by ID numbers. The faults, mapped by the recent work of EMERGEO working group (2016), are represented with red lines and plotted above the boxes' lines and the re-located earthquakes (yellow dots in the figure) for a better visualization. In Fig. 29b it is shown the same area without earthquakes to better show the MDA trends correlated to complex systems of faults.

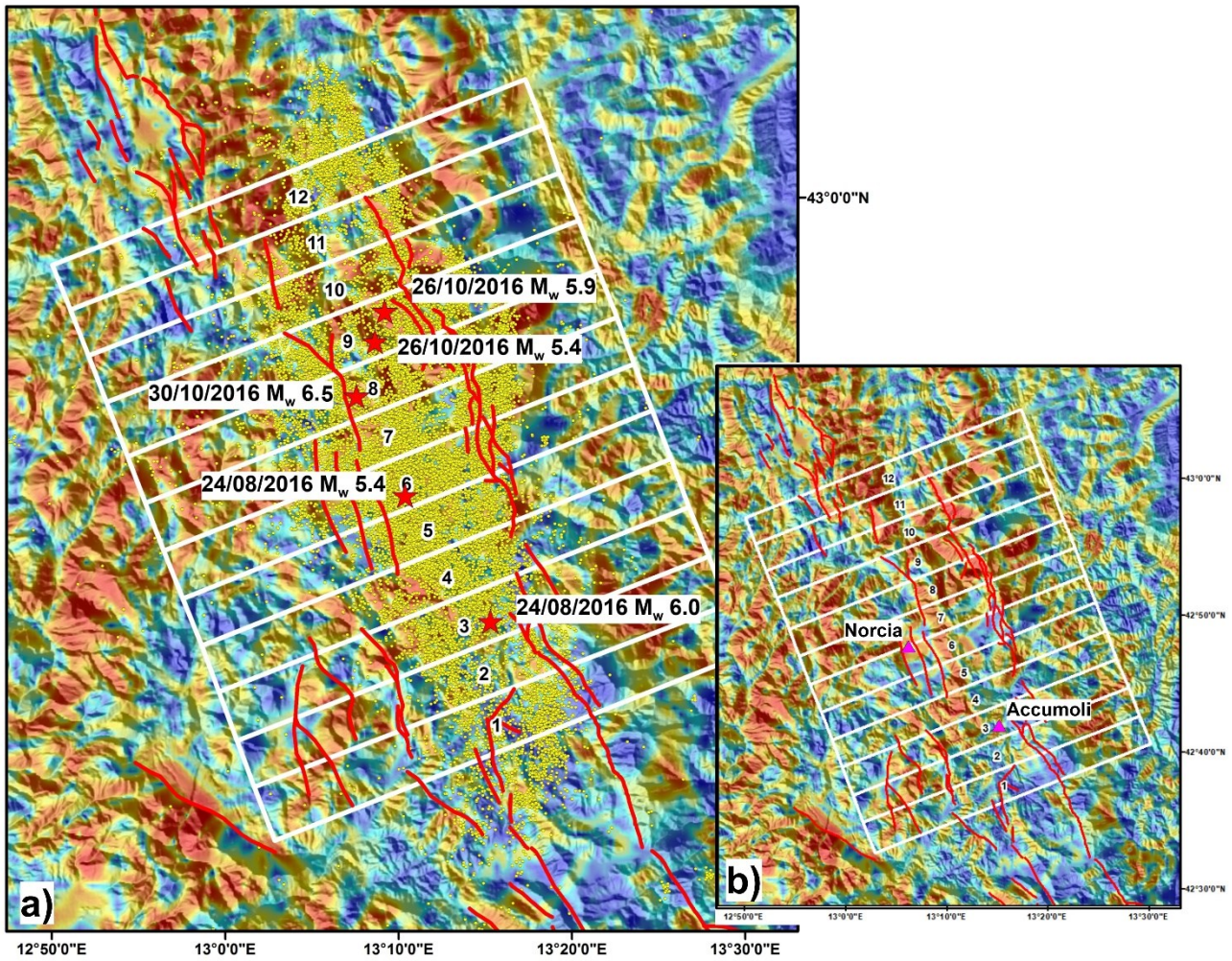

Fig. 29 *The Mt. Vettore – Mt. Bove area divided in sub-areas. White boxes: the 12 sub-areas differentiated by an ID number; red lines: faults extracted from by the EMERGEO working group report.* ***a)*** *merge of the three datasets; yellow dots: relocated events (Michele et al., 2016);* ***b)*** *the same area without earthquakes.*

In the following figures, sections are drawn from SW to NE for a total distance of about 40 km and are located at the centre of each sub-area. Several sections depict a rather complex patter of the DEXP signal likely connected to the complexity of the fault system of the area. I am plotting a zoom of the sections (i.e., mostly the central part of the 40-km long sections) for better showing these patterns. Moreover, I am plotting the sections where my combined analysis highlighted clear DEXP maxima that match with the pattern of hypocentres and the faults mapped at the surface.

In the section 1, I note a rather complex pattern of the DEXP image. Hypocentres are located from 3 km to 12 km depth with a clear SW dip, and with a minor hypocentres clustering, NE dipping. These hypocentre patterns seem matching with small maxima of the DEXP signal (white lines in Fig. 30-Section 1), extending down to a depth of about 6 and 3 km, respectively. In the north-eastern portion of section 2, from 2 km to 6 km depth I recognize two sub-vertical hypocentres clusters with two clear sub-vertical DEXP signals. Moreover, I note another cluster dipping NE, in correspondence of the San Venanzio fault, that seems matching with a strong DEXP signal extending down to a depth of 4 km (white lines in Fig.30-Section 2). In the section, a flat clustering located between 8 and 10 km depth is shown (Chiaraluce et al., 2017). The geometry of this clustering, confining at depth almost the entire fault system, is not regular but it seems to be eastward dipping of about 15°, mainly in the central portion of the fault system (see sections 4, 5, 6).

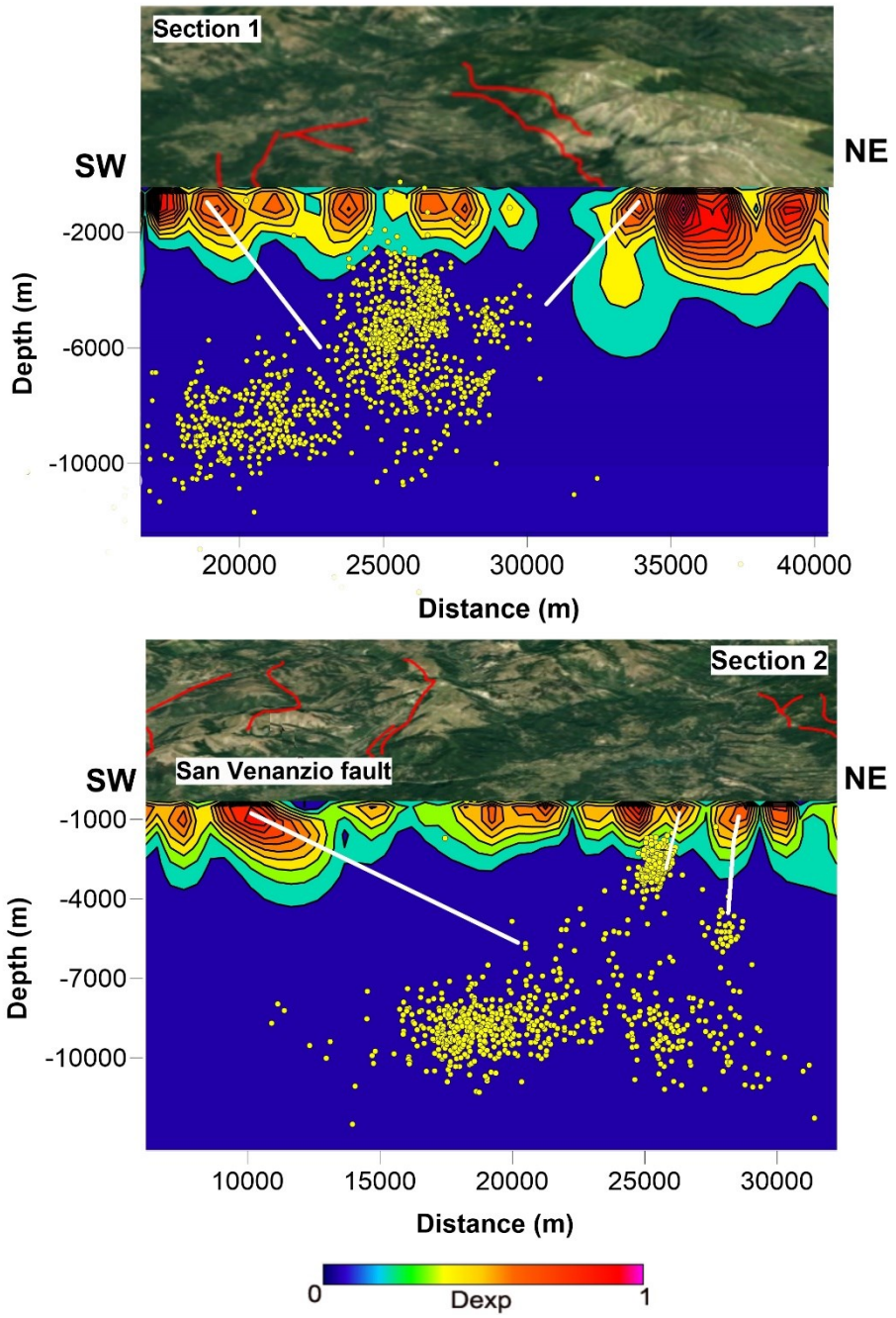

Fig. 30 *Continued*.

In section 4, the trend of the main SW-dipping clustering at about 50° (Chiaraluce et al., 2017) becomes clear. I can also observe the presence of a NE-dipping hypocentres clustering, corresponding to the antithetic fault that caused the M_w 5.4 event (Scognamiglio et al., 2016) (better visible in section 6) nucleating at the intersection with the main SW-dipping fault plane. The NE-dipping hypocentre pattern seems matching very well with a series of NE-dipping small maxima of the DEXP signal (with lines in Fig. 30-Section 4) extending down to a depth of about 4–5 km. It is

important to notice that in south-western portion of section 4, the good overlapping between DEXP signals and hypocentre section highlights the presence of an antithetic fault plain, not reported by scientific papers and geological maps, that start to be mapped from section 5. In section 5, in correspondence with the main Mt. Vettore – Mt. Bove faults' system, a hypocentre clustering dips SW with an angle of about 50°–55°. A clear DEXP signal (with line in Fig. 30-Section 5) overlaps perfectly the seismic trend down to a depth of about 5 km. In the SW portion of section 5, the Norcia antithetic fault plain is reported (Pierantoni et al., 2013 and therein) and its geometry is well-defined by the hypocentres trend. No correlation with DEXP signal is shown.

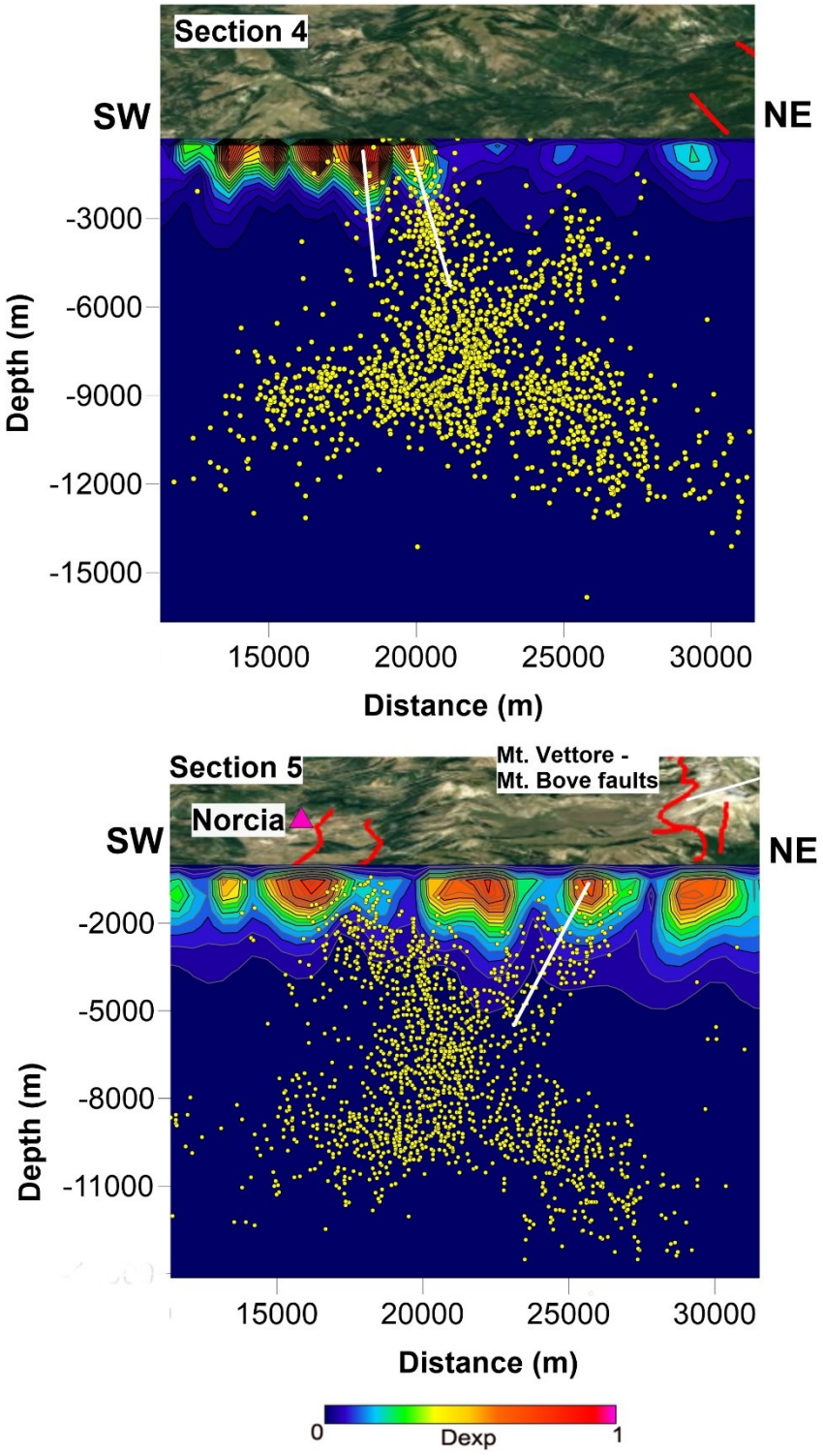

Fig. 30 *Continued.*

Instead, in section 6, hypocentres clustering, NE-dipping and corresponding to the antithetic fault that caused the M_w 5.4 event (red star in Fig. 30-Section 6), well matches with the DEXP signal down to a depth of about 4 km. In correspondence with the main Mt. Vettore – Mt. Bove faults' system, there is no correlation between hypocentre clusters and DEXP signals. This may be due to the presence of many faults splay with small length whose gravimetric signals influence each other. Moving to the north, an interesting result is shown in the section 7. The flat clustering begins to fade away and, under the main Mt. Vettore – Mt. Bove fault system, there is a clear hypocentral trend not correlated with DEXP signal. In the central part of the section, characterized by absence of mapped faults, there is a high correlation between hypocentral locations and the DEXP signal (identified by the white line), dipping SW with an angle of about 50°. This suggests that the fault plain moves deep from SW to NE until it outcrops. This is confirmed also by the correlation between hypocentral location and DEXP signals in section 9.

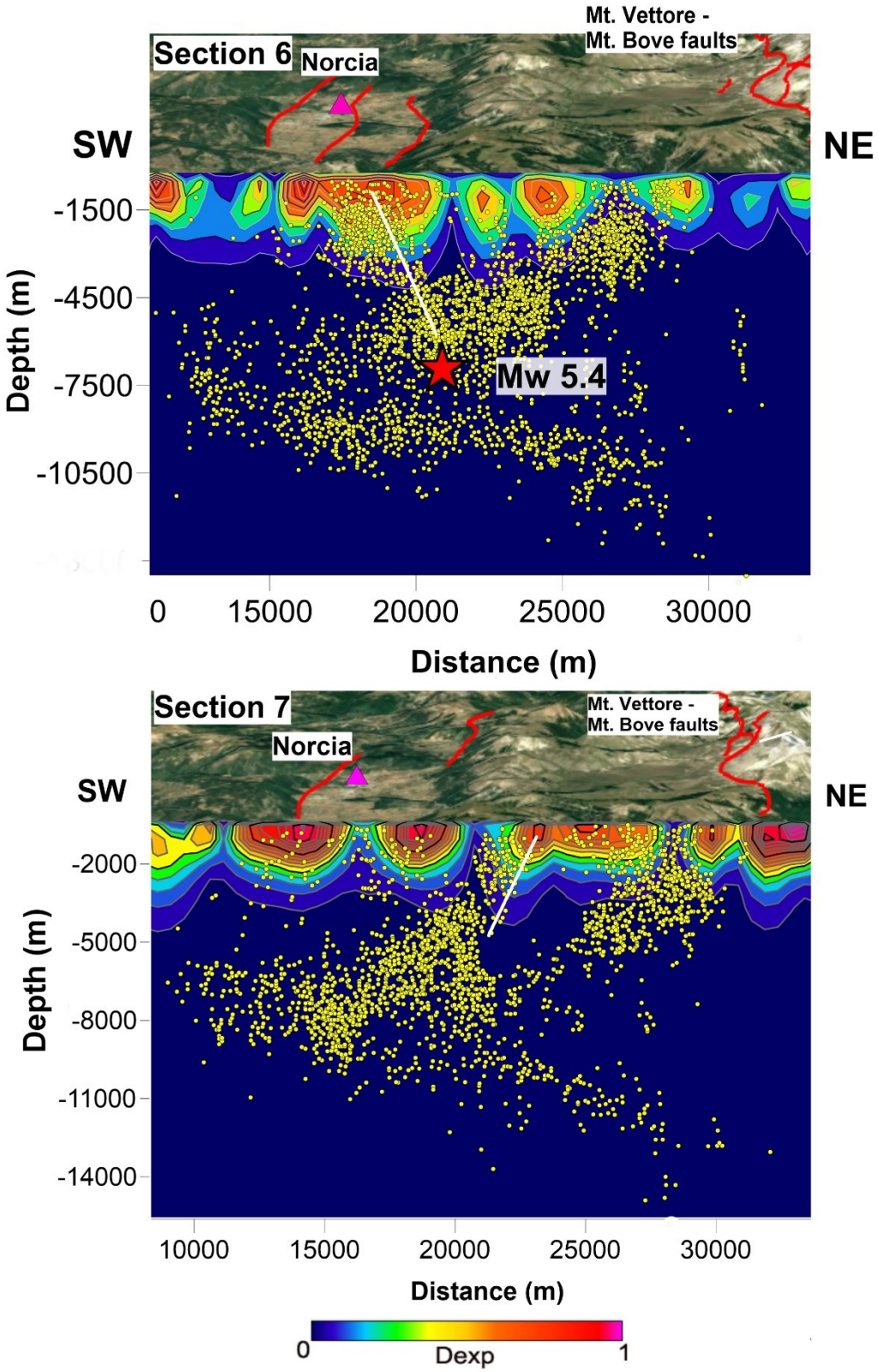

Fig. 30 *Continued.*

Section 9 shows the last two major events, with M_w 5.4 and 5.9 occurred in 26 October 2016 in the northern sector of the fault system. The trends of the hypocentres, SW dipping, agree with three major DEXP signals marked by white lines. The same good correlation is shown in the section 10. In the SW sector of section 10, the antithetic Norcia fault is highlighted by spread-out hypocentral clusters dipping NE that seems to continue below a strong DEXP signal with same dip, reaching 5 km depth. The north-easternmost sector of section 10 shows that also the main Mt. Vettore – Mt. Bove fault system is highlighted by a DEXP signal down to 5 km depth and correlated with hypocentral clusters.

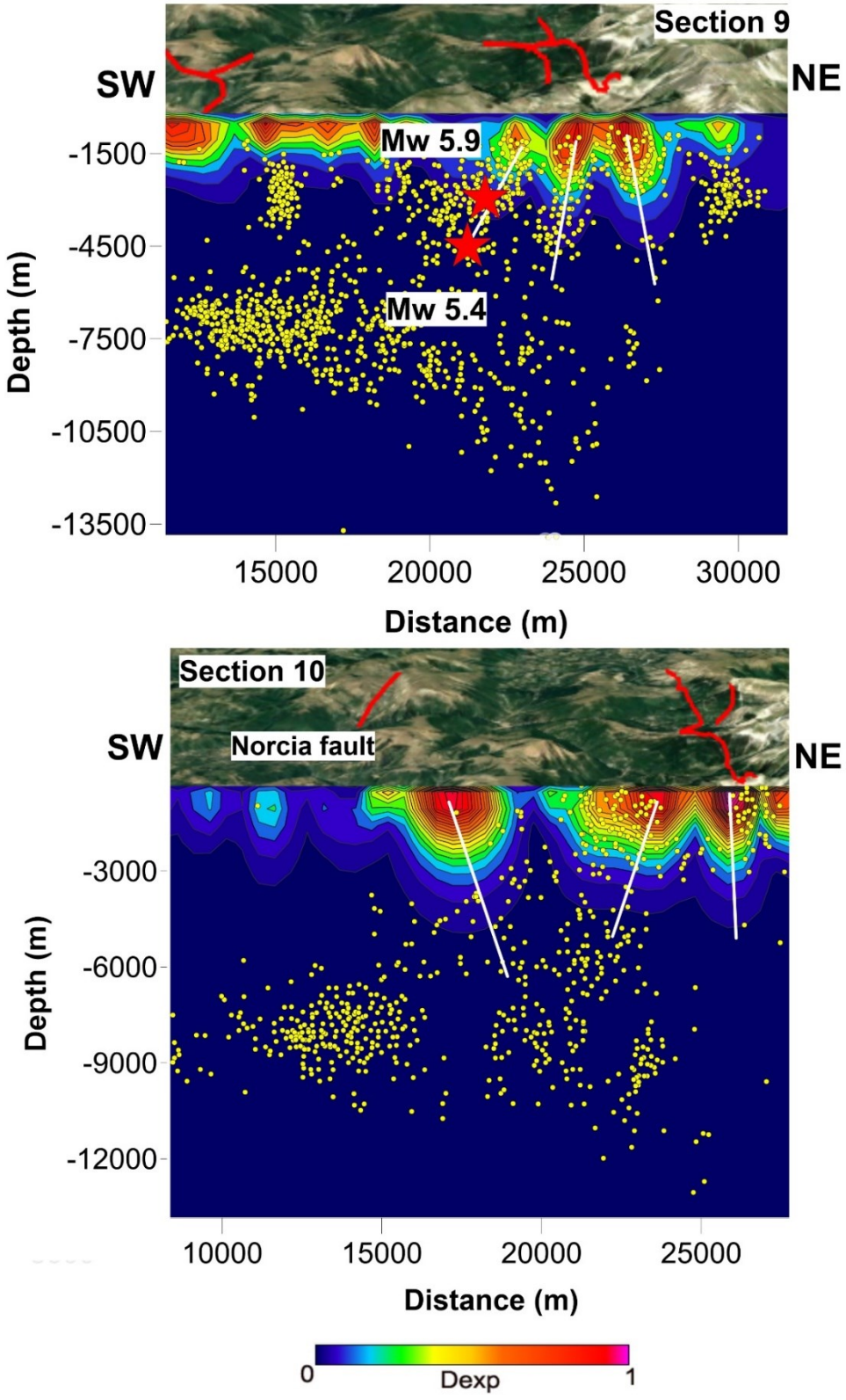

Fig. 30 *Continued.*

Section 11 shows three DEXP signals with a SW dip extended down to 4 km of depth well-correlated to hypocentres and to the main SW-dipping structures mapped at the surface, except for the DEXP signal in the middle of the section. This well fits with the seismicity, suggesting the presence of a small fault segment SW dipping but not mapped yet. On the north-easternmost side, the seismic events, with a dip of about 45°–50°, overlaps the DEXP signal down to 4 km depth.

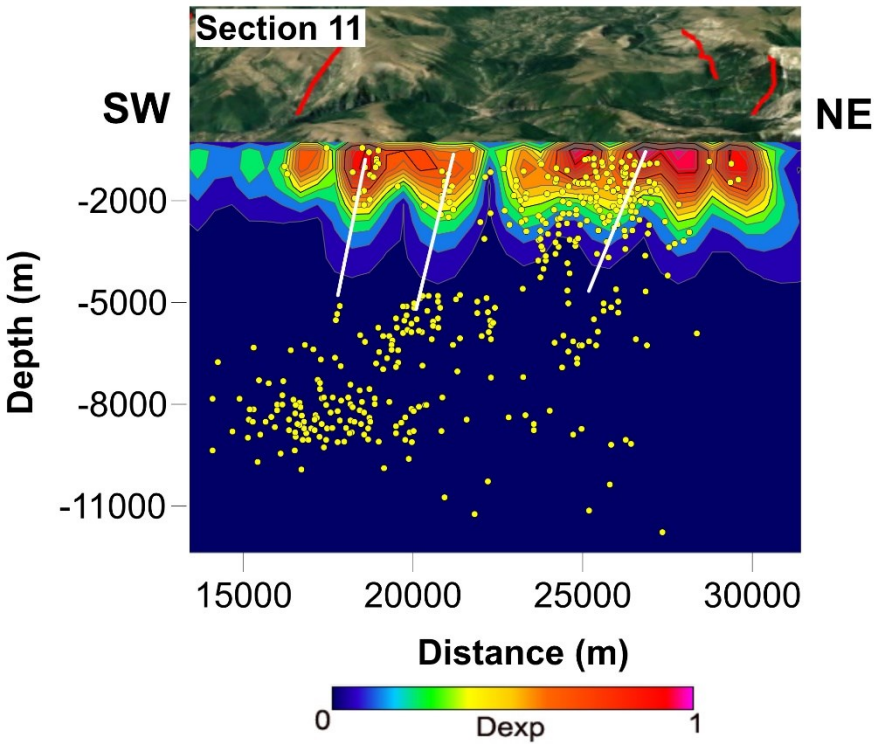

Fig. 30 *Characterization of the geometry and depth extend of the NW–SE Mt. Vettore – Mt. Bove fault system through a combined analysis of gravity and seismological data along SW–NE sections. Red lines: faults exacted from EMERGEO Working Group catalogue (2016); yellow dots: relocated earthquakes; red stars: main events of the 2016 seismic sequence; white lines: DEXP maxima signals.*

The analysis of the correlation between DEXP signals and hypocentral sections, highlights a different interpretation for the Paganica and the Mt. Vettore – Mt. Bove areas. The Paganica fault is isolated and its gravimetric field is not influenced by the gravimetric signals of nearby faults. For this reason, the DEXP maxima of the Paganica fault are clear and allow the fault plain geometry (direction and dip angle) to be constrained, also without the use of seismological information (that are useful to identify the active portion of the fault plain.

In the Mt. Vettore – Mt. Bove area the situation is more complex. The faults splay of the fault system, whose gravimetric signals influence each other, make the DEXP image rather complicated. Several DEXP signals are very close each other and overlap the shallow sector of the hypocentral lineaments,

with similar dipping. On the other hand, the antithetic faults, more isolated that the eastern fault system, are more visible with the gravimetric signals. In this case, the signals give clearer information about the faults' dip angle, matching with the fault plain geometry shown by hypocentral sections (Sections 4, 6,7, 10).

4.2.2 Mt.Massico area

To constrain the geometry of the faults bordering the Mt. Massico, I performed the DEXP analysis along a NW–SE profile about 24 km long, crossing the two NE–SW active lineaments. The DEXP maxima (highlighted by white lines, Fig. 31a) are at about the depth-to-the-top of the fault plain, and the area covered by the DEXP highs is oriented similarly to the fault dip (Luiso et al., 2017). The lineament located to the northern side of the horst is dipping NW at an angle larger than 80°. The southern fault dips towards the SE and seems to be sub-vertical down to about 7 km. The fault geometry is also constrained by 2D analysis of the re-localized hypocenters. I have isolated the relocated events for the northern and southern faults (yellow and red events in Fig. 31a, respectively) also including the events located on the continuation of the bordering faults (dotted black lines in Fig. 31a). The hypocentral sections are plotted above the DEXP outcome confirming the dip of 70°- 80° and showing a maximum depth of about 20 km. These results agree with the studies from De Rita and Giordano (1996) and Billi et al. (1997) regarding the depth geometry of both faults.

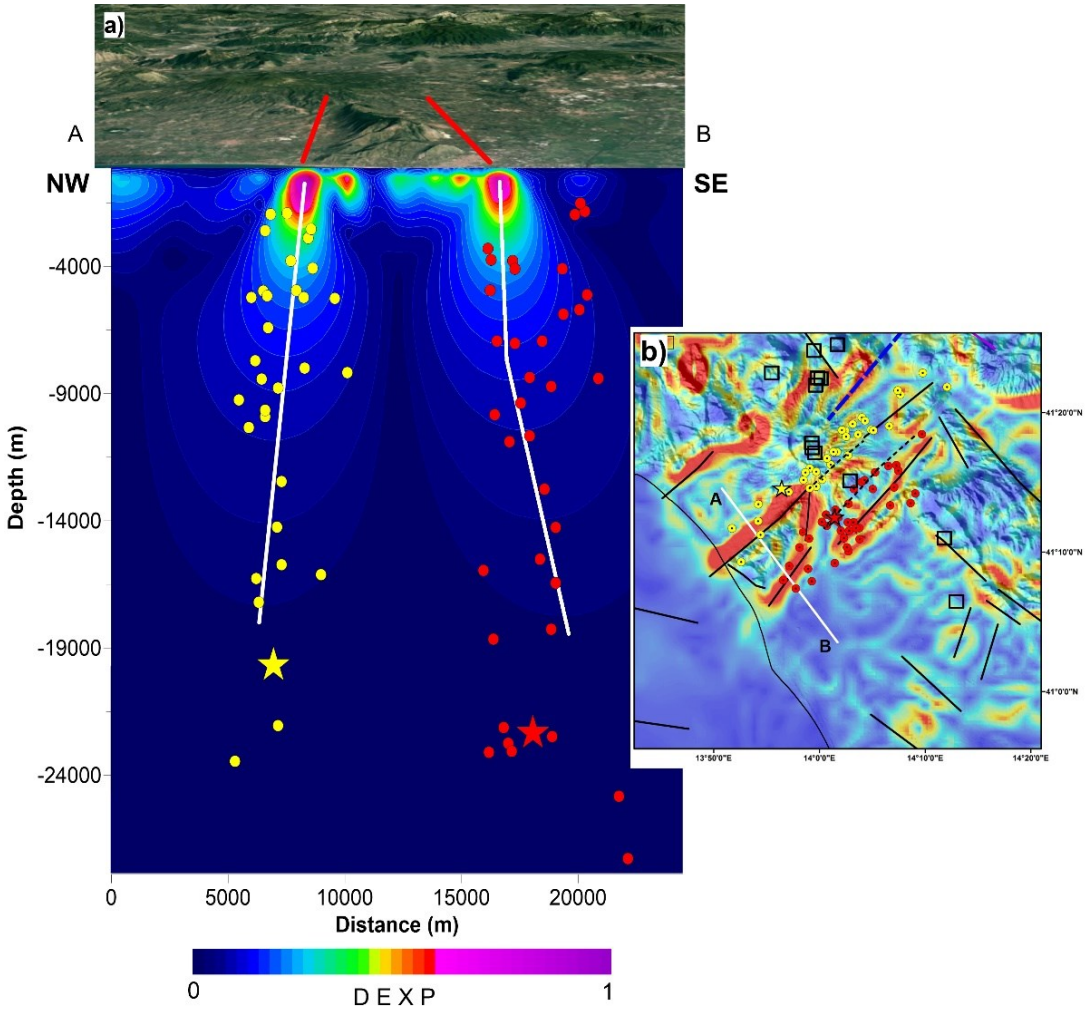

Fig. 31 *Characterization of the geometry and depth extend of the NE–SW faults bordering the Mt. Massico horst along the NW-SE profile AB; a) DEXP analysis on the two faults along AB profile; b) MDA map of Mt. Massico. Yellow dots: the earthquakes along the north-western fault; red dots: the earthquakes along the south-eastern fault. Yellow and red stars are the strongest earthquakes along the two lineaments.*

In order to clarify this depth pattern between DEXP signals and fault plains, I performed a DEXP analysis on synthetic gravity data relative to two plausible forward models with density contrast of 0.3 g/cm^3 (Fig. 32): i) a system of faults with the southeast fault deviating at an angle of 70° in its deeper section; ii) a series of down-thrown blocks of different widths on the southeast side of the horst located at 1 km, 7 km and 10 km depth, respectively. The two models return comparable DEXP synthetic outcomes. In Fig. 32, I show the DEXP outcome relative to the second model (down-thrown block model), whose pattern is in turn rather similar to the DEXP image resulting from real data (Luiso et al., 2017).

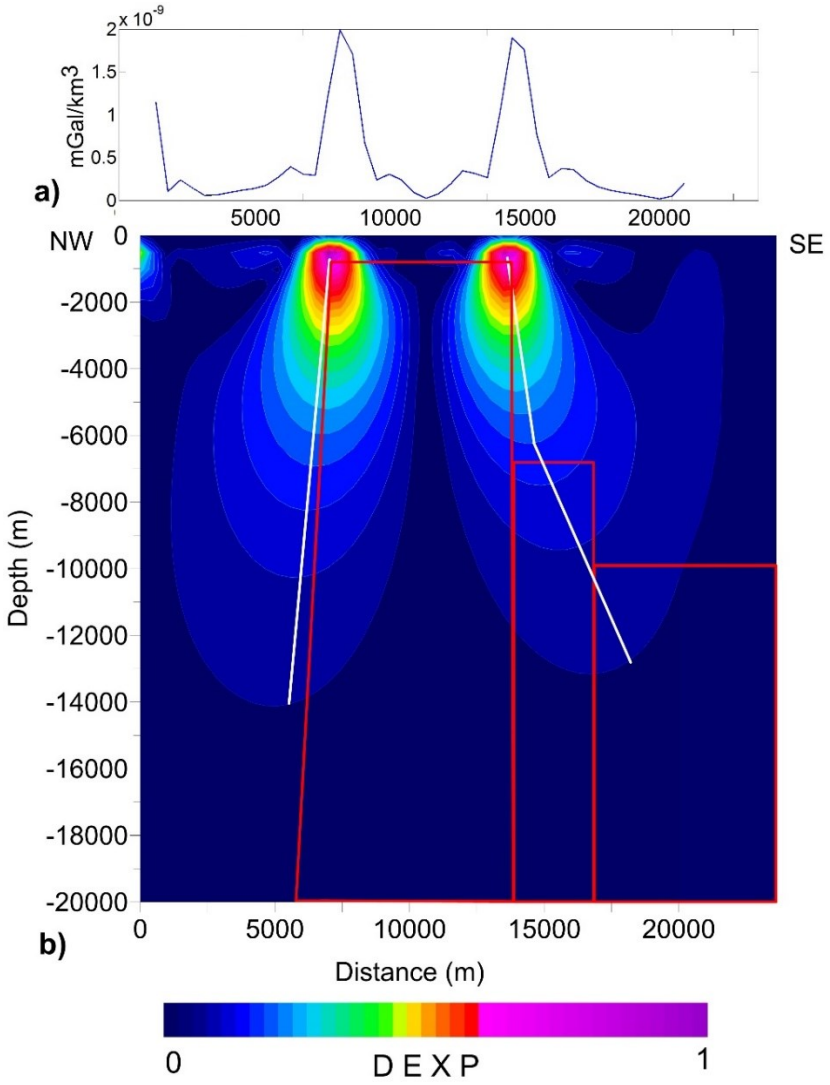

Fig. 32 *DEXP analysis on synthetic gravity data relative to two models: i) a series of down-thrown block (red blocks) with different width and same density contrast of 0.3 g/cm^3; ii) two sub-vertical faults, one of which (the southern one) has a sub-vertical trend to 6000 m of depth and then a dip of 70° (white lines);* ***a)*** *modulus of the horizontal gradient of the 2nd vertical derivative of synthetic gravity data;* ***b)*** *DEXP image.*

4.2.3 San Giuliano di Puglia area

The correlation analysis between faults, earthquakes re-localized by Chiarabba et al. (2014) and MDA lineaments at San Giuliano di Puglia, shown in section 3.1.3, suggests a strong correlation between MDA lineaments and low-angle NW–SE thrust lineament (Vezzani et al., 2010) (Fig. 33b; Chiarabba et al., 2014). Furthermore, there is a good correlation between E–W re-localized San Giuliano di Puglia earthquake seismic sequence and a MDA maximum with E–W direction, but no evidence of E–W surface mapped faults (Fig. 20d, 33b). Thus, I have analysed the DEXP images and hypocentral section along a N–S profile. The AB profile is about 20 km long and intersects the low-angle thrust lineaments (green lines in Fig. 33) mapped by Vezzani et al. (2010), the seismic clusters and the MDA lineament with E–W trend (Fig. 33b). The hypocentres section (Fig. 33a) shows a sub-vertical plane, with the aftershocks tending to cluster between 12 and 16 km depth (Chiarabba et al., 2014), well-correlated with sub-vertical DEXP maxima. More specifically, a sub-vertical DEXP signal from the surface to about 5 km depth, marked with a white line, matches the trend of the seismic clusters. My outcome of a E–W active fault with sub-vertical plain suggests a possible correlation of it with the pattern of the sub-vertical Mattinata fault system, having E–W direction. The other DEXP maxima in Fig. 33a may instead be related to the low-angle thrusts and reverse faults reported by Vezzani et al. (2010, green lines in Fig. 33a). The merge of the DEXP image and hypocentral section in the San Giuliano di Puglia area is very interesting because of the good agreement with the geological and scientific works supporting the activation of Mattinata fault in 2002 (Mucciarelli et al., 2009; Di Bucci and Mazzoli, 2003; Puglia et al., 2013).

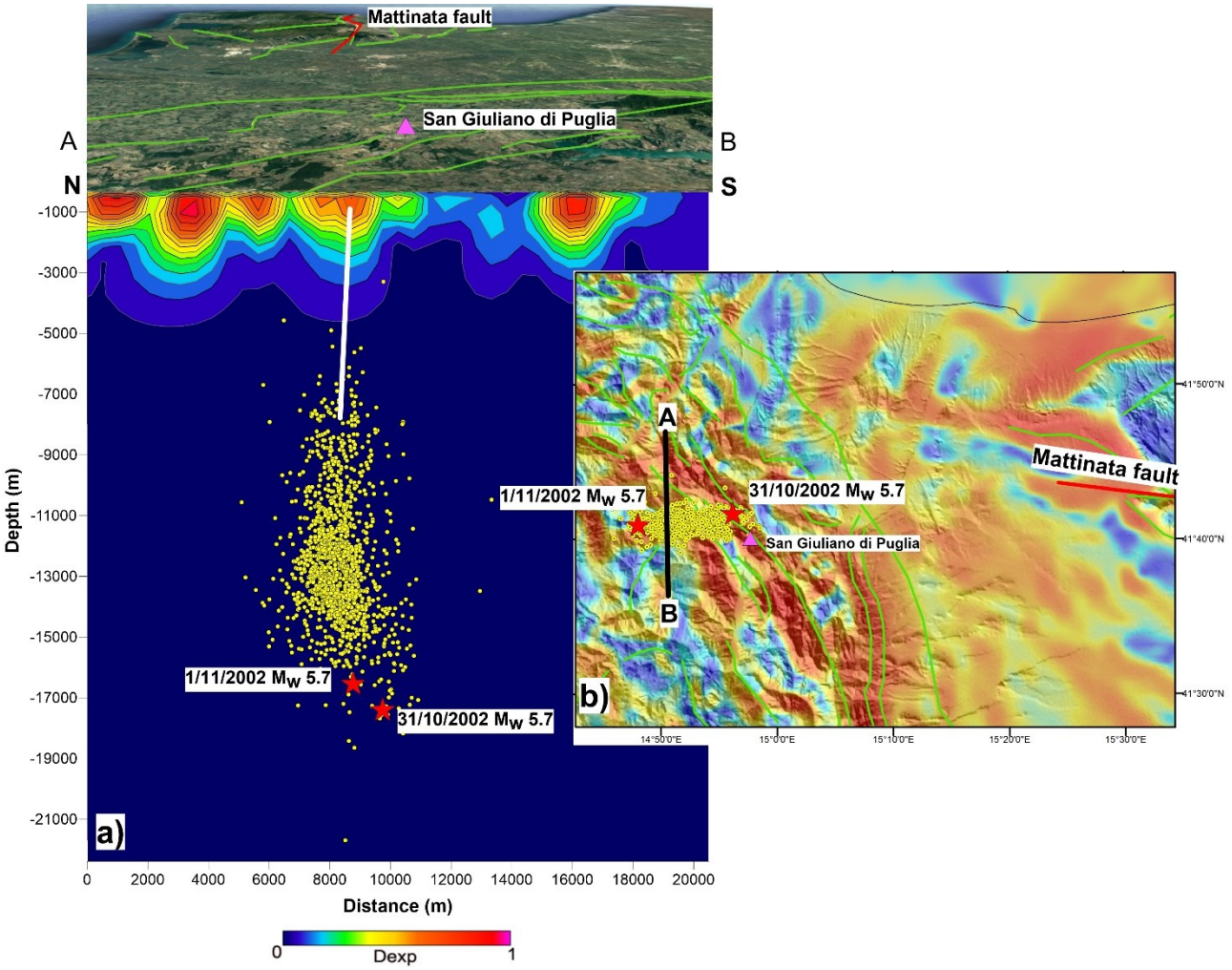

Fig. 33 *Characterization of the geometry and depth extend of the E–W fault causing the 2002 seismic sequence along a N-S profile;* ***a)*** *DEXP analysis along the AB profile;* ***b)*** *MDA map of the area. Yellow dots: relocated earthquakes; red stars: main shock and aftershocks with higher magnitudes; white lines: DEXP maxima signals matching with the hypocentre distribution.*

.

5 Conclusions

In this thesis, I present a new methodology, consisting in a combined analysis of structural, seismological and gravimetric datasets that allows characterizing active, silent and inactive faults, both outcropping and buried. I performed my multi-parametric data analysis in the Paganica and Mt. Vettore – Mt. Bove areas (high seismic hazard), and in the Mt. Massico and San Giuliano di Puglia areas (medium-low seismic hazard). My analysis aimed at contributing to the knowledge of the neotectonic activity of the study areas and identifying of the geometry of their active faults. The first step consisted in the analysis of the correlation between Multiscale Derivative Analysis (MDA; Fedi, 2002) maxima, showing the presence of density contrasts, earthquakes and faults. I found four possible scenarios of correlation between faults, earthquakes and MDA maxima:

i) the existence of active faults, revealed by a good correlation between epicentral location of seismic clusters, known fault positions and MDA maxima. This is the case of the faults edging the Massico horst, the faults of Mt. Vettore – Mt. Bove and the Paganica fault;

ii) the presence of inactive or silent faults, such as the Lucoli fault, highlighted by good correlation of gravimetric lineaments with faults reported in geological maps, with lack of earthquakes;

iii) the existence of active faults correlated with a weak MDA signal but with a good clustering of earthquakes. This is the case of the Amatrice fault, where clustered seismic locations suggest a NW propagation of the SW dipping fault plain. Weak MDA signatures could be due to the presence of faults contacting lithologies with similar densities;

iv) the existence of strong MDA signals correlated with a good clustering of earthquakes, but without faults mapped at the surface. This could suggest that the fault is active and buried. This is the case of the portion of the Paganica fault that is not mapped, and the case of the San Giuliano di Puglia area. Here the fault that caused the 2002 seismic sequence, correlated to the westward continuation of the Mattinata fault, has no surface evidences.

To better define the geometry and depth extent of the active faults in the studied areas, I performed the *Depth from Extreme Points* (DEXP, Fedi, 2007; Fedi and Pilkington, 2011) analysis on gravity data combining the DEXP images with the information derived from 2D hypocentral sections. As results, I note some relevant differences for the analysed areas in the correlation between faults,

earthquakes and gravimetric signals. As regards the Paganica and the Mt. Massico faults, I found a good correlation between the geometry of the fault plain constrained by hypocentral sections and the fault geometry shown by DEXP signals. Both the results are in very good agreement with the consulted geological maps and scientific papers. This good result is due to the presence of gravimetric maxima that, for Paganica and Mt. Massico, are not influenced by other signals generated by nearby faults. Instead, the fault system of Mt. Vettore – Mt. Bove is characterized by a set of linked faults whose gravimetric signals influence each other. Nevertheless, there is a good correlation between earthquakes and DEXP signals along:

- The Norcia antithetic faults (sections 4, 6, 10 in Fig. 30);
- Buried fault plains located far from the main fault system (sections 7, 11 in Fig. 30).

A good match between DEXP images and earthquakes was observed in the San Giuliano di Puglia area. The 2002 seismic sequence, with an E–W trend, fits with a weak E-W MDA signal with E-W direction interrupted by a stronger signal with NW–SE direction (Fig. 25). The DEXP signals are well correlated with hypocentres and show a sub-vertical fault maybe related to the buried extension, to the west, of the E–W Mattinata fault (Di Bucci and Mazzoli, 2003).

Based on these results, I point out the effectiveness of this multi-parametric approach to characterize active faults known (such us the Paganica and the Mt. Massico faults) or un-known in literature (such as the west-ward continuation of the Mattinata fault), and capable or not. Moreover, this approach allows understanding if the structure is active along the whole fault plain or only partially, as for the Paganica fault, and depict its geometry. Given the above results, this new method could contribute to the knowledge of the Apennine seismic hazard, especially in the areas where the sole seismological/structural analysis is not enough.

Acknowledgment

I would like to thank my referees, prof. A.M. Michetti and prof. S. D'Amico for their precious advices and constructive comments. I would like to thank also the professor F. Cella for his support in the analysis of gravimetric data.

References

Ambrosetti P., Bosi C., Carraro F., Ciaranfi N., Panizza M., Papani G., Vezzani L., Zanferrari, A., 1986. Neotectonic map of Italy, Modello strutturale scala 1:500.000. CNR. *Quaderni de "La Ricerca Scientifica"*, 114.

Amoresano A., Angelino A., Anselmi M., Bianchi B., Botteghi S., Brandano M., Brilli M., Bruno P.P., Caielli G., Caputi A., Cardellicchio N., Carotenuto A., Cavuoto G., Chiarabba C., Chiesa S., Ciccolella M., Corniello A., Cuoco E., de Fenzo B., De Franco R., De Lisa G., De Luca G., del Vecchio U., Di Bella G., di Fiore V., di Gregorio C., Di Leo M., Donato A., D'Oriano A., Ducci D., Fedi M., Ferrante L., Florio G., Gargiulo V., Gimelli A., Giocoli A., Giustini F., Gola G., Iavarone M., Inversi B., Iorio M., Langella G., Livani M., Losanno S., Manzella A., Maraio S., Massarotti N., Mauro A., Meo S., Mercadante A., Minissale A., Montanari D., Montegrossi G., Mussi M., Pandolfi L., Pelosi N., Petracchini L., Petruccione E., Pischiutta M., Polemio M., Punzo M., Quattrocchi F., Recanati R., Rizzo E., Romano C., Romi A., Rovelli A., Sarnacchiaro G., Scotto di Vettimo P., Scrocca D., Tamburrino S., Tarallo D., Tedesco D., Testa B., Tiano P., Vanoli L., Varriale F., 2015. VIGOR: Sviluppo geotermico nella regione Campania – Studi di Fattibilità a Mondragone e Guardia Lombardi. Progetto VIGOR – Valutazione del Potenziale Geotermico delle Regioni della Convergenza, POI Energie Rinnovabili e Risparmio Energetico 2007-2013, CNR-IGG, ISBN: 9788879580151.

Atzori S., Hunstad I., Chini M., Salvi S., Tolomei C., Bignami C., Stramondo S., Trasatti E., Antonioli A., Bosci E., 2009. Finite fault inversion of DInSAR coseismic displacement of the 2009 L'Aquila earthquake (central Italy). *Geophys. Res. Lett.,* 36, L15305, doi:10.1029/2009GL039293.

Bally A.W., Burbi L., Cooper C., Ghelardoni R., 1986. Balanced sections and seismic reflection profiles across the central Apennines. *Memorie della Società Geologica Italiana*, v. 35, p. 257–310.

Barberi F., Carapezza M.L., Ranaldi M., Tarchini L., 2007. Gas blowout from shallow boreholes at Fiumicino (Rome): induced hazard and evidence of deep CO2 degassing on the Tyrrhenian margin of central Italy. J*. Volcanol. and Geothermal Res*. 165, 17–31.

Bigi G., Cosentino D., Parotto M., Sartori R., Scandone P., 1983. Structural Model of Italy. Firenze, *Geodynamic project, C.N.R.*, S.El.Ca., scale 1: 500,000.

Billi A., Bosi V., De Meo A., 1997. Caratterizzazione strutturale del rilievo del M. Massico nell'ambito dell'evoluzione quaternaria delle depressioni costiere dei fiumi Garigliano e Volturno (Campania Settentrionale). *Italian Journal of Quaternary Sciences*, 10, 15–26.

Bonardi G., D'Argenio B., Perrone V., 1988. Carta Geologica dell'Appennino Meridionale in scala 1:250.000. *Mem. Soc. Geol. It*, 41, 1341.

Boncio P., Lavecchia G., Pace B., 2004. Defining a model of 3D seismogenic sources for seismic hazard assessment applications: the case of central Apennines (Italy). J. Seismol., 8, 407-425, doi: 10.1023/B:JOSE.0000038449.78801.05.

Bosi C., Messina P., Moro M., 2003. Nuovi procedimenti cartografici per il Quaternario continentale: l'esempio della carta geologica dell'alta Valle dell'Aterno*. Il Quaternario*. 1166 (1), 127-138.

Brozzetti F., 2011. The Campania- Lucania Extensional Fault System, southern Italy: a suggestion for a uniform model of active extension in the Italian Apennines. *Tectonics,* 30, TC5009, doi:10.1029/2010TC002794.

Brozzetti F., Cirillo D., Liberi F., Faraca E., Piluso E., 2012. The Crati Valley Extensional System: field and subsurface evidences. *Rendicont. Online Soc. Geol. Ital*., 21: 159-161.

Bruno P.P., Di Fiore V., Ventura G., 2000. Seismic study of the '41st Parallel' Fault System offshore the Campanian–Latial continental margin, Italy. *Tectonophysics*, 324 (2000), 37–55.

Carminati E., Doglioni C., Scrocca D., 2004. Alps Vs. Apennines. *Special Volume of the Italian Geological Society* for the IGC 32 Florence, 141-151.

Carrozzo M.T., Chirenti A., Luzio D., Margiotta C., Quarta T., 1986. Carta gravimetrica d'Italia. *Acts of 5° Congress* GNGTS, Rome, 2, 913-918.

Cello G., Mazzoli S., 1999. Apennine tectonics in southern Italy: a review. *J. Geodyn*. 27, 191–211.

Channell J.E.T., Mareschal J.C., 1989. Delamination and asymmetric lithospheric thickening in the development of the Tyrrhenian Rift. *The Geological Society,* London, Special Publication 45, 285–302.

Chiarabba C., De Gori P., Chiaraluce L., Bordoni P., Cattaneo M., De Martin M., Frepoli A., Michelini A., Monachesi A., Moretti M., Augliera G. P., D'Alema E., Frapiccini M., Gassi A., Marzorati S., 2005. Main shocks and aftershocks of the 2002 Molise seismic sequence, southern Italy. *J. Seismol.*, 9(4), 487–494, doi:10.1007/s10950-005-0633-9.

Chiarabba C., De Gori P., Speranza F., 2009. Deep geometry and rheology of an orogenic wedge developing above a continental subduction zone: Seismological evidence from the northern-central Apennines (Italy). *Lithosphere*, 1, 95–104, doi:10.1130/L34.1.

Chiarabba C., De Gori P., Latorre D., Amato A., 2014. Crustal structure in the area of the 2002 Molise earthquake: Clues for the evolution of the southern Apennines. *Tectonics.,* doi:10.1002/2013TC003406.

Chiaraluce L., Valoroso L., Piccinini D., Di Stefano R., De Gori P., 2011. The anatomy of the 2009 L'Aquila normal fault system (central Italy) imaged by high resolution foreshock and aftershock locations. *J. Geophys. Res.* B: Solid Earth, 116, B12311, doi: 10.1029/ 2011JB008352.

Chiaraluce L., 2012. Unravelling the complexity of Apenninic extensional fault systems: A review of the 2009 L'Aquila earthquake (central Apennines, Italy). *J. Struct. Geol*. 42, 2–18.

Chiaraluce L., Di Stefano R., Tinti E., Scognamiglio L., Michele M., Casarotti E., Cattaneo M., De Gori P., Chiarabba C., Monachesi G., Lombardi A., Valoroso L., Latorre D., Marzorati S., 2017. The 2016 Central Italy seismic sequence: a first look at the mainshocks, aftershocks, and source models. *Seismological Research Letters,* 88, 3. doi: 10.1785/0220160221.

Chiodini G., Baldini A., Barberi F., Carapezza M.L., Cardellini C., Frondini F., Granieri D., Ranaldi M., 2007. Carbon dioxide degassing at Latera caldera (Italy): evidence of geothermal reservoir and evaluation of its potential energy. *J. of Geophys. Res*. 112, B12204.

Cinque A., Ascione A., Caiazzo C., 2000. Distribuzione spazio-temporale e caratterizzazione della fagliazione quaternaria in Appennino meridionale. In F. Galadini, C. Meletti, A. Rebez (ed.) "Le ricerche del GNDT nel campo della pericolosità sismica", CNR – Gruppo Nazionale per la Difesa dai Terremoti, Rome, 203–218.

Cinti F., Pantosti D., De Martini P. M., Pucci S., Civico R., Pierdominici S., Cucci L., Brunori C. A., Pinzi S., Patera A., 2011. Evidence for surface faulting events along the Paganica Fault prior to the April 6, 2009 L'Aquila earthquake (central Italy). *J. Geophys. Res*., 116, B07308, doi:10.1029/2010JB007988.

Civico R., Pucci S., Villani F., Pizzimenti L., De Martini P.M., Nappi R., Emergeo Working Group, 2017. Surface ruptures following the 30 October 2016 Mw 6.5 Norcia earthquake, central Italy. Journal of Maps, submitted.

Corniello A., Cardellicchio N., Cavuoto G., Cuoco E., Ducci D., Minissale A., Mussi M., Petruccione E., Pelosi N., Rizzo E., Polemio M., Tamburrino S., Tedesco D., Tiano P., Iorio M., 2015. Hydrogeological characterization of a geothermal system: the case of the thermo591 mineral area of Mondragone (Campania, Italy). Intern. J. of Environ. Res. 9, 2, 523–534.

Cosentino D., Asti R., Nocentini M., Gliozzi E., Kotsakis T., Mattei M., Pennacchioni M., 2017. New insights into the onset and evolution of the central Apennine extensional intermontane basins based on the tectonically active L'Aquila Basin (central Italy). GSA Bulletin, 129, 9-10, 1314-1336.

Cuoco E., Minissale A.A., Di Leo A., Tamburrino S., Iorio M., Tedesco D., 2017. Fluid Geochemistry of the Mondragone hydrothermal systems (southern Italy): water and gas compositions versus geostructural setting. *Int. J. Earth Sci.,* 106(7), 2429–2444.

De Alteriis G., Fedi M., Passaro S., Siniscalchi A., 2006. Magneto-seismic interpretation of subsurface volcanism in the Gaeta Gulf (Italy, Tyrrhenian Sea). *Annals of Geophys*., 49, 4/5, 929–943.

De Luca G., Cattaneo M., Monachesi G., Amato A., 2009. Seismicity in central and northern Apennines integrating the Italian national and national network. *Tectonophysics* 476, 121–135, doi:10.1016/j.tecto.2008.11.032.

De Rita D., Giordano G., 1996. Volcanological and structural evolution of Roccamonfina volcano (Italy): origin of the summit caldera. From McGuire, W. J., Jones, A. P. & Neuberg, J. (eds) 1996. Volcano Instability on the Earth and Other Planets. *Geological Society*, Special Publications, 110, 209–224; doi:10.1144/GSL.SP.1996.110.01.16.

Di Bucci D., Mazzoli S., 2003. The October-November 2002 Molise seismic sequence (Southern Italy): An expression of Adria intraplate deformation. *Journal of the Geological Society*, London. 160, 503–506.

Di Luccio F., Fukuyama E., Pino N. A., 2005. The 2002 Molise earthquake sequence: What can we learn about the tectonics of southern Italy?. *Tectonophysics*, 405, 141–154, doi:10.1016/j.tecto.2005.05.024.

DISS Working Group, 2015. Database of Individual Seismogenic Sources (DISS), Version 3.2.0: A compilation of potential sources for earthquakes larger than M 5.5 in Italy and surrounding areas. *Istituto Nazionale di Geofisica e Vulcanologia*. doi:10.6092/INGV.IT-DISS3.2.0.

Doglioni C., 1991. A proposal of kinematic modelling for W-dipping subductions - Possible applications to the Tyrrhenian - Apennines system. *Terra Nova*, 3, 4, 423-434.

Doglioni C., 1995. Geological remarks on the relationships between extension and convergent geodynamic settings. *Tectonophysics,* 252, 253–267, doi: 10.1016/0040-1951(95)00087-9.

EMERGEO Working Group, 2010. Evidence for surface rupture associated with the Mw 6.3 L'Aquila earthquake sequence of April 2009 (central Italy). *Terra Nova*, doi: 10.1111/j.1365-3121.2009.00915.

EMERGEO Working Group, 2016. The 24 August 2016 Amatrice Earthquake: Coseismic Effects. doi:10.5281/zenodo.61568.

Faccenna C., Piromallo C., Crespo Blanca A., Jolivet L., Rossetti F., 2004. Lateral slab deformation and the origin of the western Mediterranean arcs. *Tectonics*, 23, TC1012, doi:10.1029/2002TC001488.

Falcucci E., Gori S., Peronace E., Fubelli G., Moro M., Saroli M., Giaccio B., Messina P., Naso G., Scardia G., Sposato A., Voltaggio M., Galli P., Galadini F.,2009. The Paganica Fault and surface coseismic ruptures caused by the 6 April 2009 earthquake (L'Aquila, central Italy). *Seism. Res. Lett.,* 80(6), 940–950. doi:10.1785/gssrl.80.6.940.

Fedi M., Florio G., 2001. Detection of Potential fields source boundaries by Enhanced Horizontal Derivative method. *Geophysical Prospecting*, 49, 1, 40 - 58.

Fedi M., 2002. Multiscale Derivative Analysis: a new tool to enhance gravity source boundaries at various scales. *Geophys. Res. Lett.* 29, 16 -1-16-4.

Fedi M., Florio G., 2002. A stable downward continuation by using ISVD method. *Geophysical Journal International,* 151, 146–156.

Fedi M., Cella F., Florio G., Rapolla A., 2005. Multiscale Derivative Analysis of the Gravity and Magnetic Fields of the Southern Apennines (Italy) - *CROP PROJECT Elsevier.*

Fedi M., 2007. DEXP: A fast method to determine the depth and the structural index of potential fields sources. *Geophysics*, 72, 1, 1–11.

Fedi M., Pilkington M., 2011. Understanding imaging methods for potential field data. *Geophysics,* 77: G13-G24.

Galadini F., Galli P., 2000. Active tectonics in the Central Apennines (Italy) – input data for seismic hazard assessment. *Nat. Haz.,* 22, 225-270.

Galadini F., Galli P., 2003. Paleoseismology of silent faults in the Central Apennines (Italy): the Mt. Vettore and Laga Mts. Faults. Annals of Geophysics, 46, 5.

Galli, P., Galadini, F., and Pantosti, D., 2008: Twenty years of paleoseismology in Italy. Earth Sci. Rev. 88, 89–117, 2008.

Galli P., Giaccio B., Messina P., 2010. The 2009 central Italy earthquake seen through 0.5 Myr-long tectonic history of the L'Aquila faults system. *Quarter. Sci. Rev.,* 29(27–28), 3768–3789.

Galli P., Molin D., 2002. Macroseismic Survey of the 2002 Molise, Italy, Earthquake and Historical Seismicity of San Giuliano di Puglia. *Earthquake Spectra*, 20, S1, S39–S52.

Galli P., Peronace E., Tertulliani A., 2016. Rapporto sugli effetti macrosismici del terremoto del 24 Agosto 2016 di Amatrice in scala MCS. Roma, rapporto congiunto DPC, CNR-IGAG, INGV, 15 pp., doi: 10.5281/zenodo.161323.

Gaudiosi G., Alessio G., Luiso P., Nappi R., Ricciolino P., 2010. A critical review of seismotectonic setting of the Campanian Plain (Southern Italy) in GIS environment. *Geophys. Res. Abstracts,* 12. Poster presentation; doi: 10.13140/RG.2.2.26245.65763.

Ghisetti F., Vezzani L., 1983. Structural map of Mt. Pollino (Southern Italy). *S.EL.CA.,* Firenze, scale 1:50,000, 1 sheet.

Ghisetti F., Vezzani L., 1991. Thrust belt development in the central Apennines (Italy): northward polarity of thrusting and out-of-sequence deformations in the Gran Sasso chain. *Tectonics*, 10, 5, p. 904–919. doi:10.1029/91TC00902.

Ghisetti F., Vezzani L., 1997. Interfering paths of deformation and development of arcs in the fold-and-thrust belt of the central Apennines (Italy). *Tectonics*, 16, 523–536. doi: 10.1029/97TC00117.

Giraudi C., Frezzotti M., 1995. Palaeoseismicity in the Gran Sasso massif (Abruzzo, central Italy*). Quaternary International,* 25, 81–93, doi: 10.1016/1040-6182(94)P3716-L.

Herrmann R. B., Malagnini L., Munafò I., 2011. Regional moment tensors of the 2009 L'Aquila earthquake sequence. *Bull. Seismol. Soc. Am.* 101, 975–993, doi:10.1785/0120100184.

ISIDe working group (2016) version 1.0, doi:10.13127/ISIDe

Lavecchia G., Ferrarini F., Brozzetti F., de Nardis R., Boncio P., Chiaraluce L., 2012. From surface geology to aftershock analysis: constraints on the geometry of the L'Aquila 2009 seismogenic fault system. *Ital. J. Geosci.,* 131, 330–347.

Lavecchia G., Adinolfi G., De Nardis M., Ferrarini F., Cirillo D., Brozzetti F., De Matteis R., Festa G., Zollo A., 2017. Faulting model for the largest aftershock of the L'Aquila 1 2009 sequence and implications for unknown active extensional sources in central Italy. *Terra Nova* 29, 77–89, doi: 10.1111/ter.12251.

Latorre D., Amato A., Chiarabba C., 2010. High-resolution seismic imaging of the M_w 5.7, 2002 Molise, southern Italy, earthquake area: Evidence of deep fault reactivation. *Tectonics*, 29, TC4014, doi:10.1029/2009TC002595.

Lee W. H. K., Lahr J. C., 1975. HYP071 (Revised): A computer program for determining hypocenter, magnitude, and first motion pattern of local earthquakes. *U. S. Geological Survey* Open File Report 75-311, 113.

Luiso P., Paoletti V., Nappi R., La Manna M., Cella F., Gaudiosi G., Fedi M., Iorio M., 2017. A multidisciplinary approach to characterize the geometry of active faults: the example of Mt. Massico, Southern Italy. *Geophysical Journal International* (submitted).

Malinvemo A., Ryan W.B.F., 1986. Extension in the Tyrrhenian Sea and Shortening in the Apennines as Result of Arc Migration Driven by Sinking of the Lithosphere. *Tectonics*, 5, 2, 227-245. doi:10.1029/TC005i002p00227

Mariotti G., Doglioni C., 2000. The dip of the foreland monocline in the Alps and Apennines, Earth Planet. *Sci. Lett.,* 181, 191–202. doi:10.1016/S0012-821X(00)00192-8.

Miccadei E., Barberi R., De Caterini G., 1997. Nuovi dati geologici sui depositi quaternari della Conca Subaequana (Appennino abruzzese). *Il Quaternario*, 10.2, 483-486.

Michele M., Di Stefano R., Chiaraluce L., Cattaneo M., De Gori P., Monachesi G., Latorre D., Marzorati S., Valoroso L., Ladina C., et al., 2016. The Amatrice 2016 seismic sequence: A preliminary look at the mainshock and aftershocks distribution. *Ann. Geophys*. 59. doi: 10.4401/ag-7227.

Michetti A.M., Audemard F. A., Marco S., 2005. Future trends in paleoseismology: Integrated study of the seismic landscape as a vital tool in seismic hazard analyses. *Tectonophysics,* 408, 3 –21, doi: 10.1016/j.tecto.2005.05.035.

Milano G., Di Giovambattista R., Ventura G., 2008. Seismic activity in the transition zone between Southern and Central Apennines (Italy): Evidences of longitudinal extension inside the Ortona–Roccamonfina tectonic line. *Tectonophysics,* 457, 102–110.

Mildon Z. K., Roberts G. P., Walker, J. P. F., Iezzi F., 2017. Coulomb stress transfer and fault interaction over millennia on non-planar active normal faults: the Mw 6.5-5.0 seismic sequence of 2016–2017, central Italy. *Geophysical Journal International*, 210, 2.

Milia A., Torrente M.M., 2011. The possible role of extensional faults in localizing magmatic activity: a crustal model for the Campanian Volcanic Zone (Eastern Tyrrhenian Sea, Italy). *J Geol Soc.,* 68, 471–484.

Mostardini F., Merlini S., 1986. Appennino centro-meridionale: Sezioni geologiche e proposta di un modello strutturale. *Memorie della Società Geologica Italiana*, 35, 177–202.

Mucciarelli M., Böhm G., Caputo R., Giocoli A., Gueguen E., Klin P., Marello L., Palmieri F., Piscitelli S., Priolo E., Romano G., Rizzo E., 2009. Caratteri geologici e geofisici dell'area di San Giuliano di Puglia. *Rivista italiana di geotecnica*, 3, 32-42.

Oldow J.S., D'Argenio B., Ferranti L., Pappone G., Marsella E., Sacchi, M., 1993. Largescale longitudinal extension in the southern Apennines contractional belt, Italy. *Geology,* 21, 1123–1126.

Pace B., Peruzza L., Lavecchia G., Boncio, P., 2006. Layered seismogenic source model and probabilistic seismic-hazard analyses in Central Italy. Bull. Soc. seism. Am., 96(1), 107–132.

Pantosti D., Valensise G., 1990. Faulting mechanism and complexity of the 23 November 1980, Campania-Lucania earthquake, inferred from surface observations. *J. of Geophys. Res.,* 95, 15,319-15,341.

Pantosti D., Schwartz D.P., Valensise G., 1993. Paleoseismology along the 1980 Irpinia earthquake fault and implication for earthquake recurrence in the southern Apennines. *Journal of Geophysical Research*, 98, 6561–6577. doi: 10.1029/92JB02277.

Patacca E., Sartori R., Scandone P., 1990. Tyrrhenian basin and Apenninic arcs: kinematic relations since Late Tortonian times. *Mem. Soc. geol. ital*., 45, 425-451.

Patacca E., Sartori R., Scandone P., 1993. Tyrrhenian basin and Apennines. Kinematic evolution and related dynamic constraints. In Boschi E., Mantovani E. and Morelli A. Eds., Recent Evolution and Seismicity of the Mediterranean Region, *Kluwer Academic Publ*., 161-171.

Patacca E., Scandone P., 2004. The Plio-Pleistocene Thrust Belt-Foredeep System in the Southern Apennines and Sicily (Italy). *Special Volume of the Italian Geological Society for the IGC 32* Florence, 2004, 94-129.

Patacca E., Scandone P., 2007. Geology of the Southern Apennines. In: Mazzotti A., Patacca E. and Scandone P. (eds), Results of the CROP Project Sub-project CROP-04, Southern Apennines (Italy), *Boll. Soc. Geol. It.*, Special Issue, 7, 75-119.

Patacca E., Scandone P., Di Luzio E., Cavinato G.P., Parotto M., 2008. Structural architecture of the central Apennines: interpretation of the CROP11 seismic profile from the Adriatic coast to the orographic divide. *Tectonics*, 27, TC3006. doi:10.1029/2005TC001917.

Pierantoni P., Deiana G., Galdenzi S., 2013. Stratigraphic and structural features of the Sibillini Mountains (Umbria-Marche Apennines, Italy). *Italian Journal of Geosciences*, 132:3, 497-520.

Pizzi A., Galadini F., 2009. Pre-existing cross-structures and active fault segmentation in the northern-central Apennines (Italy). *Tectonophysics,* 476, no. 1, 304–319.

Pondrelli S., Morelli A., Ekstrom G., Mazza S., Boschi E., Dziewonski A.M., 2002. European-Mediterranean regional centroid-moment tensors: 1997–2000. *Phys. Earth Planet. Int.* 130, 71–101.

Pucci S., Villani F., Civico R., Pantosti D., Del Carlo P., Smedile A., De Martini P. M., Pons-Branchu E., Gueli A., 2015. Quaternary geology of the Middle Aterno Valley, 2009 L'Aquila earthquake area (Abruzzi Apennines, Italy). *Journal of Maps*, 11:5, 689-697, doi:10.1080/17445647.2014.927128.

Pucci S., De Martini P. M., Civico R., Villani F., Nappi R., Ricci T., Azzaro R., Brunori C. A. Caciagli M., Cinti F. R., Sapia V., De Ritis R., Mazzarini F., Tarquini S., Gaudiosi G., Nave R., Alessio G., Smedile A., Alfonsi L., Cucci L., Pantosti D., 2019. Coseismic ruptures of the 24 August 2016, Mw 6.0 Amatrice earthquake (central Italy). *Geophys. Res. Lett*., 44, doi:10.1002/2016GL071859.

Puglia R., Vona M., Klin P., Ladina C., Masi A., Priolo E., Silvestri F., 2013. Analysis of Site Response and Building Damage Distribution Induced by the 31 October 2002 Earthquake at San Giuliano di Puglia (Italy). *Earthquake Spectra*, 29, 2, 497-526.

Roberts G.P., Michetti A.M., 2004. Spatial and temporal variations in growth rates along active normal fault systems: an example from Lazio–Abruzzo Apennines. *J. Struct. Geol.*, 26, 339-376.

Rovida A., Camassi R., Gasperini P. e Stucchi M., (eds), 2011. CPTI11, la versione 2011 del Catalogo Parametrico dei Terremoti Italiani. Milano, Bologna, http://emidius.mi.ingv.it/CPTI.

Rovida A., Locati M., Camassi R., Lolli B., Gasperini P., (eds), 2016. CPTI15, the 2015 version of the Parametric Catalogue of Italian Earthquakes. *Istituto Nazionale di Geofisica e Vulcanologia.* doi:http://doi.org/10.6092/INGV.IT-CPTI15.

Salvini F., Vittori E., 1982. Analisi strutturale della Linea Olevano- Antrodoco-Posta (Ancona-Anzio Auct.): metodologia di studio delle deformazioni fragili e presentazione del tratto meridionale. *Memorie della Società Geologica Italiana*, 24, 337–355.

Scarpato G., Giudicepietro F., Romano S.P., Martini M., Ventre G., De Cesare W., 2004. Dispositivo virtuale per l'analisi da remoto degli eventi sismici (DIVARES).

Scognamiglio L., Tinti E., Michelini A., Dreger D. S., Cirella A., Cocco M., Mazza S., Piatanesi A., 2010. Fast determination of moment tensors and rupture history: What has been learned from the 6 April 2009 L'Aquila earthquake sequence. *Seismol. Res. Lett.* 81, 892–906. doi:10.1785/gssrl.81.6.892.

Scognamiglio L., Tinti E., Quintiliani M., 2016. The first month of the 2016 Amatrice seismic sequence: Fast determination of time domain moment tensors and finite fault model analysis of the ML 5.4 aftershock. *Ann. Geophys. 59*. doi: 10.4401/ag-7246.

Stavrev P., Reid A., 2007. Degrees of homogeneity of potential fields and structural indices of Euler deconvolution. *Geophysics,* 72, L1–L12, 2007.

Tedesco D., 1997. Systematic variations in the 3He/ 4He ratio and carbon in fumarolic fluids from active volcanic areas in Italy: Evidence for radiogenic 4He and crustal carbon addition by the subducting African plate. *Earth Planet. Sci. Lett*., 151, 255–269.

Tertulliani A., Rossi A., Cucci L., Vecchi M., 2009. L'Aquila (Central Italy) earthquakes: the predecessors of the April 6, 2009 event. *Seism. Res. Lett.,* 80 (6), 1008-1013. doi: 10.1785/gssrl.80.6.1008.

Tinti E., Scognamiglio L., Michelini A., Cocco M., 2016. Slip heterogeneity and directivity of the ML 6.0, 2016, Amatrice earthquake estimated with rapid finite-fault inversion. *Geophys. Res. Lett*. 43, 10,745–10,752, doi: 10.1002/2016GL071263.

Torrente M.M., Milia A., Bellucci F., Rolandi, G., 2010. Extensional tectonics in the Campania Volcanic Zone (eastern Tyrrhenian Sea, Italy): new insights into the relationship between faulting and ignimbrite eruptions. *Ital J. Geosci,* 129, 297–315.

Valensise G., Pantosti D., Basili R., 2004. Seismology and Tectonic Setting of the 2002 Molise, Italy, Earthquake. *Earthquake Spectra*, 20, S1, S23-S37.

Valoroso L., Chiaraluce L., Piccinini D., Di Stefano R., Schaff D., Waldhauser F., 2013. Radiography of a normal fault system by 64,000 high-precision earthquake locations: The 2009 L'Aquila (central Italy) case study. *J. Geophys. Res.* 118, 3, 1156–1176.

Vezzani L., Ghisetti F., 1998. Carta geologica dell'Abruzzo, scale 1:100000. S.EL.CA, Firenze.

Vezzani L., Festa A., Ghisetti F., 2010. Geological-Structural Map of the Central-Southern Apennines, Italy, in Geology and Tectonic evolution of the Central-Southern Apennines, Italy. *Edition: Geological Society of America Special Paper 469*.

Vittori E., Sylos Labini S., Serva L., 1991. Palaeoseismology: review of the state-of-the-art. *Tectonophysics*, 193, 9–32. doi: 10.1016/0040 -1951(91)90185-U.

Vittori E., Di Manna P., Blumetti A.M., Comerci V., Guerrieri L., Esposito E., Michetti A.M., Porfido S., Piccardi L., Roberts G.P., Berlusconi A., Livio F., Sileo G., Wilkinson M., McCaffrey K.J.W., Phillips R.J., Cowie P.A., 2011. Surface faulting of the 6 April 2009 M_w 6.3 L'Aquila Earthquake in Central Italy. *Bull. seism. Soc. Am*., 101(4), 1507–1530. doi:https://doi.org/10.1785/0120100140.

Wilkinson M.W., McCaffrey K.J.W., Jones R.R., Roberts G.P., Holdsworth R.E., Gregory L.C., Walters R.J., Wedmore L., Goodall H., Iezzi F., 2017. Near-field fault slip of the 2016 Vettore Mw 6.6 earthquake (Central Italy) measured using low-cost GNSS. *Scientific reports*, 7, 4612 doi:10.1038/s41598-017-04917-w.

http://www.isprambiente.gov.it/it/progetti/suolo-e-territorio-1/ithaca-catalogo-delle-faglie-capaci

http://www.isprambiente.gov.it/it/cartografia/carte-geologiche-e-geotematiche/carta-geologica-alla-scala-1-a-50000

http://sismolab.ov.ingv.it/sismo/index.php?PAGE=SISMO/last&area=Vesuvio&rmenu=on

Annexes

Table 1. *Attribute table of the structural dataset in the Paganica area.*

ID	Type	Age	Dip	Note
22	Normal fault	Pliocene-Quaternary	N-NE	
23	Normal fault	Pliocene-Quaternary	N-NE	Supposed
24	Normal fault	Pliocene-Quaternary	N-NE	Supposed
25	Normal fault	Pliocene-Quaternary	NE	
26	Normal fault	Pleistocene middle-Holocene	E	Supposed
27	Normal fault	Pliocene-Quaternary	SW	
28	Normal fault	Pliocene-Quaternary	SW	
29	Normal fault	Pleistocene middle-Holocene	SW	
30	Normal fault	Pleistocene middle-Holocene	SW	
31	Normal fault	Pleistocene middle-Holocene	NE	
32	Normal fault	Pleistocene middle-Holocene	SW	
33	Normal fault	Pleistocene middle-Holocene	SW	
34	Indefinite	Pleistocene middle-Holocene	Indefinite	
35	Thrust	Pliocene middle-low	W	
36	Thrust	Pliocene middle-low	SW	
37	Thrust	Pliocene middle-low	W	
38	Normal fault	Pliocene-Quaternary	SW	

Table 2. *Attribute table of the structural dataset in the Mt. Vettore – Mt. Bove area.*

ID	Type	Age	Dip	Note
480	Normal fault	Pliocene-Quaternary	S	
481	Normal fault	Pliocene-Quaternary	S	
482	Indefinite	Pleistocene middle-Holocene	Indefinite	Supposed

483	Indefinite	Pleistocene middle-Holocene	Indefinite	Supposed
484	Indefinite	Pleistocene middle-Holocene	Indefinite	Supposed
485	Normal fault	Pliocene-Quaternary	Indefinite	
486	Normal fault	Pliocene-Quaternary	SW	
487	Normal fault	Pliocene-Quaternary	SW	
488	Indefinite	Pliocene-Quaternary	Indefinite	
489	Indefinite	Pliocene-Quaternary	Indefinite	
490	Normal fault	Pliocene-Quaternary	Indefinite	
491	Normal fault	Pliocene-Quaternary	NE	
492	Normal fault	Pliocene-Quaternary	NE	
493	Normal fault	Pliocene-Quaternary	E-NE	
494	Normal fault	Pliocene-Quaternary	E-NE	
495	Normal fault	Pliocene-Quaternary	SW	
496	Indefinite	Pliocene-Quaternary	SW	

Table 3. *Attribute table of the structural dataset in the Mt. Massico area.*

ID	Type	Age	Dip	Note
358	Normal fault	Pleistocene low	E	Supposed
360	Reverse fault	Pliocene-Quaternary	NE	
361	Normal fault	Pliocene-Quaternary	NW	
362	Normal fault	Pliocene-Quaternary	NW	Supposed
363	Normal fault	Pliocene-Quaternary	SE	
364	Normal fault	Pliocene-Quaternary	SW	Supposed
365	Normal fault	Pliocene-Quaternary	SE	
366	Normal fault	Pliocene-Quaternary	SW	
367	Normal fault	Pliocene-Quaternary	SW	
368	Normal fault	Pliocene-Quaternary	SW	

369	Normal fault	Pliocene-Quaternary	S-SW	
370	Indefinite	Pliocene-Quaternary	Indefinite	
371	Normal fault	Pliocene-Quaternary	SW	
372	Normal fault	Pliocene-Quaternary	W-NW	
373	Normal fault	Pliocene-Quaternary	W	Supposed
374	Normal fault	Pliocene-Quaternary	NW	
375	Normal fault	Pre- Pliocene-Quaternary	N	
376	Normal fault	Pre- Pliocene-Quaternary	SE	

Table 4. *Attribute table of the structural dataset in the San Giuliano di Puglia area.*

ID	Type	Dip
1	Buried external front of the Apenninic accretionary prism	SW
2	Thrust and reverse fault	SW
3	Thrust and reverse fault	SW
4	Thrust and reverse fault	SW
5	Thrust and reverse fault	SW
6	Thrust and reverse fault	SW
7	Thrust and reverse fault	SW
8	Thrust and reverse fault	SW
9	Thrust and reverse fault	SW
10	Thrust and reverse fault	SW

Table 5. *Velocity model from Gaudiosi et al. (2010).*

P Velocity (km/s)	Depth (km)
2.8	0
5.3	2
6.2	8
7.2	12
8.2	25

Table 6a. *Attribute table of the gravimetric dataset in the Paganica area.*

ID	Topog. Correlation	Fault Correlation	Earthquake Correlation	Note
22	Medium	Low	Low	Faults correlation is high in the lower part of the anomaly
23	Medium	Medium	Medium	Topography correlation is high in the upper part of the anomaly
24	High	Medium	High	The anomaly is perpendicular to the mountain ranges
25	Medium	Low	High	
26	High	High	High	The anomaly is perpendicular to the faults
27	High	Low	High	The anomaly is perpendicular to the faults
28	Low	Low	High	
29	High	High	Low	
30	Medium	Low	Low	
31	High	Medium	Medium	
32	High	Low	Low	The anomaly is perpendicular to the faults

33	High	Low	Low	
34	High	Low	Low	
35	Medium	Low	Low	
36	High	Low	Low	

Table 6b. *Attribute table of the gravimetric dataset in the Mt. Vettore – Mt. Bove area.*

ID	Topog. Correlation	Fault Correlation	Earthquake Correlation	Note
274	High	High	High	
275	Medium	Medium	Low	The anomaly is perpendicular to the mountain ranges and faults
276	High	Low	Low	The anomaly is perpendicular to the mountain ranges
277	High	Low	High	
278	High	High	High	
279	High	High	High	
280	Low	Low	Medium	
281	High	Low	High	The anomaly is perpendicular to the mountain ranges
282	High	Low	Low	The anomaly is perpendicular to the mountain ranges
283	High	Low	Low	The anomaly is perpendicular to the mountain ranges
284	High	Low	High	The anomaly is perpendicular to the mountain ranges
285	High	Low	Low	
286	High	Low	Low	
287	High	Medium	High	
288	High	Low	Low	The anomaly is perpendicular to the mountain ranges
289	High	Low	Low	The anomaly is perpendicular to the mountain ranges
290	Medium	High	Low	

Table 6c. *Attribute table of the gravimetric dataset in the Mt. Massico area.*

ID	Topog. Correlation	Fault Correlation	Earthquake Correlation	Note
200	High	Medium	Low	
201	High	Low	Low	
202	High	Low	Low	
203	High	Medium	High	
204	Low	Low	Low	
205	Medium	Low	Low	
206	Medium	High	Low	
207	High	High	Medium	
208	High	High	Medium	
209	Medium	High	Low	
210	Medium	Medium	Low	Topography correlation is high only in the upper part of the anomaly
211	Medium	Medium	Low	
212	High	Medium	Low	
213	High	Medium	Low	
214	High	High	Low	
215	Low	High	Low	
216	High	High	Low	
217	Low	Low	Low	

Table 6d. *Attribute table of the gravimetric dataset in the San Giuliano di Puglia area.*

ID	Topog. Correlation	Fault Correlation	Earthquake Correlation	Note
26	Low	Medium	Low	
27	Low	Medium	High	
28	Low	Low	Low	
29	Low	Low	Low	
30	Low	Low	Low	
31	Low	Low	Low	
32	Low	High	Low	
33	Low	High	Low	
34	Low	High	Low	
36	High	Low	Medium	
37	High	Low	Low	
38	High	Low	Low	
39	Low	Medium	Low	
40	Medium	Medium	Low	
41	Medium	Low	Low	
42	High	Low	Low	The signal is perpendicular to the topography high
43	High	Low	Low	

Table 7. *Attribute table of the most accredited faults in the Paganica area.*

ID	Type	Dip	Sources
1	Normal fault	NE	ITHACA; CARG project
2	Normal fault	NE	ITHACA; CARG project
3	Normal fault	SW	ITHACA; CARG project
4	Normal fault	NE	ITHACA; CARG project; Galadini and Galli (2003); Neotectonic map of Italy (Ambrosetti et al., 1986)
6	Normal fault	SW	ITHACA; CARG project; Neotectonic map of Italy (Ambrosetti et al., 1986)
11	Normal fault	SW	ITHACA; CARG project

Table 8. *Attribute table of the most accredited faults in the Mt. Vettore – Mt. Bove area.*

ID	Type	Dip	Sources
1	Normal fault	W-SW	EMERGEO W.G.; Galadini and Galli (2003); Neotectonic map of Italy (1986)
2	Normal fault	E-NE	EMERGEO W.G.; Galadini and Galli (2003); Neotectonic map of Italy (1986)
3	Normal fault	E-NE	EMERGEO W.G.; Neotectonic map of Italy (1986)
4	Normal fault	E-NE	EMERGEO W.G.; Neotectonic map of Italy (1986)
5	Normal fault	W-SW	EMERGEO W.G.; Galadini and Galli (2003);
6	Normal fault	W-SW	EMERGEO W.G.; Galadini and Galli (2003);
7	Normal fault	W-SW	EMERGEO W.G.; Galadini and Galli (2003);
8	Normal fault	W-SW	EMERGEO W.G.; Galadini and Galli (2003);
9	Normal fault	W-SW	EMERGEO W.G.; Galadini and Galli (2003);
10	Normal fault	E-NE	EMERGEO W.G.; Galadini and Galli (2003);
11	Normal fault	E-NE	EMERGEO W.G.; Neotectonic map of Italy (1986)
12	Normal fault	W	EMERGEO W.G.; Neotectonic map of Italy (1986)
13	Normal fault	E-NE	EMERGEO W.G.; Neotectonic map of Italy (1986)
14	Normal fault	E-NE	EMERGEO W.G.; Neotectonic map of Italy (1986)

15	Normal fault	SW	EMERGEO W.G.; Galadini and Galli (2003); CARG project; Neotectonic map of Italy (1986)

Table 9. *Attribute table of the most accredited faults in the Mt. Massico area.*

ID	Type	Dip	Sources
1	Normal fault	NW	ITHACA; Neotectonic map of Italy (1986); Structural map of Italy (Bigi et al., 1983); Carta geologica dell'Appennino meridionale (Bonard et al., 1988)
2	Normal fault	NW	ITHACA; Neotectonic map of Italy (1986); Structural map of Italy (Bigi et al., 1983);
3	Normal fault	SE	ITHACA; Neotectonic map of Italy (1986);
4	Normal fault	Sub-Vertical	ITHACA; Neotectonic map of Italy (1986);
5	Normal fault	NW	Neotectonic map of Italy (1986); Structural map of Italy (Bigi et al., 1983);
6	Normal fault	SE	ITHACA; Neotectonic map of Italy (1986); Structural map of Italy (Bigi et al., 1983); Carta geologica dell'Appennino meridionale (Bonard et al., 1988)
7	Normal fault	SE	Neotectonic map of Italy (1986); Structural map of Italy (Bigi et al., 1983);
8	Normal fault	SW	Carta geologica dell'Appennino meridionale (Bonard et al., 1988); Carta delle faglie tardo quaternarie (Cinque et al., 2000)
9	Normal fault	SW	Neotectonic map of Italy (1986); Carta delle faglie tardo quaternarie (Cinque et al., 2000)
10	Normal fault	SW	Neotectonic map of Italy (1986); Carta delle faglie tardo quaternarie (Cinque et al., 2000)
11	Normal fault	SW	ITHACA; Carta delle faglie tardo quaternarie (Cinque et al., 2000)
12	Normal fault	SW	Neotectonic map of Italy (1986); Carta delle faglie tardo quaternarie (Cinque et al., 2000)

Table 10. *Attribute table of the most accredited faults in the San Giuliano di Puglia area.*

ID	Type	Dip	Sources
1	Thrust	SW	Vezzani et al. (2010); Neotectonic map of Italy (1986);
2	Thrust	SW	Vezzani et al. (2010); Neotectonic map of Italy (1986);
3	Thrust	NE	Vezzani et al. (2010); Neotectonic map of Italy (1986);
4	Reverse fault	S	Vezzani et al. (2010); Neotectonic map of Italy (1986);
5	Normal fault	SW	Vezzani et al. (2010); Neotectonic map of Italy (1986);
6	Reverse fault	SW	Vezzani et al. (2010); Neotectonic map of Italy (1986);
7	Reverse fault	NE	Vezzani et al. (2010); Neotectonic map of Italy (1986);
8	Reverse fault	SW	Vezzani et al. (2010); Neotectonic map of Italy (1986);
9	Reverse fault	SW	Vezzani et al. (2010); Neotectonic map of Italy (1986);
10	Reverse fault	SW	Vezzani et al. (2010); Neotectonic map of Italy (1986);
11	Thrust	W-SW	Vezzani et al. (2010); Neotectonic map of Italy (1986);
12	Normal fault	W	ITHACA; Vezzani et al. (2010); Neotectonic map of Italy (1986); Carta delle faglie tardo quaternarie (Cinque et al., 2000)
13	Normal fault	Sub-Vertical	ITHACA; Vezzani et al. (2010);
14	Normal fault	SW	ITHACA; Vezzani et al. (2010);